Universidad
Carlos III de Madrid
www.uc3m.es

TESIS DOCTORAL

ESTUDIOS FUNCIONALES MEDIANTE RESONANCIA MAGNÉTICA EN PEQUEÑOS ANIMALES

FUNCTIONAL MAGNETIC RESONANCE IMAGING STUDIES IN SMALL ANIMALS

Autor:

Cristina Chavarrías Navas

Directores:

Manuel Desco Menéndez

Juan Felipe Pérez-Juste Abascal

DEPARTAMENTO DE BIOINGENIERÍA E INGENIERÍA AEROESPACIAL

Leganés, diciembre de 2015

Universidad
Carlos III de Madrid
www.uc3m.es

TESIS DOCTORAL

ESTUDIOS FUNCIONALES MEDIANTE RESONANCIA MAGNÉTICA EN PEQUEÑOS ANIMALES

Autor: Cristina Chavarrías Navas

Directores:

Manuel Desco Menéndez

Juan Felipe Pérez-Juste Abascal

Firma del Tribunal Calificador:

Firma

Presidente:

Vocal:

Secretario:

Calificación:

Leganés, de de

A ti, papá.

Tu incansable lucha obrera me ha permitido
llegar hasta aquí, donde quizá tú
debieras haber llegado.

"La lucha del hombre contra el poder es la lucha de la memoria contra el olvido"

Milan Kundera

AGRADECIMIENTOS

A mis directores de tesis.

A Manolo por haberme sacado del cascarón y haber confiado en mí desde el primer momento. Gracias por tu esfuerzo, a veces poco apreciado, que nos ha permitido hacer lo que nos gusta durante tantos años. Además de mucho conocimiento me llevo valiosas lecciones de inconformismo, escepticismo y espíritu crítico.

A Juan por ser un faro en mitad de la noche. Tu paciencia, optimismo y comprensión han sido imprescindibles para poder encontrar la salida del túnel. Gracias por tantas horas de generosa dedicación.

A todos los que me ayudaron en los comienzos con su saber hacer o con sus consejos: un gallego encantador y muy docente, Marina, Sandra, Ángela, Ángel, Yasser, Vero, Chema, Juanjo, Balaban. Todos formáis parte en mayor o menor medida de este trabajo, muchas gracias.

Gonzalo, tú has sido mi apoyo durante todos estos años. Contigo he aprendido tanto o más que dentro del laboratorio, y probablemente enseñanzas más valiosas. Gracias por ser un señor de los pies a la cabeza.

A Paula, por tu inmenso cariño. Siempre me has apoyado laboralmente y personalmente. Dicen que más vale tarde que nunca, y contigo este refrán se ha personificado. No sólo tienes unos valores personales que son un tesoro sino que además tienes la inteligencia, serenidad y humildad características de los investigadores más brillantes. Eres una grande y vas a llegar muy lejos. ¡¡¡Y quiero estar ahí para verlo!!!

Sin duda en los últimos años el mayor apoyo lo he encontrado cada mañana frente al café o por la tarde frente a la sidra. Gracias a mi pequeño Santidrín por acogerme con los brazos abiertos, cuidarme, aconsejarme o simplemente escuchar. Os quiero mucho… y lo sabéis (insert meme here :P).

Eu, mi torbellino hermano, ten paciencia, que todo llega. Aptitudes y energía te sobran a borbotones. Gracias por tu frescura, alegría, por tus abrazos, y por tener siempre un plan genial para mí.

Esta tesis no resume mi estancia en el LIM, sólo una pequeña parte, pero es ahora cuando freno, miro atrás y siento nostalgia por la familia que fuimos. Echo de menos aquel núcleo duro que me sacaba a olvidar las penas: Tra, Sisni, Esther, Juanolas, Edu, Alvarico, Gus, Josete, Irina, Angelito, Santi Reig, Gonzalo, los neuros, Yassel, Jafi,

Kike, Fidel, María, y seguro que algunos otros que me estoy olvidando. Vaya recuerdos me quedan. Gracias también a las nuevas adquisiciones por seguir cuidándome, sois unos encantos e irradiáis talento. No dejéis que se pierdan estos lazos, que te ayudan a sujetarte cuando te estás cayendo. En general gracias a todos mis compañeros del LIM, pasados y presentes, que siempre estáis y habéis estado dispuestos a echar una mano. Son tantas horas compartidas que de verdad os siento como mi familia de acogida.

Y cómo no, a mi familia real, por apoyarme en todo aunque a veces no entendieran una sola de mis palabras o acciones.

TABLE OF CONTENTS

RESUMEN

Esta tesis se enmarca dentro del ámbito de la imagen biomédica preclínica, y específicamente trata sobre la técnica de imagen de resonancia magnética funcional (fMRI) en pequeños animales. La complejidad de dicha técnica tanto a nivel experimental como tecnológico ha limitado considerablemente su ámbito de uso, y por ello no es una modalidad de imagen que se realice de manera habitual. Sin embargo ofrece información muy valiosa tanto a nivel fisiológico, para el estudio de los mecanismos del cerebro normal durante la actividad neuronal, como a nivel patológico, para la búsqueda y estudio de fármacos aplicables a diferentes disfunciones cerebrales.

En esta tesis se han estudiado técnicas y métodos para intentar aliviar estas dificultades y facilitar su utilización por parte de la comunidad científica. El trabajo incluye aportaciones en los ámbitos de la configuración del experimento, de la adquisición de los datos y su reconstrucción, y por último del análisis cuantitativo final de las imágenes.

En el primer capítulo se trata el problema del uso de anestesia durante el experimento. Para obtener medidas funcionales es necesario establecer un protocolo anestésico que facilite la sedación del animal pero sin llegar a un estado anestésico profundo. Por otra parte, es deseable que sea de rápida inducción y recuperación, y que no sea tóxico para que pueda usarse en estudios longitudinales. En esta parte de la tesis se realizaron experimentos de fMRI en rata sedada con sevofluorano, para lo cual fue necesario realizar un estudio dosis-respuesta y un barrido de frecuencias de estimulación. Además, la señal obtenida en la corteza cerebral se comparó con la de otro protocolo de sedación más tradicional, con medetomidina subdérmica. La señal obtenida fue de intensidad similar a la obtenida con medetomidina, pero el tiempo de preparación del animal se incrementó considerablemente, lo cual constituye un grave inconveniente práctico para el uso de este anestésico.

El segundo capítulo está dedicado al estudio de un entorno de adquisición comprimida o "compressed sensing" que permita reducir sustancialmente el tiempo de adquisición sin degradar la calidad de la imagen, gracias a la adquisición de una cantidad mucho menor de datos. En este trabajo se muestra que sería posible acelerar la adquisición a altas tasas que incumplen el criterio de Nyquist-Shannon siempre y cuando se explote la redundancia de información temporal y al mismo tiempo se empleen algoritmos de reconstrucción de imagen iterativos no lineales. En concreto se compara la eficacia de tres algoritmos de reconstrucción que explotan la redundancia temporal para recuperar el contraste BOLD y que han arrojado buenos resultados en otras aplicaciones o modalidades de imagen: tomografía por rayos X, estudios dinámicos de corazón por resonancia magnética, y resonancia funcional en reposo o "resting state". La comparativa se realizó en dos escenarios de relación señal a ruido y se concluye que el algoritmo que utiliza una imagen a priori (PICCS) es el que mejores resultados obtiene en la reconstrucción.

El tercer capítulo aborda el postprocesado y análisis de las imágenes. Existen varias herramientas gratuitas y de código abierto para este fin, pero fueron diseñadas para imagen de cerebro humano, y su adaptación a imágenes de roedores requiere el uso de herramientas adicionales o la realización de transformaciones en la imagen que implican conocimientos de programación. Además, para obtener valores cuantitativos es imprescindible el uso de extensiones o herramientas adicionales. En este trabajo se han estudiado las herramientas existentes y se ha propuesto y desarrollado un nuevo software, fMRat, que realiza el análisis completo de varios sujetos de manera automática, desde el cambio de formato de las imágenes hasta la obtención de valores numéricos de las regiones de interés elegidas por el usuario. La herramienta está programada en Matlab como una extensión de un paquete SPM ya existente, y fue validada con 460 estudios reales de ratas. El código está publicado como "open-software" en el sitio web de Github y es accesible a cualquier neurocientífico que desee utilizarlo.

ABSTRACT

This thesis is framed within the field of preclinical biomedical imaging, and specifically devoted to the study of functional magnetic resonance imaging (fMRI) technique in small animals. The experimental and technological complexity of this modality has greatly limited its use, and therefore it is not a routine imaging modality. However, it provides valuable information both at the physiological level, to study the mechanisms of normal brain during neuronal activity, and at the pathological level, to study drugs intended for different brain dysfunctions.

In this work we have studied techniques and methods that intend to alleviate these difficulties and facilitate their use by the scientific community. The work includes contributions at several stages: the experimental setup, the data acquisition and reconstruction, and the quantitative image analysis.

The first section addresses the problem of using anesthesia during the experiment. In order to perform functional measurements, it is necessary to establish a protocol to induce anesthetic sedation of the animal rather than a deep anesthetic state. Moreover, the use of non-toxic drugs with fast induction and recovery is desirable. In this section of the thesis we conducted fMRI experiments in rats sedated with sevoflurane, and since this agent had not been previously reported for fMRI, it was necessary to conduct strategies in order to determine the optimum dose-response and stimulation frequency. Furthermore, the signal obtained in the cerebral cortex was compared with a more traditional protocol sedation, subdermal medetomidine. The signal obtained was similar to that obtained under medetomidine, but the animal preparation time increased considerably, which constitutes a serious practical drawback for the use of sevoflurane.

The second section is devoted to the study of a compressed sensing framework that allows a substantial reduction on the acquisition time without degrading image quality. The acquisition of a much reduced amount of data, thus at high rates of acceleration

that violate the Nyquist-Shannon criterion, is possible by means of a wise exploitation of the temporal information redundancy and by the use of nonlinear iterative reconstruction algorithms. In this study we evaluated the performance of three compressed-sensing reconstruction algorithms that exploit temporal redundancy to recover the BOLD contrast and which have proved successful in other applications or imaging modalities such as: X-ray tomography, dynamic cardiac MRI, and resting state MRI studies. The comparison was performed in two signal-to-noise ratio scenarios and the conclusion drawn is that the algorithm which uses an a priori image (PICCS) yields the best reconstruction.

The third section deals with the post-processing and image analysis. There are several open-source tools available to this purpose, but they were originally designed for human studies. Their adaptation to rodent images requires the use of additional tools or some image transformation processing that involve programming skills. Moreover, to obtain quantitative values, the user would need to use additional extensions or external software. In this work we have studied the existing tools and proposed and developed a new software, fMRat, which automatically performs a full multi-subject analysis, from the initial format conversion to the extraction of numerical values from the regions interest chosen by the user. The tool was programmed in Matlab as an extension of the existing SPM package, and was validated with 460 real rat studies. The code has been published as "open-software" in Github website and is accessible to the neuroscience community.

1 GLOSSARY OF TERMS

ATP:	adenosintriphosphat
AUC:	area under the curve, typically under a ROC curve
BOLD (signal):	blood oxygenation level-dependent (signal)
CBF:	cerebral blood flow
CL:	alpha-chloralose
$CMRO_2$:	cerebral metabolic rate of oxygen
CO_2:	carbon dioxide
CS:	compressed sensing
dHB:	deoxyhemoglobin
EPI:	echo planar imaging
EVI:	echo volumar imaging
fMRI:	functional magnetic resonance
FOV:	field of view
FPF:	false positive fraction
FWE:	family-wise error
FWHM:	full width at half maximum
GABA:	gamma-aminobutyric acid (neurotransmitter)
GLM:	general linear model
GUI:	graphical user interface
HRF:	hemodynamic response function
HYPR:	highly constrained back-projection —algorithm—
HYPR LR:	HYPR local reconstruction —algorithm—
HYPRIT:	HYPR by iterative estimation
I-HYPR:	iterative HYPR
KLT:	Karhunen-Loève transformation
k-t BLAST:	broad-use linear acquisition speed-up technique —algorithm—
k-t FASTER:	fMRI accelerated in space-time via truncation of effective rank —algorithm—
k-t FOCUSS:	k-t focal underdetermined system solver —algorithm—
k-t SENSE:	k-t sensitivity encoding —algorithm—

k-t SPARSE:	high frame-rate dynamic imaging exploiting spatio-temporal sparsity —algorithm—
L1:	L1 norm, noted as $\|\cdot\|_1$. Also called taxicab distance or Manhattan distance.
L2:	L2 norm, noted as $\|\cdot\|_2$. Also called Euclidean distance.
MC:	matrix completion
MR:	magnetic resonance
MRI:	magnetic resonance imaging
pCO_2:	carbon dioxide arterial tension
PCA:	principal component analysis
PET:	positron emission tomography
PICCS:	prior image constrained compressed sensing —algorithm—
RARE:	rapid acquisition with relaxation enhancement
rCBF:	regional cerebral blood flow
ROC:	receiver operating curve (of a detection system)
ROI:	region of interest
S1:	somatosensorial primary cortex
S1FL:	left forelimb somatosensorial primary cortex
S1FR:	right forelimb somatosensorial primary cortex
S1HL:	left hindlimb somatosensorial primary cortex
S1HR:	right hindlimb somatosensorial primary cortex
SE-EPI:	spin-echo (SE) echo planar imaging (EPI)
SER:	simultaneous echo refocusing
SIR:	simultaneous image refocused
SNR:	signal to noise ratio
SPM:	[1]statistical parametrical mapping (in general) [2]software package developed by the Wellcome Trust Centre for Neuroimaging, UK, for statistical parametrical mapping
SPM5:	SPM, version 5
SPM8:	SPM, version 8
SPM12:	SPM, version 12
T1:	longitudinal magnetization relaxation time constant
T2:	transversal magnetization relaxation time constant

TE:	echo time
TTL:	transistor-transistor logic (digital electronics standard)
TTV:	spatio-temporal total variation —algorithm—
TV:	total variation (spatial)
TPF:	true positive fraction
TR:	repetition time
VD:	variable density

2 MOTIVATION AND OBJECTIVES

Functional magnetic resonance imaging (fMRI) in rodents has been used for decades to study brain function and dysfunction [1-6]. Such a technique has enabled a finer study of the brain hemodynamics thanks to the higher resolution it provides as compared to human fMRI –one order of magnitude higher-[3]. Moreover, these studies in rodents have also enabled simultaneous measurements of the electrical activity and the BOLD (blood oxygenation level-dependent) signal for a deeper understanding of the neuro-vascular coupling and its associated mechanisms [3]. However, the complexity of the experimental setup, the variability of the subject physiological conditions, the long acquisition times and the intricacy of the image analysis have prevented this technique from being widely used in preclinical studies.

Keeping a sedative state is critical in rodent fMRI for obtaining a robust and reproducible BOLD signal with minimal head movement, and this was traditionally achieved by using alpha-chloralose (CL) as the anesthetic agent [7-10]. This drug was reported to produce the strongest brain activation as compared to other anesthetics, probably because CL preserves better the functional-metabolic coupling [7, 8]. Unfortunately, it has significant toxic side effects, such as acidosis and seizure-like activity, and it has a very long recovery time [11-14]. Therefore it is not recommended for survival procedures [9]. The latest research on anesthetics for fMRI preclinical experiments has focused on survival-compatible drugs such as medetomidine or isoflurane which may substitute alpha-chloralose and enable longitudinal studies [10-14]. Inhaled anesthetics are particularly preferred because of the easier animal manipulation required and fast recovery. In this line, sevoflurane is widely used in the human clinical practice since it is well tolerated by adult and pediatric patients, with a low incidence of mild airway complications, and particularly better tolerated than isoflurane or halothane during rapid induction [15]. Nonetheless, its adequacy for preclinical fMRI studies has not been tested yet.

Another challenge regarding fMRI experiments is the long duration of the acquisition sequences, and the consequent excessive time required by the whole protocol. In a typical experiment, the animal preparation and the image adjustments and localization may take about one hour. In addition, several fMRI runs have to be acquired at the beginning to ensure the stimuli adequacy, the synchronization of the stimuli with the scanner and the animal physiological conditions. After that, the aimed fMRI series are acquired under the different circumstances required by the study. Between runs, the animal is typically allowed to rest for 5-10 minutes in order to avoid developing stimuli tolerance. All these steps result in a total experiment duration of several hours, which adds some extra difficulty to maintain anesthesia and to avoid stimuli tolerance.

An additional difficulty in fMRI comes from the fact that BOLD contrast is very small in comparison with the background noise (both physiological and electronic), and therefore the image has to be acquired repeatedly to build a temporal series that is statistically analyzed at later stages. There is a trade-off between acquisition time and final statistical power achieved.

Efforts have not been spared to shorten the series acquisition time by exploiting parallel imaging techniques [16, 17], by multiplexing along different dimensions [18, 19], or by using single-shot 3D trajectories [20-22]. Although most of these approaches are prone to artifacts at high acceleration factors, the compressed sensing (CS) framework [23-25] has relieved those effects and is nowadays one of the strategies with the highest potential for accelerating fMRI acquisitions. In addition, it can be combined with parallel imaging or single-shot trajectories to achieve even faster acquisitions. The theory behind CS states that a full recovery of the signal is possible from a partial measurement of the k-space if certain conditions are fulfilled: the signal must be sparse in some transform domain, the undersampling must be random or pseudo-random in order to ensure incoherent artifacts and a non-linear optimization algorithm should be used for reconstruction [23, 24, 26]. Many CS algorithms have been tested for dynamic cardiac MRI but very few of them have been tested for fMRI (k-t FOCUSS [27], generalized series [28] and low-rank approaches [29]).

Some of the works mentioned above intended to exploit the compressed sensing framework to increase the spatial or temporal resolutions instead of reducing scan time. Higher spatial resolution translates into better localization of the neurological activity, and higher temporal resolution helps to attenuate susceptibility artifacts, chemical shifts and physiological noise. The reduction of the readout periods may also be used to improve the statistical power in the final fMRI maps if more repetitions are acquired within the same acquisition time [28].

The typical analysis of fMRI series comprises several preprocessing steps, the fitting of a regression model and a voxel-by-voxel statistical test, but every single step has to be performed with different algorithms and software implementations, which makes the methodology cumbersome and subject to controversy. Moreover, most of the research in this field was carried out for human fMRI [30-33], and thus available software tools such as SPM (*Statistical Parametric Mapping*, The Wellcome Trust Centre for Neuroimaging), AFNI [34] or FEAT [35], are oriented to this type of images. The large difference in resolution between human and rodent images demands adjustments of the realignment, normalization, smoothing and visualization steps as well as the adaptation of the hemodynamic function model involved in the regression model. An extension for rodents, a software named SPMMouse was developed for a previous version of SPM (SPMMouse, Wolfson Brain Imaging Centre, University of Cambridge [39]), but is no longer maintained. Simpler software packages, such as Bruker proprietary software or Stimulate (University of Minnesota [40]), provide a fast and straightforward analysis, but they lack relevant features such as series realignment, adjustment to a general linear model (GLM), multiple comparisons correction, or ROI (region of interest) quantification.

In summary, fMRI is a technology with high potential for a deeper knowledge of brain functioning but there are several aspects which impair its daily use in rodent studies: physiological considerations, experimental issues such as the acquisition time, and the post-processing complexity.

2.1 OBJECTIVES

The main objective of this thesis is to contribute to improving fMRI technique in rat brains, at three main different stages: the experimental setup, the acquisition, and the statistical analysis. The specific objectives of each content block are:

1. To define and validate an optimum experimental setup able to conduct electrical somatosensorial fMRI experiments in normal rats, under a recoverable sedation and producing a strong BOLD contrast.

2. To investigate the applicability of compressed sensing techniques to reduce total scan time while preserving BOLD contrast, by defining a new acquisition scheme able to exploit the temporal redundancy of fMRI series.

3. To study the specific requirements for the automatic analysis of rodent fMRI, and to develop and validate a new and versatile solution fulfilling the needs of both expert and non-expert users.

3 INTRODUCTION

This chapter introduces the physiological mechanisms that produce the BOLD contrast, and reviews the MRI sequences used in fMRI together with the required image postprocessing and statistical analysis.

3.1 FMRI BASICS

Neurovascular coupling

BOLD (Blood Oxygenation Level-Dependent) contrast was first described by Ogawa et al. [36, 37] as an endogenous MRI contrast agent reflecting the blood oxygenation level in-vivo. They observed a reduction in the MRI signal intensity of gradient-echo sequences in the bigger venous blood vessels produced by the presence of deoxy-hemoglobin, which had already been described as paramagnetic by Pauling in 1936 [38]. However, it was not until 1993 that the first rat stimuli-related positive BOLD contrast was observed [39]. In this thesis the term "BOLD contrast" will denote the change in MR signal intensity related to a neuronal activation induced by some external stimulation.

Since deoxy-hemoglobin (dHb) is paramagnetic, it produces a noticeable difference in susceptibility between the vessels and the surrounding tissues:

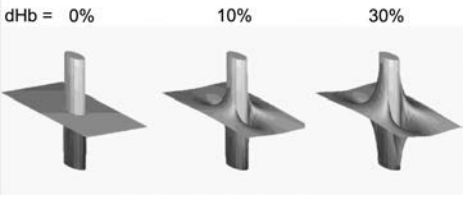

Figure 1.Susceptibility effects of the concentration of deoxy-hemoglobin around a vessel [40].

The paramagnetic core of Hb is surrounded by a hydrophobic structure, and this explains why the T1 relaxation time is preserved, while the T2 relaxation time is shortened, especially where deoxy-hemoglobin is compartmentalized –vessels and red blood cells- [41].

During brain stimulation, local oxygen demands from the neurons produce an initial increase in the deoxy-hemoglobin content of the surrounding capillary bed. Subsequent vasodilation and regional increase in cerebral blood flow (CBF) takes place to increase the oxygen supply. This compensatory increase in regional cerebral blood flow (rCBF) and oxygen supply exceeds the tissue oxygen extraction, and therefore produces a net dHb decrease. The initial increase in dHb translates into an MRI signal decrease due to the spin-spin dephasing, commonly known as the "initial dip" [42]. The following dHb decrease leads to a main BOLD signal increase or "primary response", after which a latter "post-stimulus undershoot" takes place [43]. All these dynamic changes in MRI contrast are typically called 'brain hemodynamic response function' (HRF), which actually constitutes the system impulse response function. The biological mechanisms underlying this signal response are called 'neurovascular coupling' and have been studied through electrophysiology, spectral optical imaging, ultrasound, photoacoustic microscopy and MRI studies in both human and rodents [3, 42, 44-53].

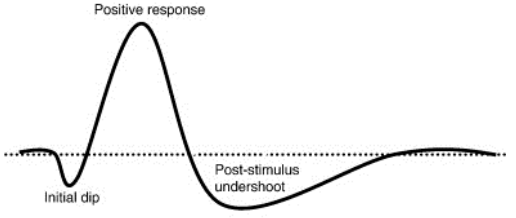

Figure 2. Hemodynamic response function and its parts: the initial dip, the positive response and the post-stimulus undershoot [42].

Therefore, the vasoreactivity or vascular tone and the cerebral blood flow play an important role in the BOLD contrast generation [43]. Three different phenomena

influence the level of cerebral blood flow: the hyperemic response or flow-metabolism coupling described above, the mechanical cerebral autoregulation, and the CO_2 reactivity [54]. Under physiological conditions, the brain has the capability of maintaining a stable blood flow under a range of cerebral perfusion pressures, which is called cerebral autoregulation [55], but the underlying mechanisms of this regulation are still under study [56, 57]. They have been hypothesized to depend on the transmural pressure caused by changes in perfusion pressure (myogenic reflex), but also to depend on adenosine levels (metabolic response) and sympathetic/parasympathetic innervation (neurogenic mechanism) [54, 56, 57]. Astrocytes seem to be the origin of the substances involved in both the regulation (prostaglandins, nitric oxide, and arachidonic acid) and the synapse mechanisms (glutamate, ATP, adenosine, GABA, D-serine) [47, 58, 59].

On the other hand, carbon dioxide is a well-known modulator of the vascular tone since changes in arterial blood carbon dioxide partial pressure lead to vasodilation or constriction and therefore they alter the CBF. However, the way it modifies the CBF/CPP regulation curve remains unknown [60].

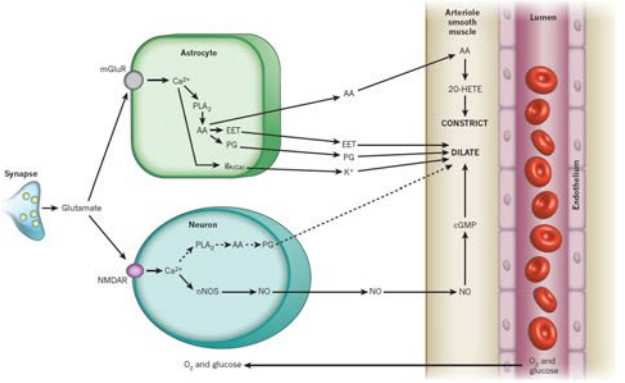

Figure 3. Major pathways that regulate blood flow from astrocytes and neurons [58]

Applications

Since functional magnetic resonance provides an indirect measurement of the neural activity, it has proven to be a very useful technique to study both brain physiology and pathology [2-6, 41, 48, 50, 61-63]. More specifically, it has been widely used to study the hemodynamic coupling and uncoupling processes, to study how the different brain networks work and interact, or to study vascular or neural injuries and treatments. In this regard, animal studies have been of great help in the assessment of the neural and vascular responses simultaneously, in order to study the timing and coupling of both responses. Many researchers have reported simultaneous acquisition of fMRI images and electrical recordings of the neuronal firing with microelectrodes inserted in the brain or through external EEG measurements performed during fMRI scanning. Others have tried to assess and understand the BOLD signal generation by comparison with optical measurements of the capillaries blood oxygenation or even with photoacoustic measurements [46, 64-66]. All these recordings are not possible in human volunteers, since they require the surgical exposure of the cerebral cortex, and thus imply an interesting advantage of rodent fMRI as compared to human fMRI.

As illustrative examples of its potential, cortical layer-dependent BOLD and CBF were measured in cat fMRI studies already in 2006 [67], and lately in 2012, contributions of macrovascular and microvascular BOLD signals have been independently identified (Figure 4 left) and studied throughout the rat barrel cortical layers (Figure 4 right) [68].

Another interesting research field where rodent fMRI outstrips human fMRI is the assessment of pain. Rodent fMRI has allowed studying the brain responses to nociceptive stimuli, either electrical or mechanical or chemical [63, 69-77], and it has enabled imaging hyperalgesia [78].

Nevertheless, the killing application for rodent fMRI is definitely drug development research [5]. Pharmacological fMRI is critical in preclinical and clinical trials for drug development studies, since it saves money and efforts in further stages. fMRI technique helps in the target validation, in the patient stratification and in the evaluation of the

drug response. In fact, as it can be applied to both rodents and human, it helps to assess correspondences in tests of mechanisms [79].

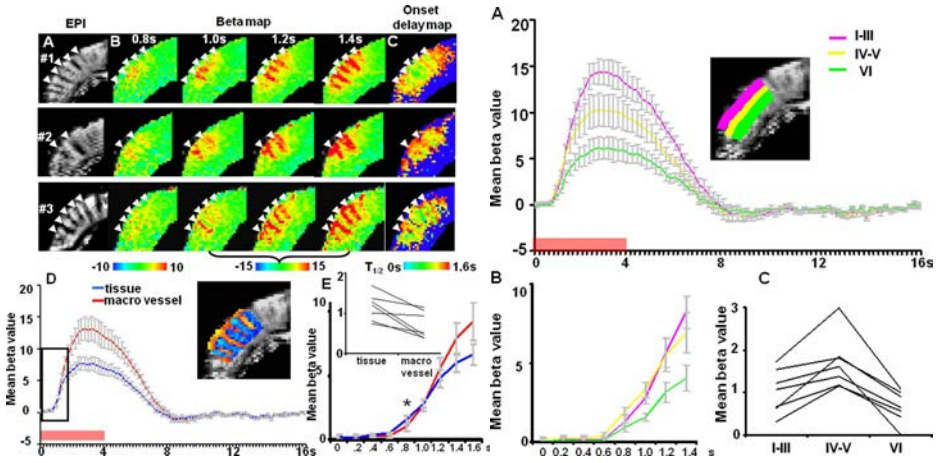

Figure 4. Left: BOLD signal from the barrel cortex at different time points shows different delays for macro vessels and the surrounding tissue. Right: BOLD signal from layers IV-V rise faster than signal from layers I-III and VI. [68].

Regarding the pathological brain, rodent fMRI has facilitated the study of the ischemic brain lesion [80-82] brain plasticity after stroke [83, 84], peripheral nerve injury [85], or spinal cord injury [86-88]. Actually preoperative fMRI before epilepsy surgery has helped other intraoperative electrophysiological techniques to localize motor, sensorial, language-related and memory-related functions, or the epileptogenic areas [89-92]. Clinical fMRI has also guided tumor resection [93, 94], has contributed to follow neurological rehabilitation patients after stroke [95], and helped to guide pre-surgical training to take enhance plasticity and reallocate a function before tissue removal [96]. Further details on clinical fMRI for surgery planning or plasticity concerns can be found in [97].

Obviously, the translation of rodent fMRI to humans is limited by the inherent anatomical and physiological species differences. The variety of applications in

humans exceeds that of rodents, since not only supports the study basic functions as those related to sensorial/motor stimuli, but it also enables more intricate analyses of superior cognitive processes.

3.2 EXPERIMENTAL CONSIDERATIONS

The typical experiment in fMRI consists on sequentially acquiring several T2* weighted images at rest and several images during some type of stimulus, and statistically comparing both groups of images in a voxel-by-voxel fashion. In order to group them correctly, the image acquisition must be physically synchronized with the stimuli presentation, and this requires some hardware and/or software modifications of the stimulating device, the scanner or both. Figure 5 shows an example of an experimental setup: the animal is placed inside the scanner with several monitoring sensors attached in order to keep its physiological variables under control, and it is also connected to the stimulation device (electrical stimulator in this case). The synchronization of the scanner and the stimulator is depicted with green and red lines carrying a TTL signal and the stimulation electrical pulses respectively.

The experimental protocol consists on anesthesia induction, placement of the animal on the scanner bed, where all the monitoring sensors must be attached to the subject and some heating system should be accommodated, and where the stimulation device must be attached to the animal and tested (Figure 5). Then the head coil, which is usually a surface coil to ensure a high signal-to-noise ratio (SNR), is placed on the animal head, and the animal is positioned inside the field of view (FOV), ensuring that the target part of the brain is in the center of the scanner. Radiofrequency and field adjustments are performed, and a structural image is usually acquired per subject for later visualization purposes. Then the functional slices are planned and various fMRI trials (fMRI series of T2 images) are acquired to assess different experimental conditions, typically

allowing for resting periods of 5-15 minutes between trials to avoid adaptation to the stimuli.

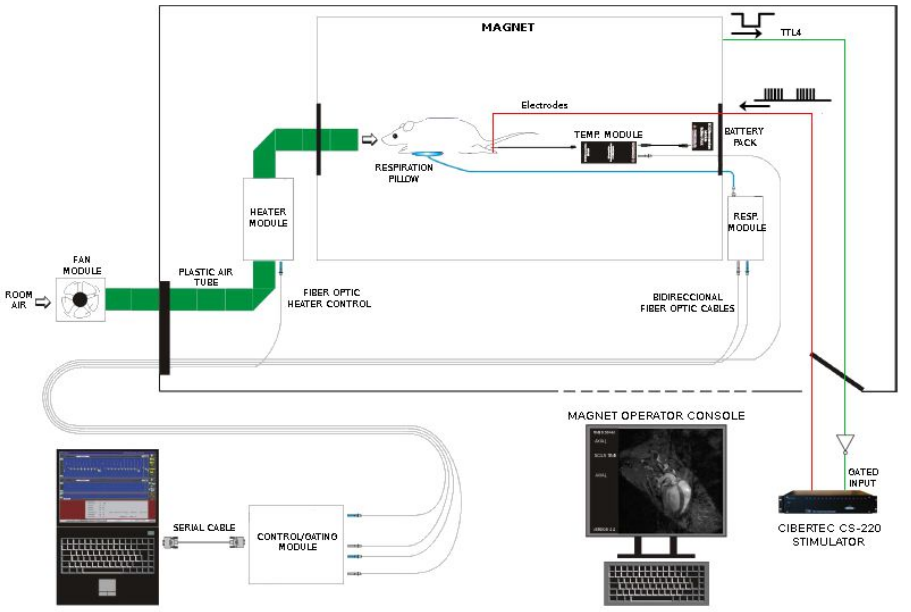

Figure 5. Example of an experimental setup. The sensors and stimulation electrodes are attached to the animal inside the MRI scanner, whereas the monitoring computer, the scanner control computer and the stimulation device are placed in the operation room, outside the magnetic field.

Functional paradigm and stimulation

The sequence of stimuli or tasks presented to the subject during one trial is called the fMRI paradigm, and numerous possibilities have been tested (Figure 6). The stimuli can be arranged as a block design, inherited from the positron emission tomography (PET) field and used in the first fMRI experiments. In this paradigm all the stimuli inside a block are exactly the same. Alternatively, they can be presented in a randomized fashion, but separated enough to let the BOLD signal reach the baseline between stimuli, which produces an individual response of equal intensity for each

event. This is called a 'slow event-related paradigm'. Finally, stimuli can be presented in a randomized fashion but faster than the HRF drop, which makes responses to accumulate and produces stronger final responses provided that the events are close. This is called a 'rapid event-related paradigm' and the responses to individual stimuli can be disentangled by deconvolution.

All these types of paradigms have been tested in rodent fMRI, but the block design is typically preferred for simplicity. On the contrary, in human trials, fMRI event-related paradigms are more popular since they avoid cognitive adaptation to the stimuli from the subject [97]. From all the rodent studies referenced in this manuscript, only one of them presented randomized stimuli [74], and corresponded to a pain study, where adaptation to stimuli is more critical. All the rest were block designed paradigms.

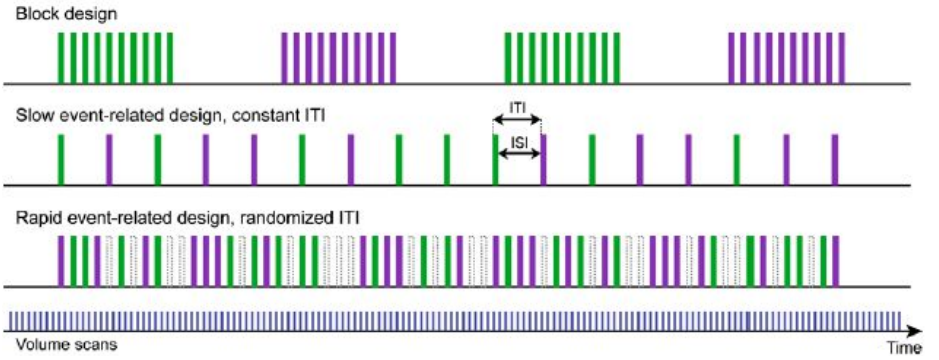

Figure 6. Typical types of fMRI paradigms: block design, slow event-related design and rapid event-related design.

Regarding the stimuli nature, the simplest approach relies on electrical stimulation of the forelimbs or hindlimbs [14, 69, 84, 98-102] and therefore it is the most widely used procedure. However, mechanical stimuli applied through filaments [6, 73] or chemicals [75, 76] have also been reported, mainly in nociception studies. Heat stimulation is another possibility [78, 103], and a controlled air flow has also been used for whisker stimulation [104]. In the literature, a few examples of odorous [105] and visual stimuli [106, 107] can also be found.

Anesthesia

Besides the endogenous factors of cerebral autoregulation presented in the previous subsection, anesthesia may be a confounding factor, since it plays a role in the BOLD signal by modulating CO_2 reactivity [108] and affecting neuro-vascular coupling. It increases basal CBF [108-110] and therefore reduces BOLD contrast. In addition, the vascular reaction produced by anesthetics may be vasodilation or constriction depending on the dose, as described by Kolbitsch et al. [111], and a high dose can dramatically suppress brain activity [109, 112] and spinal transmission [113]. These phenomena have also been studied in animals [46, 109, 114, 115], where the anesthesia control is critical to avoid head movement and image artifacts. In addition, other exogenous factors such as mental stress [62] or pain [63, 116] may influence these flow-related mechanisms. However, anesthesia is not only a confounder in rodent research, it should also be taken into account in human studies performed under anesthetics on noncollaborative patients [117-121].

For instance, different timings for the onset and duration of the hemodynamic response have been reported under different anesthetics, which also differ from those of the awake response [46]. The BOLD signal in awake animals has been found to be stronger than under sedation in most brain areas, but also bilateral and less specific activations were found, which are more difficult to interpret and may confound the target measurements [46].

Therefore the number of studies carried out on awake animals has grown in the past decade. Animals can also be paralyzed with some neuromuscular blocking agents such as pancuronium [99, 100, 122], tubocurarine [123] , vecuronium, mivacurium [115, 124], or atracurium [125], but this demands mechanical ventilation during the fMRI experiment, and patently complicates the experimental procedures. On the one hand, oxygenation and pCO_2 may be altered if not properly monitored and controlled during ventilation, and on the other hand, special care must be taken to avoid an excess of histamine release [9]. A blocking agent may also interfere with the anesthetic, for example, inhaled anesthetics potentiate the effect of neuromuscular blockers [126], and

the histamine release might be excessive as compared to the use of the neuromuscular agent alone. Besides, the usage of neuromuscular blockers without any anesthetics or sedative agents is controversial because the animal would be paralyzed but not sedated and this is hardly permitted by animal handling regulations, in order to avoid animal stress. This, in turn, may cause side-effects related to the vascular tone, undesirable for fMRI.

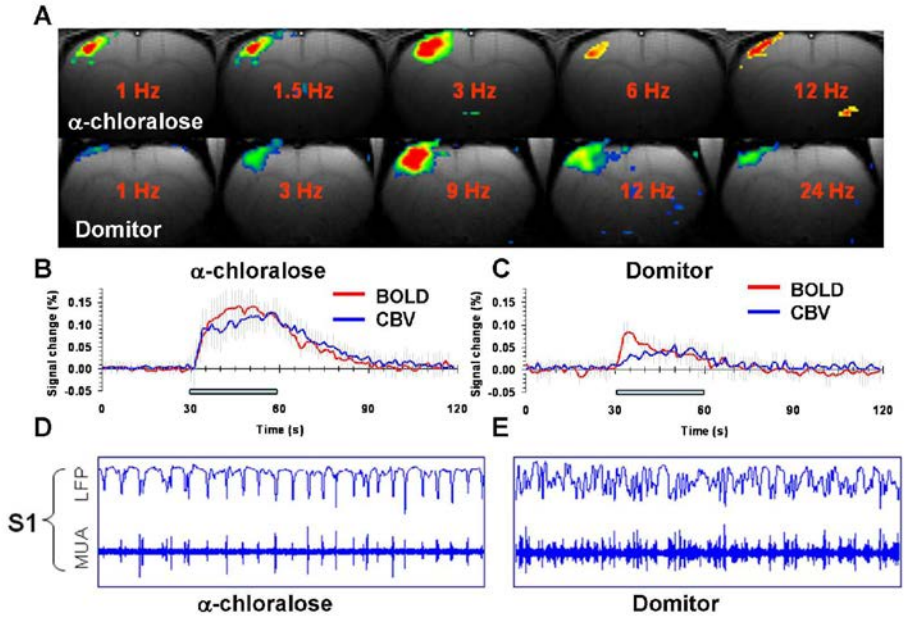

Figure 7. Effects of chloralose and medetomidine on (D,E) the electrical brain activity at the primary somatosensorial cortex, (B,C)their corresponding average BOLD and CBV responses and (A,B) the stimulation frequency for the strongest BOLD signal. Figure reproduced from [12].

Another option to perform awake studies would be to restrain the animals movement and/or to train them to keep still during image acquisition [127-129] by acclimatization to the restraining procedures, the MR noise and the stimuli. However it requires an expert operator to conduct them, hours of training per subject and, in the end, the movement is not completely suppressed. Even a slight movement has a strong impact on the acquisition and produces artifacts in the fMRI activation maps [115].

All these technical and physiological obstacles for awake fMRI still support the execution of studies under sedation as the typical approach to conduct functional experiments in rodents. The main types of anesthetics used in rodent fMRI are: 1) hypnotics, such as alpha-chloralose (CL) or urethane; 2) sedatives, such as medetomidine; and 3) inhaled volatile compounds, such as halothane, enflurane, isoflurane or sevoflurane. As mentioned previously, each anesthetic leads to different effects on the neuro-vascular coupling and therefore different BOLD response characteristics. As an example, Figure 7 shows the electrical signals and BOLD responses measured under different anesthetics.

There has been extensive research on survival-compatible anesthetic protocols that would enable long fMRI sessions involving repeated fMRI runs, while maintaining stable physiological conditions during hours of experiment [10, 11, 14, 104, 113].

Analysis

Once the data have been acquired within a controlled and stable physiological environment, a postprocessing of the images provides the final statistical maps. Regarding the neurovascular brain response, there have been various attempts through the literature to mathematically model the hemodynamic mechanisms, like the balloon model proposed by Buxton et al. [43]. In a controlled environment, it is traditionally accepted that the HRF is a sum of gamma functions [130], and the BOLD contrast measured by the MRI is proportional to this hemodynamic response. Then, the data are typically adjusted to a gamma model (and optionally its derivatives) by linear regression. However, in order to account for other physiological/psychological/behavioural variables involved, more regressors or covariates can be added to the equation system and therefore the data are commonly fitted using the so-called General Linear Model (GLM) [31].

These linear analyses are based on the hypothesis that, during the trial, the cerebral blood flow is not influenced by other variables other than the oxygen consumption by

neurons and thus the BOLD signal is interpreted to be proportional to the underlying neuronal activity. However, in order to account for cerebral blood flow variations during the experiment, more sophisticated compartmental models of BOLD signal have been proposed [44, 131], which express the relationship between the increment in BOLD signal, the changes in CBF and the oxygen consumption ($CMRO_2$). These methodologies, named "calibrated fMRI", require special acquisition techniques in order to measure BOLD signal and CBF in an interleaved manner, for example interleaving the BOLD T2 weighted images with arterial-spin labeling sequences [44, 131-133]. These models have been validated by assessment of the $CMRO_2$ through ^{13}C spectroscopy measurements [45, 134, 135], but they include several parameters that require extra measurements, which are field, subject, and session-specific. Furthermore, some of the assumptions that simplify the models do not always hold for patients [136]. However, there is an increasing interest in measuring the oxygen consumption and deoxy-hemoglobin concentration with accuracy in the stroke and oncology research fields. A review of calibrated fMRI can be found in [136].

As mentioned above, the simplest approach consists of assuming a linear relationship between the BOLD signal measured and the stimuli applied, regardless of the possible CBF variability and avoiding extra acquisitions. Once the general linear model, GLM, is fitted, statistical inference is accomplished by means of t-tests between the time points acquired at rest and those under stimulation or task performance. This final step provides the activity maps, which are typically thresholded by statistical significance and spatial cluster size and finally overlaid on a structural image.

These steps constitute the core of an fMRI analysis, but actually the fitting to a GLM usually includes some other corrections like high-pass filtering to remove scanner drifts or slow physiological signals, and a whitening of the data. Compensation for spatial and temporal correlations is recommended, since a voxel-wise analysis, with a final t-test of all the volumes sampled, is implicitly assuming spatiotemporal independence of the voxels. Furthermore, before fitting the fMRI signals to the GLM, it is critical to

apply spatial realignment, normalization and smoothing to avoid artifacts and improve the sensitivity and specificity of the BOLD detection.

To summarize the image processing, from the raw data collected in the scanner to the final statistical maps, these are the typical analysis steps performed in sequential order [137]:

1. Data conversion to a standardized format. Nifti format [138] has been widely adopted by the neuroscience community.

2. Realignment of the volumes that constitute each trial to correct for the subject movement. Rigid registrations are the most adequate here, since it is an intrasubject, intramodality transformation.

3. Normalization of the different acquisitions to a common spatial reference for posterior group analysis. In this case elastic or affine transformations are recommended since it is an intersubject registration.

4. Spatial smoothing to allow a better correction for degrees of freedom and therefore improve the statistics [139, 140].

5. Fitting to the GLM. This is typically performed in two steps. The first one estimates temporal correlations in the image voxels or correlations between the levels of a factor. The second pass fits an augmented model, which includes a whitening correction. The correlation parameters estimated in the first pass are used in the posterior statistical inference to correct the number of degrees of freedom.

6. Estimation and thresholding of a statistical map, by performing statistical contrasts on the fitted regressors. The resulting statistical map is usually thresholded through a combination of a p-level threshold and a cluster size threshold.

7. Visualization of the thresholded map overlaid on a structural image.

3.3 PRECLINICAL FMRI: ADVANTAGES AND CHALLENGES

In a rat fMRI experiment, all the physiological factors mentioned above must be considered. Since the anesthesia produces hypothermia, and this may cause vascular constriction, the animal is usually kept warm with an external heating system that helps to control the animal temperature during the scan. As mentioned before, the anesthetic dose should be enough to avoid the animal stress and prevent its movement during image acquisition, but not as high as to suppress the electrical brain activity [112]. It is crucial to avoid long periods of vasodilation or constriction, such as the one produced with high dose of volatile anesthetics during induction, because they can reduce vascular reactivity. Normal levels of pCO_2 are also required, and therefore ventilation, expiratory gas exhaust and/or neuromuscular blocking agents should be carefully handled.

There are other technical issues that make rodent fMRI differ from human fMRI. The most important one is the difference in the magnetic field strength, which entails both advantages and disadvantages. The higher field strength together with a reduced bore size and smaller radiofrequency coils enable resolutions approximately one order magnitude higher than in human scanners, and considerably higher temporal resolution too [3]. On the other side, a higher magnetic field implies stronger deviations from the expected precession frequencies and therefore more obvious susceptibility artefacts, which in turn requires finer shimming strategies.

The field strength also influences the way water diffusivity affects the BOLD signal. Changes in T2 relaxation time actually occur wherever there is an interface of magnetic susceptibility change, and this happens both in the vessel walls and around the red

blood cells, inside the vessels. Therefore, the BOLD signal actually has several contributions, the extravascular component generated around the vessels and the intravascular signal coming from the blood stream. In fact, the interesting signal that closely reflects neuronal oxygen consumption is the one coming from extravascular very small vessels (capillaries). This extravascular dephasing of spins related to dHb can be averaged around small vessels due to diffusion during the echo time and have little contribution to the total BOLD signal. This is what happens in gradient echo sequences at low field strengths. Contrary to this, with spin echo sequences the contribution from capillaries is still noticeable, since the 180º refocusing pulse cancels this effect. In addition, the higher the field strength, the lesser the contribution from the intravascular signal (Table 1). To summarize, working with rodents at high field strengths and with spin echo sequences allows measuring a BOLD signal mainly from the extravascular interface of capillaries, which ensures higher spatial specificity [40, 133, 141, 142].

Table 1. Contributions of macro/microvasculature and extra/intravascular signals to the BOLD contrast measured at different field strengths and with GE or SE sequences.

	Gradient echo (GE)	Spin Echo (SE)
↓ B0	macrovasculature extra- and intravascular	macro- and microvasculature extra- and intravascular
↑B0	macro- and microvasculature extravascular	microvasculature extravascular

The physiological issues described in this section, mostly those related to anesthesia and movement, make rodent fMRI experiments still complex to set up and perform under accurate control. Moreover, the experiments usually last for hours. This can

produce adaptation of the subject to the stimuli, it leads to higher variability on the physiological variables which are supposed to be stable during the trials, and also implies an intensive usage of the scanner.

3.4 THE NEED FOR SPEED

MRI accelerations techniques before compressed sensing

All these experimental problems of physiological stability and motion artifact avoidance urge the need of shortening the acquisition time. Among the traditional "fast" MRI sequences, where several k-space lines are acquired for the same excitation RF pulse, the echo-planar imaging or EPI sequence [143] has been the most widespread sequence in the field of fMRI. It enables the acquisition of the k-space of a complete slice (or even several slices) within a single readout. Its implementation consists of opposite gradient readouts interleaved with "blips", or small phase encoding gradients. The typical readout pathway is a cartesian zig-zag, but other alternatives have also been applied to fMRI studies with success, such as radial, spiral or rosette trajectories. However not all trajectories allow acquiring a complete plane within a single readout, as it is the case with radial trajectories or the PROPELLER sequence.

Following the same principle, efforts were made to acquire a whole volume in a single readout in the shortest time possible. Cartesian sequences such as the single-shot EVI (echo-volumar imaging) [147] or multi-shot cartesian 3D sequences were proposed [21] for those scenarios where high temporal resolution is required. Three-dimensional spirals [151] and radial trajectories [20] have also been investigated, either single shot or covering the volume with several shots. In order to reconstruct MRI images these singular trajectories require either a regridding step to locate the measurements in a regular grid suitable for the traditional Fourier transform, or a non-uniform Fourier transformation.

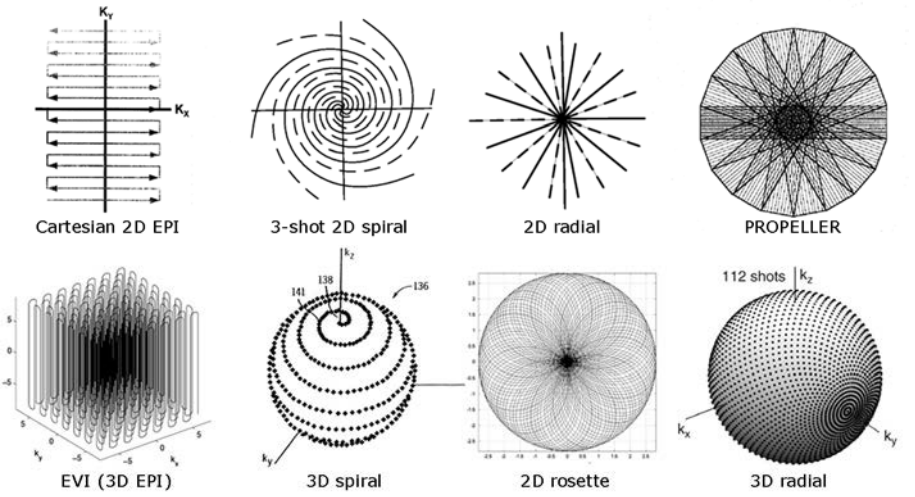

Figure 8. Examples of different k-space sampling trajectories, both two- and three-dimensional. Figure composed by adaptations from [144-150].

In general, single-shot sequences have the advantage of a faster readout but at the cost of larger off-resonance effects, which in the end translate into image artifacts and distortion [152]. Thus single-shot implies higher temporal resolution at the cost of lower spatial quality. This led the efforts towards multi-shot sequences, such as the multi-slab 3D sequences, built as stacks of spirals [153] or as stacks of EVIs [154].

Besides fast sequences, parallel imaging and undersampled acquisitions are other acceleration techniques typically implemented in most scanners. Parallel imaging consists in using arrays of coils to acquire less number of samples while preserving the final image quality [16, 17]. The preservation of the final SNR is possible because the coils share part of the field of view and therefore they measure redundant information. Combinations of parallel imaging with fast sequences enabled high resolution fMRI imaging in a cognitive Stroop experiment already in 2009 [21, 155].

On the other hand, undersampled acquisitions rely on acquiring only part of the k-space. For example, it is possible to acquire only the central part of the k-space (the 'zero filling' technique), or more than a half of the k-space on the phase encoding direction ("partial Fourier") or more than a half of it in the readout direction ("partial echo" technique).. Other undersampling strategies rely on regularly skipping measurements along the phase encoding direction, the temporal dimension or both, like k-t BLAST or k-t SENSE [156, 157]. All these techniques lead to aliasing artifacts, which may be mitigated with correction algorithms or carefully designed undersampling patterns.

Another recent possibility for the acceleration of the acquisition is multiplexing in either the readout time or the frequency domain (Figure 9).

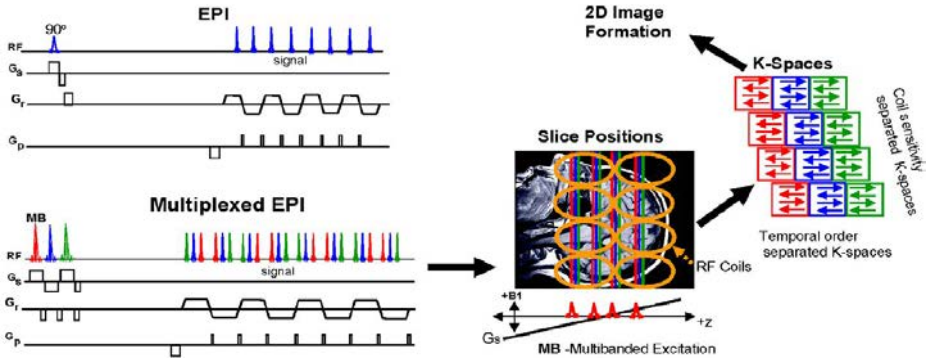

Figure 9. Acquisition scheme for a multi-slice multiplexed EPI. This scheme combines readout multiplexing, frequency multiplexing and parallel imaging acceleration techniques [158].

In the first case, two different slices are excited sequentially and read within the same readout gradient [18]. This technique was originally called SER (Simultaneous Echo Refocusing) and afterwards SIR (Simultaneous Image Refocused). With frequency domain multiplexing several slices are excited simultaneously at frequencies far apart from each other so that the multiplexing is performed in a spectral band fashion [19]. One limitation is that, in both cases, aliasing between the multiplexed measurements

must be carefully handled. On the other hand, both strategies can be combined with parallel imaging for even higher acceleration factors [18, 19, 158].

Compressed sensing

The compressed sensing framework emerged in 2004-2006 [23, 24] and notably surpassed the efficiency of the previous undersampling approaches intended for accelerated MRI acquisition. Traditional undersampling theory sustained that a band-limited signal could only be completely recovered without aliasing if sampling meets the Nyquist-Shannon criterion, which states that the sampling frequency ought to be higher than twice the signal bandwidth. The compressed sensing framework generalizes the sampling process and allows aliasing to occur as long as it can be compensated during the posterior reconstruction.

This theoretical frame entailed a revolution in the signal processing field, and specifically in the medical imaging scenario, since datasets of the same quality could be obtained at one fourth of the traditional acquisition time or even less. In addition, as we will discuss later, it can be potentially combined with the previous acceleration techniques, such as fast sequences, parallel imaging or data multiplexing.

In short, feasibility of the compressive sensing requires three conditions to be satisfied [159]:

1. The signal must have a sparse representation in some transformed domain.
2. The undersampling operator must be incoherent with the transformation base.
3. The signal can be recovered without loses if a non-linear convex optimization is used for reconstruction.

Regarding the transformed domain, the gradient, the wavelet transform and the discrete cosine are the most frequent transformations due to their sparsifying properties when

applied to medical images [25]. The discrete cosine and wavelet transforms had traditionally been exploited in graphics and video compression algorithms.

Nevertheless, theoretically the data can be transformed into any domain where data become sparse, where sparse means that very few samples of the signal are different from zero (the zero norm is minimized). This is why the first attempts to apply compressed sensing to MRI focused on angiography, since the image is already sparse in its original domain, considering that the transformation in this case is the identity transform, and it is also sparse after the computation of its finite-differences (see Figure 10) [25].

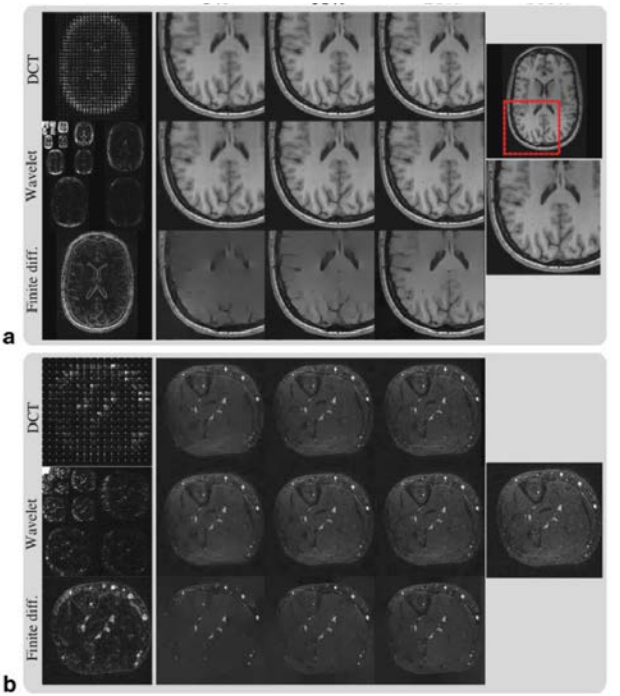

Figure 10. Example of two sparsifying transforms applied to a) a brain T1 image and b)a leg angiography. Figure from [25].

Moreover, not only medical images are typically sparse, but also the higher the dimensionality of the measurements, the higher the acceleration that can be achieved, and fMRI is a good example due to its temporal redundancy. However, each type of

study may have a sparser representation in a different transformed domain according to its characteristics. For example, periodic signals will be sparser in the Fourier domain, and other signals may become sparser with shearlets, with the Karhunen-Loeve transform (KLT), or with the discrete cosine transform.

Until the emergence of CS, undersampling was typically performed in a regular fashion, and aliasing was estimated and filtered out to avoid image artifacts. These regular patterns can be found in the k-t BLAST, k-t SENSE or UNFOLD algorithms [145, 157]. However, the acceleration factor that can be achieved is modest compared with the compressed sensing framework, where the undersampling is random or quasi-random [25].

Formally, the non-linear optimization algorithm required for the reconstruction can be expressed as:

$$\min_u \|\Psi u\|_o \text{ such that } Fu = f \tag{1.1}$$

Where u is the target image reconstruction, ψ is the sparsifying transform, F stands for the Fourier transform and f are the undersampled k-space measurements acquired.

However, solving this problem is not computationally tractable, and it is more effective to solve its corresponding L1 norm convex problem:

$$\min_u \|\Psi u\|_1 \text{ such that } Fu = f \tag{1.2}$$

This equation can also be expressed as:

$$\min_u \|\Psi u\|_1 \text{ such that } \|Fu - f\|_2^2 < \sigma \tag{1.3}$$

Where σ accounts for the noise in the measurements. The first term of the equation imposes sparsity whereas the second term imposes data fidelity, although other sparsity terms can be found in the CS literature.

Even though the framework already existed for some years, the first application of compressed sensing techniques to the MRI field was conducted by Lustig et al. in 2007 [25]. It was tested with angiographic and structural brain images at first, and suddenly

gained popularity in dynamic MR imaging since the exploitation of the temporal redundancy enables higher acceleration factors than those of conventional imaging [27, 160, 161].

Cardiac imaging has been an excellent field for testing different algorithms and the scientific production on this application has been ample during the past years. However, there are much fewer works on the application of compressed sensing to fMRI.

The first acceleration algorithm tested in fMRI was the k-t FOCCUSS proposed by Jung et al. in 2007 [27, 162] followed by the k-t SPARSE proposed by Lustig et al., which was applied to fMRI by several groups [163-165]. In 2013, Nguyen et al. successfully tested a new compressed sensing approach based on generalized series with variable density (VD) spiral trajectory EPIs. One year later, this group explored the algorithms exploiting the low-rank characteristics of the data, which became more popular lately [166]. More recently, Chiew et al. successfully evaluated one of these approaches, k-t FASTER, for studying human resting state networks with fMRI [29]. However, we could only find in the literature one study in rodent fMRI, for the detection of BOLD signal in the rat olfactory bulb [105].

fMRI is an application which can strongly benefit from the application of compressed sensing algorithms, because of its temporal redundancy. However its specific characteristics also make it a challenging application in comparison with other MRI protocols. Firstly, the contrast-to-noise ratio and the spatial resolution of the BOLD signal are much lower than in other dynamic MRI techniques. Secondly, the imaging postprocessing required in fMRI makes it harder to evaluate the achievable acceleration since the target is the statistical assessment of the BOLD contrast and not the images themselves. Given the technical issues existing in high field MRI mentioned in the previous subsection regarding long acquisition times and susceptibility artefacts, further developments on compressed sensing methodology applied to rodent fMRI are warranted.

3.5 ANALYSIS OF RODENT FMRI

There are several software packages available for the analysis of fMRI series, most of them originally conceived for human datasets.

The most popular tools in the scientific community are SPM (Statistical Parametric Mapping, The Wellcome Trust Centre for Neuroimaging) and FSL [167], but their use on rodent studies requires adapting the image resolution and tuning some registration parameters. This optimization requires some computing skills, or alternatively the use of plugins such as SPMMouse (SPMMouse, Wolfson Brain Imaging Centre, University of Cambridge) [168]. A fully automated analysis is possible with these tools, though it is recommended to check all intermediate results to avoid mistakes, and SPM offers a batch mode for this purpose.

Other simpler alternatives available do not perform all the data corrections and assume that volumes are perfectly realigned, without any head motion, do not allow registration to a common space for further group analysis or do not take into account the spatiotemporal voxel correlations. They typically carry out a voxel-wise statistical test and threshold and display the resulting map. Some examples are the Bruker proprietary tool FunTool [169] or the Stimulate package from the University of Minnesota Medical School [170].

In the end, the fMRI analysis involves the tuning and checking of numerous parameters in each workflow step, which require a deeper understanding of image processing, and is highly demanding from a computational point of view. This often discourages researchers from analyzing their images themselves and forces them to delegate the analysis to some third party.

4 EXPERIMENTAL SETUP

This chapter presents the details of an experimental setup designed to assess fMRI studies carried out under sevoflurane anesthesia and its comparison with the already settled medetomidine protocol.

4.1 INTRODUCTION

Functional magnetic resonance (fMRI) in rats is being widely used to study brain pathologies as well as normal brain functioning, usually under chloralose or medetomidine anesthesia [14, 171]. However, the anesthetic agent may greatly influence the underlying neuro-vascular mechanisms, actually in a different way for different anesthetics. The differences in hemodynamic response between different anesthetics are a consequence of a different action of anesthetics on both electrical and vascular responses. It has been demonstrated that these drugs affect the vascular tone, and therefore the neuro-vascular coupling and the BOLD signal [172].

Hyder et al. were the first researchers who performed rat fMRI with alpha-chloralose [98] in 1994, following the dose schemes tested by Lindauer and colleagues [173]. They already knew that hypnotics like alpha-chloralose or urethane preserve cortical activity better than other anesthetics [7, 8] and that alpha-chloralose specifically produces a minimal depression of the cardiac and respiratory functions [174], preserves the metabolic coupling, provides a stable blood flow baseline and also preserves vascular reactivity [108, 173, 175]. Since then, several stimuli tests were reported by varying the electrical stimulation frequency or pulse width in order to achieve the strongest BOLD contrast possible [102, 176, 177]. The strongest activations were found at stimulation frequencies ranging 3 Hz - 5 Hz. Nevertheless, alpha chloralose is known to be toxic and produces severe side effects [7, 174], so its use in fMRI remains controversial [104] and soon other alternatives were proposed.

In 2002, intravenous medetomidine arose as a suitable alternative to alpha-chloralose [178]. Some years later a medetomidine subdermal infusion protocol was proposed and optimized [14, 179], and it was soon adopted by the scientific community due to its better stability and safety as compared to alpha-chloralose. This protocol was compared to alpha-chloralose by Weber et al. in 2006 [14], and two years later Zhao et al. performed a task-induced study under medetomidine but also proposed this anesthetic for resting state functional magnetic resonance [171]. In this study, the BOLD signal peaked with an electrical stimulation of 9 Hz and 0.3 ms of duration. Further improvements were proposed for the anesthetic protocol in order to prolong the experiments up to 6 hours by stepping up the infusion dosage after 2.5 hours from 100 µg/kg/h to 300 µg/kg/h [11].

Another important group of anesthetics is that of volatile compounds. Since 1960 several derivatives of methoxiflurane (a methyl ethyl ether) such as halothane, isoflurane and sevoflurane had been used for veterinary purposes. Their advantage over injected anesthetics was their lower blood solubility, which enables faster induction and recovery [180, 181]. Additionally the administration via face mask avoids the need of any catheter or infusion pump and enables a much simpler experimental setup. In 2004, Liu et al. [182] performed the first fMRI experiments under isoflurane anesthesia, and later works appeared comparing the signal obtained with isoflurane and the traditional alpha-chloralose [10, 113]. In the study by Masamoto et al. 2007 (Figure 11), electrical stimuli at 3, 6, 12 and 20 Hz were compared, and 12 Hz was found to provide the strongest cortical activation at the primary somatosensory region [10]. The pulse width and amplitude had been previously optimized and set to 1.0 ms and 1.4 mA respectively.

Halothane has also been proposed for spinal fMRI [102, 183], but its use has not been widely reported in brain function studies, probably because it depresses respiration and cardiac activity and produces arrhythmias [180], alters cerebral blood flow more than sevoflurane [184] and provides a slower induction and recovery as compared to isoflurane and sevoflurane [181].

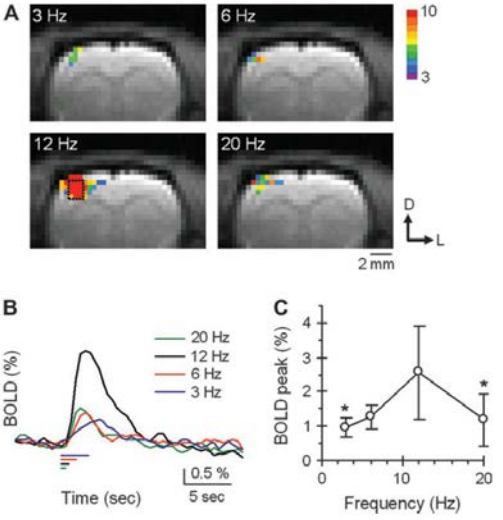

Figure 11. Frequency study performed under isoflurane anesthesia [10].

From all the volatile anesthetics, the most popular in clinical applications is sevoflurane, since it is the fastest one for induction and recovery, it is similar to isoflurane regarding the cardiovascular effects, and it is significantly safer than halothane in the degree to which it sensitizes the myocardium to the arrhythmias [185]. This fact, together with the lack of airway irritation makes sevoflurane the preferred volatile anesthetic for pediatrics [117].

There is some experience on the use of sevoflurane for functional human studies. One work compared the BOLD response under sevoflurane during an auditory paradigm with that found in the awake state, and the BOLD signal was found to be weaker under sevoflurane anesthesia [186]. Other study conducted resting state experiments under sevoflurane and in awake subjects, and the basal resting activity was found to be more heterogeneous over the brain in the anesthetized group [120]. Regarding animal studies, sevoflurane has been found to produce cerebrovasodilatory effects that increase intracranial pressure in a dose-dependent manner and reduce vessel resistance [15, 184, 187]. However, since these studies measured perfusion at rest using radiolabeled

microspheres, actual effects on BOLD signal in fMRI studies under sevoflurane are not known.

In our work, we compare an fMRI protocol under medetomidine (as described by Weber at al. [14]) with another protocol under sevoflurane anesthesia. To this purpose, we conducted a dose-response to find the optimal sevoflurane sedative dose and characterized the BOLD response to different electrical stimulation frequencies

4.2 METHODS

Animal preparation

We performed fMRI somatosensorial studies with electrical stimulation on Wistar and Sprague-Dawley rats (~350g) under two types of anesthesia: subcutaneous medetomidine (Domtor®) and inhaled sevoflurane. The animals under medetomidine anesthesia were prepared and anesthetized following the protocol described in [14], although the dose for the sevoflurane group needed to be adjusted and validated, as described in the Experimental design subsection.

Animals were handled according to the European Communities Council Directive (2010/63/UE) and national regulations (RD 53/2013), and with the approval of the Animal Experimentation Ethics Committee of Hospital General Universitario Gregorio Marañón. The animals were housed in a constant-temperature and humidity-controlled vivarium with a 12 h light-dark cycle. Commercial rodent laboratory chow and water were available ad libitum.

For anesthesia induction we used an induction box with sevoflurane at 7%. Afterwards the animals were transferred to the scanner bed, equipped with a face mask, where they were kept warm with a circulating water blanket. At this point the sevoflurane was decreased to 4% during animal preparation to monitor temperature, respiration, ECG and peripheral oxygen saturation. When the animal was stable, we inserted the stimulation electrodes in the forepaws, tested the stimulation current and started specific anesthetic protocols in each experimental group, as described in detail below.

Once the anesthetic optimal point was reached, we acquired the fMRI studies, alternating left and right stimulation to avoid adaptation.

Experimental design

We divided the animals into two groups according to the anesthetic used for maintenance: medetomidine (n=5) or sevoflurane (n=7). For the medetomidine group we followed an already established protocol [14] and for the sevoflurane group we performed a dose-response test and a stimulation frequency study.

A group scheme is shown below:

GROUPS		
A) Medetomidine (n=5)	0.05 mg/kg bolus + ci 0.15 mg/kg	9 Hz [2]
B) Sevoflurane (n=7)	**Dose-response test (n=7):** **Frequency test (n=3):**	**4% - (0.25% / 15min)** **(3,5,7,9,10,11,12) Hz**

Group A: For the medetomidine group, we switched the anesthetic from 4% sevoflurane used for induction to medetomidine. We administered a bolus of 0.05 mg/kg subdermal medetomidine and placed a catheter for subdermal infusion in the back of the animal. Then we started a constant infusion of 0.15 mg/kg/h while slowly reducing sevoflurane to zero during 15 minutes approximately. Once the animal was stable with only the subcutaneous medetomidine, we introduced it inside the scanner.

Group B: For the sevoflurane group, we introduced the animals in the scanner with sevoflurane at 4%. Firstly we performed a dose-response test with each individual in order to find an optimal anesthetic point at which there is no body movement but the animal still shows BOLD signal. From the initial 4% of sevoflurane, we decreased the dose at a rate of 0.25% every 15 minutes until we obtained BOLD contrast. Whenever we observed movement, we increased the dose again to the

last stable value. At BOLD signal emergence, we recorded the dose and performed 3-5 assessment runs per subject for the between-groups comparison. Finally we performed a frequency study in n=3 subjects, randomly selected from this group, by acquiring additional fMRI runs (one per frequency) at frequencies of 3, 5, 7, 9, 10, 11 and 12 Hz.

Imaging parameters

All studies were conducted in a 7T Bruker Biospec 70/20 scanner. Firstly we acquired structural axial and sagittal images covering the whole brain in order to localize the subsequent functional images. These structural references were 2D RARE images with RARE factor=8, TR/TE (effective) = 4000/33 ms, FOV 2.9 x 2.9, matrix= 256 x 256, 17 slices of 1 mm thickness, resolution 0.11 x 0.11 x 1 mm, and 3 averages.

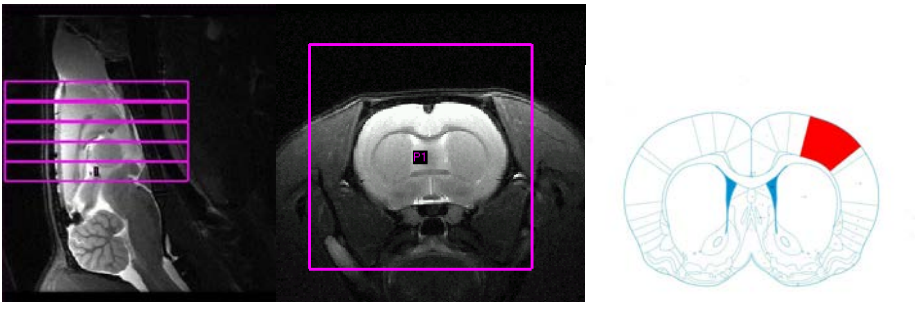

Figure 12. Localization of the functional images. Left, Centre: planning of the functional slices with the help of sagittal and axial structural RARE sequences. Right: central slice of S1 (approximately Bregma +1mm) from Paxinos atlas which was used as a reference.

Then we acquired the functional image series following the protocol described in [14]: SE-EPI 2D images with axial orientation, TE/TR = 30 / 3000 ms; FOV 1.92 x 1.92 x 1 cm; matrix of 64 x 64, 5 slices of 2 mm thickness, 115 repetitions. We used a surface phased array coil of four elements for reception and combined the data from the different coils through a weighted sum of squares.

Functional paradigm and stimulation details

The stimulation consisted on non-noxious electrical pulses of 1 mA, 0.3 ms duration delivered by a synchronized stimuli generator (STG 4002, Multi Channel Systems GmbH, Reutlingen, Germany). The stimulation frequency was 9 Hz [170], except for the frequency study in group B.

To enable synchronization, we modified the sequence acquisition code in the scanner in order to generate a TTL signal trigger for the stimulator. We stimulated the animal's forepaws through subdermal needle electrodes following a block paradigm, starting and ending with resting blocks (see Figure 13). We allowed 5 minutes of rest between fMRI runs to avoid adaptation. Each fMRI series comprised 115 volumes acquired in sequential stimulation blocks of 5 images and resting blocks of 15 images, thus following the pattern: 15 OFF +5ON +15 OFF +5ON +15 OFF +5ON+15 OFF +5ON+15 OFF +5ON+15 OFF.

Figure 13. Left: Electrical stimulation was applied through subdermal needle electrodes inserted in the forepaws. Right: The block stimulation paradigm followed during the acquisition of each fMRI run.

Image analysis

We analyzed the fMRI datasets with the fMRat tool described in chapter "5. fMRI analysis" of this thesis. The statistical maps were thresholded at p=0.001 with cluster size=4 voxels and were saved as uncompressed .tiff images. We analyzed the primary sensorial cortex regions of interest S1FL and S1FR (according to Paxinos atlas [183]) by means of the atlas and ROI functionalities included in the tool. The percentage of signal change was computed for each voxel inside the corresponding contralateral region of interest. Their maximum and mean signal change values were obtained, printed to a text file and compared for groups A and B by means of a repeated measurement GLM analysis of variance, performed with SPSS software package.

4.3 RESULTS

We could observe consistent BOLD responses in the S1 cortex of all rats under medetomidine, and in 6 out of 7 rats under sevoflurane. Figure 14 shows an example of activation maps.

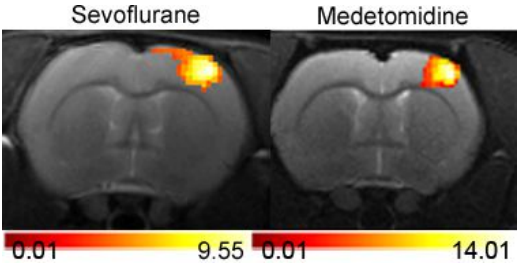

Figure 14. Example of activation maps from each group: sevoflurane (left) and medetomidine (right)

Regarding the definition of an optimal sevoflurane dose, we tested the higher dose (to avoid movement artifacts in the images) which at the same time provided BOLD signal in S1. The final doses for the different subjects are shown in Table 2; the average stable sevoflurane dose was [Mean ± SD] = 1.8% ± 0.8% sevoflurane (n=7), thus showing a high intersubject variability. The time required to stabilize the animal and obtain BOLD signal was 103 minutes on average, whereas in all animals under medetomidine, BOLD signal was present from the beginning.

Table 2. Dose-response test for sevoflurane

	% Sevoflurane	Time to BOLD (min)
Animal 1	1.00%	109
Animal 2	1.50%	126
Animal 3	2%	156
Animal 4	1.50%	104
Animal 5	1.50%	135
Animal 6	3.50%	28
Animal 7	1.75%	67
	1.82%	103.6

Figure 15 shows maximum percentage signal change at S1 cortex, mean percentage signal change at S1 cortex and total number of activated voxels over the thresholds, across the different frequencies tested under sevoflurane anesthesia.

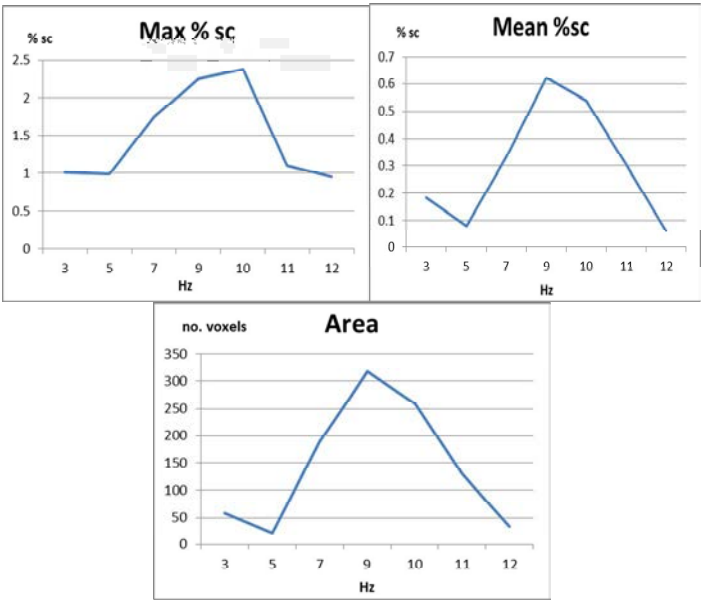

Figure 15. Results of the frequency test performed for n=3 animals from the sevoflurane group.

The maximum signal change peaked at 10 Hz, providing a signal change of 2.4% whereas the mean signal change and the number of activated voxels peaked at 9 Hz, where they showed values of 0.6% and 317 voxels respectively. Thus the stimulation frequency which provided the higher signal change and the wider activated area overall was 9 Hz, the same value reported for medetomidine [170], and different from the 12 Hz previously reported for isoflurane [10].

Regarding the comparison between medetomidine and sevoflurane, the maximum and mean percentage signal changes at S1 were higher for the medetomidine group, see Table 3, though the differences in maximum or mean values were not significant in a repeated-measurements GLM analysis. From a total number of 57 fMRI runs, 17 cases

without consistent activation in S1 (less than 50 voxels) were excluded from the analysis.

Table 3. Anesthesia dependency of BOLD contrast: values estimated by GLM statistical analysis.

	Medetomidine (n=22 runs)	Sevoflurane (n=18 runs)
Max % signal change at S1	2.42	2.17
Mean % signal change at S1	0.60	0.59

4.4 DISCUSSION

We successfully optimized a sevoflurane protocol for rat fMRI studies. The optimal dose was 1.8 % for a sedative state which did not suppress brain activity as assessed by BOLD signal, and the best electrical stimulation frequency was 9 Hz for a maximum BOLD contrast at S1 of 2.4% of signal change.

The signal change obtained with sevoflurane was lower than under medetomidine, but the differences were not statistically significant.

However, the time necessary to stabilize the animal and obtain BOLD signal with sevoflurane was around 100 minutes, whereas medetomidine yielded significant BOLD contrast from the beginning of the experiment.

In summary, a researcher willing to use sevoflurane would spend around 2 hours of animal preparation in total, which would prolong the already lengthy fMRI experiments. Both the delay on the BOLD emergence and the difficulty in finding the optimal anesthetic dose for each subject entail severe practical impairments to its use.

Therefore we can conclude that rat fMRI studies are feasible under sevoflurane anesthesia and might help to understand the effects of sevoflurane on the neurovascular coupling, but does not seem advisable as a standardized protocol for fMRI because of practical reasons.

5 ACQUISITION AND RECONSTRUCTION

This chapter investigates three different algorithms which exploit the temporal redundancy for the reconstruction of two retrospectively undersampled fMRI datasets, with high and low SNR respectively.

5.1 INTRODUCTION

Functional magnetic resonance imaging (fMRI) has been used for more than 20 years to study normal and pathological brain functioning in rodents [2, 39, 61, 184, 185]. However, the complexity of the experimental setup and the long acquisition times required still prevent its widespread application in preclinical research.

Prior to the development of compressed sensing for magnetic resonance imaging (MRI), attempts had been made to decrease acquisition times using parallel imaging, reduced K-space acquisitions, multiplexed acquisitions and single-shot readouts [16, 17, 19-22, 147, 151, 186], although image quality worsened at high acceleration rates. In contrast, the compressed sensing framework enabled accurate reconstructions from few phase encoding data using convex optimization, provided that the image is sparse in the transformed domain [23, 24, 26] and undersampling is random or quasi-random.

A commonly used transformed domain is the spatial gradient. This operator generates the functional known as total variation (TV) [24, 25, 187-189], which efficiently removes the noise and artifacts caused by undersampling. Furthermore, its extension to the temporal dimension, i.e. spatiotemporal total variation (TTV), has provided encouraging results in dynamic MRI [161, 190, 191]. However, to our knowledge TTV has not been applied to fMRI.

TV has also been combined with an initial image estimate in the prior image constrained compressed sensing (PICCS) algorithm, which is applied mainly in X-ray computed tomography. In this context, the prior image is typically constructed as the

average of all undersampled datasets [192-197]. To our knowledge, PICCS reconstruction has not been applied in MRI, and our hypothesis was that the undersampled fMRI series itself could provide an efficient prior image owing to its temporal redundancy. This idea of using a prior image or initial estimate was already presented in k-t FOCUSS [27], and in HYPR algorithms [198] and its modifications, HYPR LR[199], I-HYPR[200] or HYPRIT [201]. However, PICCS constitutes a more generalized framework since it imposes the sparsity constraints on the CS formulation[189].

Other recent approaches rely on the exploitation of low rank components along different dimensions of the data matrix in some transformed domain [29, 166, 191, 202] and have also provided effective compressed sensing reconstructions of fMRI datasets [29, 166, 202]. Few methods that explicitly exploited the temporal dimension in fMRI studies —k-t FOCUSS [27, 105], low-rank [29, 166, 202] or generalized series [28]— achieved acceleration factors of x4-x5.

In this study, our objective was to determine whether the PICCS algorithm could improve the statistical maps in fMRI better than other strategies that also exploit temporal redundancy. TTV and k-t FASTER were chosen as the reference algorithms since they have already shown high performance and robustness in other MRI applications, such as cardiac MRI and resting state fMRI [29]. Therefore, we tested and compared the maximum values of acceleration achievable using PICCS, TTV and k-t FASTER reconstructions. Different pseudo-random undersampling patterns were applied at five acceleration factors to 2 fully acquired rat fMRI series, and reconstructed images were obtained with the three algorithms. To our knowledge, this is the first study reporting on the application of PICCS and TTV algorithms to fMRI data. The evaluation was carried out on the final statistical maps in terms of the sensitivity/specificity of the detection of cortex activation (measured as the area under the ROC curve referenced to the fully sampled map), together with a visual inspection of the resulting maps.

5.2 THEORY

Compressed sensing

Compressed sensing theory states that it is possible to obtain an exact reconstruction of signals sampled below the Nyquist limit provided that the data are sparse in a transformed domain, the sampling operator is incoherent in that domain and a specific non-linear method is used for reconstruction [23].

Therefore, the reconstruction in our MRI context solves the following constrained problem:

$$\min_{u} \left\|\Psi u\right\|_1 \text{ such that } \left\|\tilde{F}u - f\right\|_2^2 < \sigma^2 \tag{5.1}$$

where $\left\|\cdot\right\|_1$ denotes the L1 norm, ψ is the sparsifying transform, $\tilde{F} = RF$ is the undersampled Fourier transform, f are the measured data and σ^2 accounts for the variance of the noise. The L1 norm of the transformed image imposes sparsity, whereas the term $\left\|\tilde{F}u - f\right\|_2^2 < \sigma^2$ enforces data fidelity.

When the spatial derivative is used as the transform domain, $\Psi = \nabla = (\nabla_x, \nabla_y)$, the functional $TV(u) = \left\|\nabla u\right\|_1$ is known as total variation.

The Split Bregman method

Constrained optimization problems based on L1 penalty functions can be solved using classic constrained optimization methods, but this approach is computationally intensive. Splitting strategies such as the Split Bregman method enable decoupling of the L1 and L2 components of the functional, so that the L1 component of the problem can be efficiently solved through shrinkage formulas and the L2 component of the problem can be solved analytically [203]. The Split Bregman formulation [203] makes the unconstrained algorithm efficiently converge to the solution of the constrained

problem. It has been successfully applied in signal processing [204], fluorescence tomography [205] and MRI [161, 203, 206].

TTV

The extension of TV in (5.1) to both spatial and temporal dimensions yields the following constrained problem [161]:

$$\min_u \left\| \left(\nabla_x u, \nabla_y u \right) \right\|_2 + \left\| \nabla_t u \right\|_1 \text{ such that } \left\| RFu - f \right\|_2^2 < \sigma^2 \tag{5.2}$$

where ∇_t is the temporal gradient, $\left\| \nabla_t u \right\|_1$ is the temporal TV and the spatial TV is computed as an isotropic model:

$$\left\| \left(\nabla_x \mathrm{u}, \nabla_y u \right) \right\|_2 = \sqrt{\left(\nabla_x u \right)^2 + \left(\nabla_y u \right)^2} \tag{5.3}$$

By adding one parameter, α, to equation (5.2), we can weight the degree of spatial and temporal sparsity:

$$\min_u \left(1-\alpha\right) \left\| \left(\nabla_x u, \nabla_y u \right) \right\|_2 + \alpha \left\| \nabla_t u \right\|_1 \text{ such that } \left\| RFu - f \right\|_2^2 < \sigma^2 \tag{5.4}$$

The problem (5.4) is easily solved using the Split Bregman framework, which enables splitting of L1 and L2 [203]. The L2 component of the problem is solved analytically in the Fourier domain, and the L1 component of the problem is solved through shrinkage formulas. The formulation and pseudocode of the algorithm can be found in [161] and are not replicated here. Values of $\mu = 1$, $\lambda = 1$ were chosen according to previous tests [206], values for α were tested as described in the next subsection, and a maximum of 5000 iterations was chosen as the stopping criterion.

PICCS

The PICCS algorithm solves the convex constrained optimization problem:

$$\min_u (1-\alpha)\left\|\psi_1 u\right\|_1 + \alpha\left\|\psi_2(u-u_p)\right\|_1 \quad \text{such that } \left\|RFu-f\right\|^2 \le \sigma^2 \qquad (5.5)$$

where u_p denotes the prior image, α stands for the weight of the prior penalty function and ψ_1 and ψ_2 are sparsifying transforms. Since ψ_1 and ψ_2 are usually chosen to be the spatial gradient, the first functional represents the spatial total variation of u, $TV(u)$, whereas the second functional represents the spatial total variation of $\left(u-u_p\right)$.

We also extended the PICCS formulation with a stability functional, $\gamma\left\|Vu\right\|_1$, as suggested by Goldstein [203], obtaining the problem:

$$\min_u \ (1-\alpha)TV(u) + \alpha TV(u-u_p) + \gamma\left\|Vu\right\|_1 \quad \text{such that } \left\|RFu-f\right\|^2 \le \sigma^2 \qquad (5.6)$$

The introduction of the variables $d_x = \nabla_x u$, $d_y = \nabla_y u$, $w_x = \nabla_x(u-u_p)$, $w_y = \nabla_y(u-u_p)$ and $v = Vu$ (in this case we choose $V = I$) enable splitting of L1 and L2, and the Bregman iterations b_i^k and f^k enable conversion of (5.6) into an equivalent unconstrained problem:

$$\begin{aligned}\min_{u,d_x,d_y,v,w_x,w_y} \ & (1\text{-}\alpha)\left\|(d_x,d_y)\right\|_1 + \alpha\left\|(w_x,w_y)\right\|_1 + \gamma\left\|v\right\|_1 + \frac{\mu}{2}\left\|RFu-f^k\right\|_2^2 + \\ & + \frac{\lambda}{2}\left\|d_x-\nabla_x u-b_x^k\right\|_2^2 + \frac{\lambda}{2}\left\|d_y-\nabla_y u-b_y^k\right\|_2^2 + \\ & + \frac{\lambda}{2}\left\|w_x-\nabla_x(u-u_p)-b_{wx}^k\right\|_2^2 + \frac{\lambda}{2}\left\|w_y-\nabla_y(u-u_p)-b_{wy}^k\right\|_2^2 + \\ & + \frac{\lambda}{2}\left\|v-Vu-b_v^k\right\|_2^2\end{aligned} \qquad (5.7)$$

The Bregman iterations are updated as follows:

$$
\begin{aligned}
b_x^{k+1} &= b_x^{k} + \nabla_x u^{k+1} - d_x^{k+1} \\
b_y^{k+1} &= b_y^{k} + \nabla_y u^{k+1} - d_y^{k+1} \\
b_{wx}^{k+1} &= b_{wx}^{k} + \nabla_x (u^{k+1} - u_p) - w_x^{k+1} \\
b_{wy}^{k+1} &= b_{wy}^{k} + \nabla_y (u^{k+1} - u_p) - w_y^{k+1} \\
b_v^{k+1} &= b_v^{k} + Vu^{k+1} - v^{k+1} \\
f^{k+1} &= f^{k} + f - Fu^{k+1}
\end{aligned}
\tag{5.8}
$$

Therefore u , d_i , w_i and v can be solved separately. d_i and w_i are solved as in TTV [161], through shrinkage formulas:

$$
\begin{aligned}
d_x^{k+1}, d_y^{k+1} &= \max\left(s^k\text{-}(1\text{-}\alpha)/\lambda, 0\right)\frac{\left|\nabla_j u^{k+1} + b_j^k\right|}{s^k}, \\
s^k &= \sqrt{\left|\nabla_x u^{k+1} + b_x^k\right|^2 + \left|\nabla_y u^{k+1} + b_y^k\right|^2},\ j = x, y
\end{aligned}
\tag{5.9}
$$

$$
\begin{aligned}
w_x^{k+1}, w_y^{k+1} &= \max(\mathrm{p}^k - \alpha/\lambda, 0)\frac{\left|\nabla_j (u^{k+1} - u_p) + b_{wj}^k\right|}{p^k}, \\
p^k &= \sqrt{\left|\nabla_x (\mathrm{u}^{k+1} - \mathrm{u}_p) + b_{wx}^k\right|^2 + \left|\nabla_y (\mathrm{u}^{k+1} - \mathrm{u}_p) + b_{wy}^k\right|^2},\ j = x, y
\end{aligned}
\tag{5.10}
$$

$$
v^{k+1} = \max\left(\left|Vu^{k+1} + b_v^k\right| - \gamma / \lambda, 0\right)\mathrm{sign}(Vu^{k+1} + b_v^k) \tag{5.11}
$$

For the resolution of u^{k+1} we obtain the following expression:

$$
\begin{aligned}
u^{k+1} = \min_u \ & \frac{\mu}{2}\left\|RFu - f^k\right\|_2^2 + \frac{\lambda}{2}\left\|d_x^k - \nabla_x u - b_x^k\right\|_2^2 + \frac{\lambda}{2}\left\|d_y^k - \nabla_y u - b_y^k\right\|_2^2 + \\
& + \frac{\lambda}{2}\left\|w_x^k - \nabla_x (u - u_p) - b_{wx}^k\right\|_2^2 + \frac{\lambda}{2}\left\|w_y^k - \nabla_y (u - u_p) - b_{wy}^k\right\|_2^2 + \\
& + \frac{\lambda}{2}\left\|v^k - Vu - b_v^k\right\|_2^2
\end{aligned}
\tag{5.12}
$$

By differentiating (5.12) with respect to u and equating to zero and then choosing $V = I$, which stabilizes the solution [203],

$$
\begin{aligned}
&Ku^{k+1} = r^k \\
&K = (\mu \mathrm{F}^T \mathrm{R}^T \mathrm{RF} + 2\lambda\nabla_x^T\nabla_x + 2\lambda\nabla_y^T\nabla_y + \lambda \mathrm{I}) \\
&\mathrm{r}^k = \mu \mathrm{F}^T \mathrm{R}^T f^k + \lambda\nabla_x^T(\mathrm{d}_x^k - \mathrm{b}_x^k) + \lambda\nabla_y^T(\mathrm{d}_y^k - \mathrm{b}_y^k) + \\
&\quad + \lambda\nabla_x^T(\mathrm{w}_x^k + \nabla_x u_p - \mathrm{b}_{wx}^k) + \lambda\nabla_y^T(\mathrm{w}_y^k + \nabla_y u_p - \mathrm{b}_{wy}^k) + \lambda u^k
\end{aligned}
\tag{5.13}
$$

The linear system (5.13) can be solved in the Fourier domain as

$$
u^{k+1} = F^{-1}\left[F(r^k) / \widehat{K} \right] \tag{5.14}
$$

where $\widehat{K} = \mu R - 2\lambda\Delta + \lambda I$, as described in [203].

Values of $\mu = 1$, $\lambda = 1$, and $\gamma = 2$ were chosen according to previous tests [206] with the undersampled datasets. All results were obtained using these values and a maximum of 5000 iterations as the stopping criterion.

We tested both TTV and PICCS algorithms using alpha values of 0.05, 0.5, and 0.95 on 2 datasets with 3 different undersampling patterns at an acceleration factor of x5 (20% of k-space lines preserved from each dataset) (see Methods section for datasets and undersampling details). In all cases BOLD contrast was better preserved for $\alpha = 0.95$.

The prior, u_p in equation (5.5), was the mean of the undersampled k-spaces across the temporal dimension and was the same for all volumes in the fMRI series; therefore, it was replicated to match the dimensions of u.

k-t FASTER

The k-t FASTER method consists on using a nonlinear algorithm to fill the non-sampled locations of the k-space data matrix using a low-rank constraint. This matrix completion (MC) technique was first described in [207]. The algorithm and its application to fMRI were thoroughly described in [29] and will not be replicated here. Different values were tested at an acceleration factor of x5 (20% lines) for each of the three parameters involved in its performance, mu, c and R (rank) and the best

combination [mu=0.95, c=0.5, R=114] was selected. All subsequent results were obtained using these values and a maximum of 100000 iterations.

5.3 METHODS

Datasets

All the reconstructions in the present study were obtained from undersampled versions of fully sampled studies acquired in a Bruker Biospec 70/20 7T preclinical MRI scanner. In order to consider the high variability in BOLD contrast and extension on either inter- and intrasubject studies, two datasets (named A and B) were analyzed. Dataset A exhibited a high signal-to-noise ratio (SNR) and a large activation region (58 voxels, maximum t-value of 13.64), whereas dataset B presented a lower SNR together with a smaller activation region (16 voxels, maximum t-value of 4.64).

Dataset A was obtained from an fMRI experiment based on a block design paradigm of forepaw somatosensorial electrical stimulation (2mA, 0.3ms, 8Hz rectangular pulses) in an adult Wistar rat (~300g) sedated with medetomidine [190, 208]. The fully sampled data from dataset A consisted of 115 spin echo–echo planar imaging (SE-EPI) volumes with TR/TE = 3000/30 ms, five slices and a resolution of 0.3 x 0.3 x 2 mm with a 0.1 mm gap between slices, for a total acquisition time of 5'45". The resting blocks comprised 15 volumes (45 s), whereas the stimulation blocks comprised five volumes (15 s). The first and last blocks corresponded to resting periods, for a total of 11 alternating blocks (OFF-ON-OFF-ON-OFF-ON-OFF-ON-OFF-ON-OFF).

For dataset B, all values were the same except the number of slices (11), the stimulation of the left hindpaw instead of the right forepaw, and the sedation maintenance protocol (alpha-chloralose) [209].

In both cases, a phased array coil of four elements was used for reception, and the data from the different coils were detrended, undersampled and reconstructed separately before being combined using a weighted sum of squares.

Animals were treated according to the European Communities Council Directive (86/609/EEC) and local regulations, with the approval of the Animal Experimentation Ethics Committee of Hospital General Universitario Gregorio Marañón.

Undersampling

From the complete dataset (A), the central slice (located at the primary somatosensorial cortex corresponding to the right forelimb, S1FL) was extracted, since it showed the highest functional activation. For dataset B, the fifth slice was selected for analysis (located at the contralateral primary somatosensorial cortex corresponding to the left hindlimb, S1HR).

The detrended k-space corresponding to the selected slice was undersampled at 5 different ratios by removing some of the phase encoding lines from the fully sampled EPI, assuming that in a real scenario the subsampling EPI artifacts could be corrected *a posteriori* using a reference scan [105].

The final ky-t undersampling was quasi-randomly distributed, because a different ky undersampling pattern was applied for each frame or time point within the fMRI series. The selection of ky lines was performed in a quasi-random fashion according to [161] —adapted from [25]— following a polynomial probability density function with higher weight at the center of the k-space (delimited by the distance *rad*) and decay towards the higher frequencies:

$$\begin{cases} (1-r)^p & if \quad |r| \geq rad \\ 1 & if \quad |r| \prec rad \end{cases} \tag{5.15}$$

Parameter values of the probability density function were chosen heuristically to densely sample the lower frequencies and gradually varied for the 5 undersampling factors. Three different realizations were generated for each distribution function, yielding 3 different undersampling patterns at each undersampling factor.

The 5 different factors preserve 5% (acceleration x20), 10% (x10), 12.5% (x8), 20% (x5) and 50% (x2) of the original number of k-space lines. Figure 16 shows an example of the undersampling patterns obtained for 50% of the lines acquired.

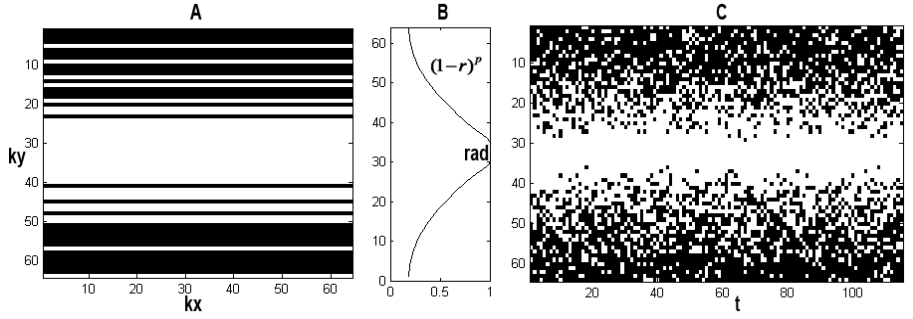

Figure 16. Example of the undersampling patterns generated for 50% of the preserved k-space lines (x2 acceleration). A) Example of a kx-ky pattern. B) Probability density function in the ky direction. C) ky-t sampling.

For the PICCS algorithm, the prior image was constructed from the sum over time of these undersampled k-spaces.

Image analysis

We compared the reconstruction algorithms after statistical processing of the fMRI series using SPM8 (The Wellcome Trust Centre for Neuroimaging) and the SPMMouse toolbox (Wolfson Brain Imaging Centre, University of Cambridge [210]).

Images were realigned to their mean, smoothed with a 1.2 mm FWHM gaussian kernel, and fitted to the block design through the general linear model. The resulting maps were thresholded at $p_{uncorr}<0.05$, with a cluster size of 12 voxels [10, 13, 211] for dataset A and cluster size of 4 voxels for dataset B.

In the fully sampled datasets (which serve as the reference for the compressed sensing evaluation), activation was only observed in the contralateral somatosensorial cortex (see reference "full" map in Figure 17 and Figure 18).

Evaluation of the statistical maps

We visually compared the statistical maps obtained with the TTV, PICCS and k-t FASTER algorithms with the fully sampled map in 3 realizations for each scenario. To assess the sensitivity/specificity of the BOLD detection for each reconstruction, we computed the receiver operating characteristic (ROC) curves using the fully sampled maps as the ground truth. A ROC curve depicts the true positive fraction (TPF) versus the false positive fraction (FPF). In the context of detection of fMRI activation, according to the definitions given in [27] "TPF means the ratio of the number of detected voxels as activated among truly activated voxels to the total number of truly activated brain voxels and FPF indicates the ratio of the number of detected voxels as activated among truly non-activated brain voxels to the total number of truly non-activated brain voxels". Therefore, the higher the area under the curve (AUC), the more robust the detection algorithm. We compared the areas under the curves for TTV, PICCS and k-t FASTER in all undersampling scenarios for the realizations generated (n=3).

5.4 RESULTS

Activation maps

Figure 17 shows examples of the activation maps for the fully sampled dataset A (high SNR) and five undersampling factors –columns– using the three algorithms –rows—. Artifacts resulting from aliasing are obvious at high undersampling factors, particularly for the TTV, although BOLD contrast is preserved at the region of interest, S1FL. The functional images reconstructed (shown as the background) appear more “patchy” for TTV, as previously described in [212]. Visual inspection suggests similar activation intensities for PICCS and k-t FASTER, and in both cases higher than those of TTV.

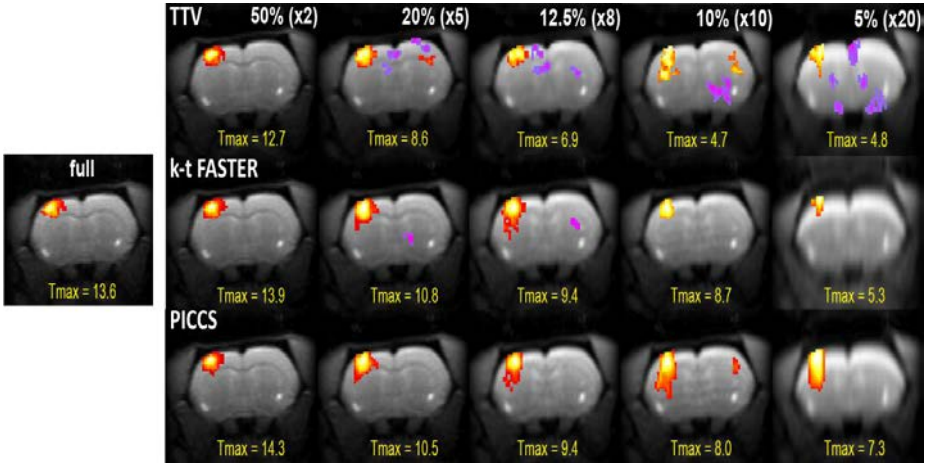

Figure 17. Example of the activation maps generated for dataset A by the three reconstruction algorithms at several undersampling factors. The percentages indicate the amount of k-space lines preserved from the full dataset. The acceleration factor is shown in parentheses. Maximum t-values are shown in yellow below each map.

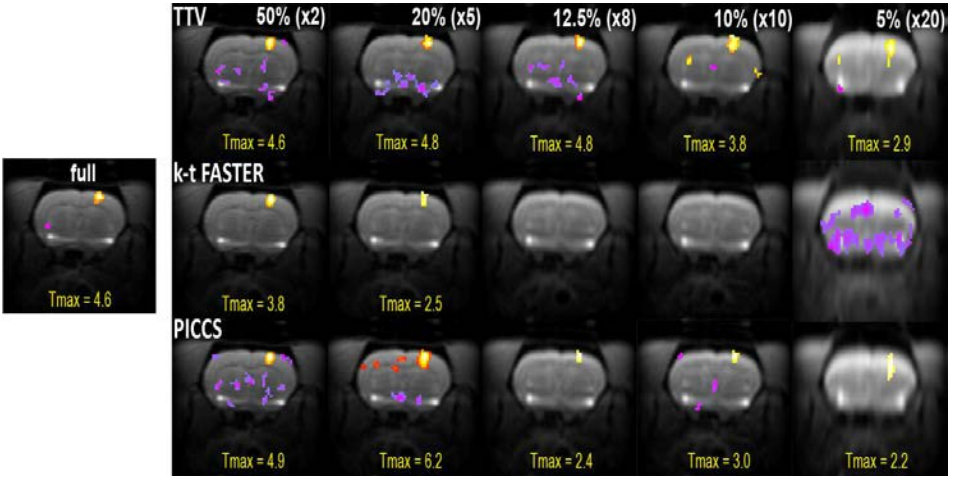

Figure 18. Example of the activation maps for the noisy dataset (B) generated by the three reconstruction algorithms at several undersampling factors. The percentages indicate the amount of k-space lines preserved from the full dataset. The acceleration factor is shown in parentheses. Maximum t-values are shown in yellow below each map.

Figure 18 shows examples of the activation maps for the fully sampled dataset B (low SNR) and the five undersampling factors –columns– using the three algorithms –rows—. In general acceleration-related artifacts appear earlier than for dataset A, probably due to the lower SNR of this dataset. Visual inspection suggests slightly higher BOLD contrast for the TTV than for the PICCS algorithm and more "patchy"[212] images for TTV at high acceleration factors. K-t FASTER produced significant activation maps at x2 and x5 accelerations, but failed to detect significance ($p<0.05$ uncorrected and cluster size $k\geq4$) at higher acceleration factors.

Sensitivity, specificity and acceleration

For dataset A, the areas under the ROC curves were very similar for all the three algorithms at low acceleration factors, and slightly lower for TTV at high undersampling rates (Figure 19).

For dataset B, the performance of the three reconstruction algorithms was very similar at low acceleration factors (Figure 20), as with dataset A. However, PICCS yielded the highest AUC values at high acceleration factors, thus indicating better sensitivity/specificity than TTV or k-t FASTER.

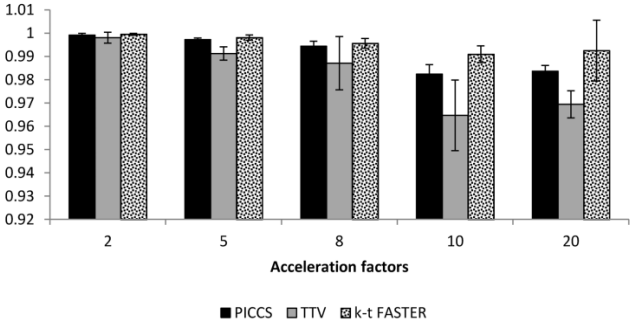

Figure 19 Areas under the ROC curves for the three reconstruction methods at different sampling factors. Three different realizations of the undersampling function were averaged for each acceleration factor and method. Error bars indicate 1 standard deviation from the mean (n=3).

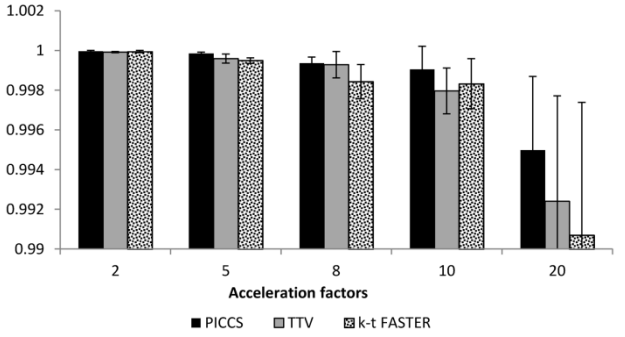

Figure 20. Areas under the ROC curve for the three reconstruction methods at different sampling factors. Three different realizations of the undersampling function were averaged for each acceleration factor and method. Error bars indicate 1 standard deviation from the mean (n=3).

5.5 DISCUSSION

We performed a comparison of the TTV [161] and PICCS [192, 193, 195, 197], two algorithms which had never been applied to fMRI, with k-t FASTER [29], recently proposed for resting state fMRI. This comparison was carried out using previously acquired rat functional magnetic resonance datasets, which were retrospectively undersampled. Although all algorithms exploit temporal redundancy, PICCS proved to be more robust in a noisy scenario where k-t FASTER failed to provide significant maps at high acceleration factors. TTV also provided acceptable maps but reached lower sensitivity/specificity than the other two algorithms. In general, according to the visual inspection of the statistical maps and the AUC values obtained, PICCS seems able to achieve acceleration factors within the range x5-x8. TTV can also reach this acceleration but providing worse spatial localization of the BOLD contrast, whereas k-t FASTER reached a maximum acceleration of x5 in noisy scenarios. Acceleration values of x4 and x5 have been previously reported in the literature for fMRI applications [27-29, 105, 165, 166, 202, 213]. The acceleration factor of x8 reached by

PICCS doubles the value reported in the only existing article about compressed sensing applied to preclinical rodent studies [105] based on k-t FOCUSS reconstruction. However, direct comparison would be unfair, since the aim of the authors in [105] was not to find the maximum possible acceleration. In general, any direct comparison with other methods applied to fMRI, such as k-t FOCUSS [27, 105] and generalized series [28], is fairly difficult, given the numerous variables which differ between the applications (e.g., biological model, acquisition sequence, SNR and resolution, implementation, etc.).

The exploitation of temporal redundancy by averaging all available undersampled k-spaces to build a prior image has provided robust results. It takes advantage of all the available information acquired, and greatly constrains the problem. The prior image seems to provide good spatial support for the slight BOLD temporal changes and thus facilitates their recovery by the PICCS algorithm.

We can hypothesize that, at high acceleration factors, combinations of this prior-based strategy with other frameworks such as k-t FOCUSS, TTV or k-t FASTER might also perform better than any method alone. Further studies to corroborate this hypothesis are warranted.

Regarding the two methodologies specifically developed by the authors for this context, the formal difference between PICCS and TTV algorithms lies in the use of temporal redundancy. In the case of TTV, the use of a temporal gradient leads to image quality degradation at high acceleration factors, probably because neighboring frames have very few k-space lines. On the other hand, PICCS makes use of a prior image containing all the temporal information compressed into a single volume. Since this prior image is replicated along the temporal dimension, each volume of the series under reconstruction uses the same prior volume. Thus, PICCS builds images upon a prior image with a good SNR, thus leading to better image quality than TTV. This may be the reason why PICCS performs better than TTV regarding sensitivity/specificity.

It is remarkable that all the algorithms presented here could also be used for other sequences, such as traditional gradient echo sequences (as suggested in [105]), variable density spirals [28, 214] and 3D EPIs [29].

In all cases, the acceleration achieved could be exploited either to reduce total scan time or to increase temporal or spatial resolutions. In 2014, Zong et al. [105] studied the advantages of total scan time reduction using a gradient echo sequence accelerated with compressed sensing instead of EPI. Alternatively, if the acceleration is exploited by reducing the TR (increased temporal resolution), the saved scan time could allow us to acquire more repetitions of the fMRI series, thus improving the BOLD signal [214]. Following the same principle, the spatial resolution of the fMRI maps could be improved by acquiring more spatial data within the same total acquisition time, as demonstrated with spiral trajectories [214]. In the specific case of EPI and other fast sequences, the compressed sensing framework enables the reduction of the train length, which is often desirable when attempting to attenuate susceptibility artifacts, chemical shifts and physiological noise [28, 214].

One limitation of our study is that results were obtained by simulating a compressed sensing acquisition via undersampling of a fully acquired EPI dataset. In a real scenario, data would have to undergo a correction step before reconstruction, which is usually performed by means of a reference scan with the phase encoding switched off, as reported in [105].

Another limitation is that we did not systematically test the parameters of the undersampling probability density function in order to find their optimum value, since the aim of the study was to compare the two reconstruction algorithms under the same circumstances. Therefore, optimized parameters could lead to even higher accelerations.

We chose the gradient as our sparsifying transform because it is generally used with the PICCS method. However, other transforms such as wavelets, shearlets or discrete cosine transforms might lead to sparser representations and provide even higher accelerations; consequently, further testing is warranted. These transforms can be

easily implemented within the framework we present based on the Split Bregman formulation, which provides an efficient solution to the problem. The Split Bregman formulation also solves a constrained optimization problem by obviating the search for appropriate regularization parameters [160, 161, 203, 205] and thus considerably reducing the computational burden.

5.6 CONCLUSIONS

In the present study, we successfully applied three reconstruction algorithms that exploit the temporal redundancy of dynamic acquisitions to undersampled rat fMRI data: TTV, which has previously been applied in cardiac MRI[161]; PICCS, which has been widely used in compressed sensing frameworks for computed tomography imaging [192, 193, 195, 197]; and k-t FASTER [29], which has recently been tested with resting state human fMRI data. The PICCS algorithm performed similarly to k-t FASTER in a high SNR scenario, but much better in a low SNR scenario, where k-t FASTER failed to provide significant maps. TTV also provided consistent statistical maps but with less sensitivity/specificity on the BOLD contrast detection than the other two algorithms. Our results suggest that acceleration factors up to x8 are feasible with the PICCS algorithm.

6 FMRI ANALYSIS: FMRAT

This chapter proposes a new tool for the fully automatic analysis of rodent fMRI studies, fMRat. The tool is programmed in Matlab as an extension for SPM package and makes use of several SPM functions . In addition to a simple and friendly user interface, it also loads appropriate parameters for rodents, offers optional advanced processing steps and obtains percentage signal changes in user-defined ROIs. Therefore fMRat gathers functionalities of several software packages into a single tool for an automatic multi-subject analysis.

6.1 INTRODUCTION

Functional imaging of rodent brains using BOLD (blood-oxygen-level-dependent) contrast has been widely applied in preclinical research for the past 20 years, as it enables indirect measurement of neurological responses to induced stimuli [2, 39, 61, 98, 185]. Neurology, radiology, and behavioral sciences are the main areas of application of rodent fMRI imaging, which makes it possible to map the BOLD signal in the brain by means of statistical analysis of the voxel signal changes in voxel time-series [2, 140, 215].

A typical fMRI analysis addresses acquisition inaccuracies through several preprocessing steps, namely, spatial realignment of the volumes constituting the series, optional normalization to standard spatial coordinates to ensure further between-group comparison, and spatial smoothing. Statistical analysis of fMRI studies is usually carried out by applying a general linear model (GLM), where the measured voxel values represent linear responses to the convolution of the applied stimuli with a hemodynamic response function (HRF). The linear coefficients in the model are estimated from both the acquisition data and a user-provided design matrix, which is composed mainly of HRF-convolved stimuli regressors and covariate regressors. Once

the model is estimated by means of a restricted maximum likelihood algorithm, a voxel-wise paired t test produces the final parametric image.

Although several fMRI tools are available, few perform these preprocessing steps appropriately for the analysis of fMRI preclinical data. The most user-friendly tools usually offer few features and only provide elementary preprocessing algorithms. Among them, we can cite the Bruker proprietary FunTool [169] and the Stimulate package from the University of Minnesota Medical School [170].

SPM (Statistical Parametric Mapping, The Wellcome Trust Centre for Neuroimaging), one of the most widely used software packages in neuroscience, produces thorough analyses and implements the full possible span of preprocessing and processing routines. However, it was originally designed for human application and therefore requires adjustment (with totally new default values) before being applied in preclinical studies. In order to address this problem, an SPM extension tool was developed for rodent studies (SPMMouse, Wolfson Brain Imaging Centre, University of Cambridge). SPMMouse allows the user to work with rodent fMRI studies by adapting several SPM functions and defining specific preprocessing and display settings but it is no longer maintained [210].

Another toolbox that can be applied in preclinical environments is 'SPM batch' (from release SPM8), which enables fully automated multisubject analyses. However, prior to execution, it is necessary to manually select each subject and define the acquisition parameters. Once the SPM model has been estimated for each fMRI series and the statistical inference performed, other SPM extensions such as MarsBar [216] and the VBM tools [217] can generate quantitative results for specific regions of interest (ROIs).

In summary, an expert user can complete the analysis of rodent fMRI data by using four different tools to load appropriate default parameters with SPMMouse, to create an SPM batch template, to run this batch, and to extract quantitative ROIs data with some of the SPM extensions mentioned above.

However, all of these steps involve significant user interaction, which prevents a fully automated pipeline and makes the analysis prone to user errors, and require some expertise in programming. The purpose of our work was to develop a multiplatform automatic tool for full processing of fMRI rodent studies. Based on a user-friendly interface, the tool provides first-level statistical parametric brain maps (t and Z) by means of an automatic pipeline that loads appropriate default parameters for preclinical studies and processes multiple subjects in batch mode. The workflow and several software parameters were specifically tuned for rat brain analysis and validated with real fMRI data.

6.2 METHODS

Architecture

The multiplatform (Windows, Linux and MAC) tool was implemented in Matlab (MathWorks ®). It uses several functions from the SPM package (e.g., spm_realign m, spm_coreg m, spm_affreg, spm_smooth, spm_run_fmri_design m, and spm_spm) complemented with functions taken from other toolboxes: the CBMGmosaic (Northwestern Cognitive Brain Mapping Group) (ortho viewer code) and SPMMouse (Wolfson Brain Imaging Centre, University of Cambridge [168]) (preset loading function).

Since SPMMouse was originally designed for SPM5, we had to ensure compatibility with SPM5, SPM8 and SPM12 by introducing some minor modifications into the original SPMMouse code. An overview of the program flow is presented in Figure 21. The workflow was designed to run in separate modules that communicate via disk files in such a way that modules can be executed independently from a command line. The typical execution workflow recommended for non-expert users is described below.

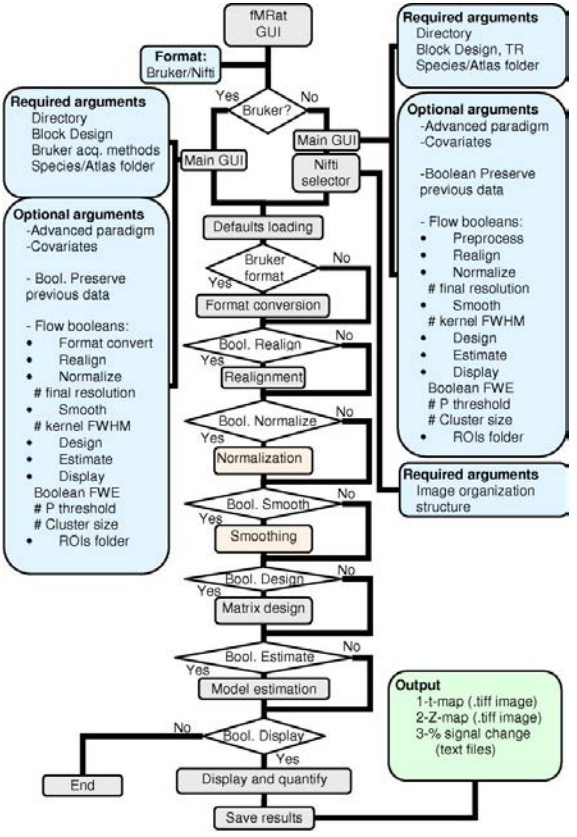

Figure 21. Flow diagram. User input is displayed in *blue*, output in *green*, and optional steps in *light orange*.The default pipeline includes each processing step, as shown in the "Advanced Options" of Figure 22.

Graphical user interface (GUI)

The GUI prompts the user for the image format, in either Bruker raw format or in Nifti format [138]. For both image formats the main window interface (Figure 22) asks for a directory of interest, which can host multiple studies from different subjects, and the stimulation paradigm. Advanced users can provide onsets and durations of the stimuli/tasks, covariates data and customize optional parameters for image registration (such as the final resolution desired) and statistical analysis (optional multiple

comparisons correction, statistical p threshold, or cluster threshold). The content of the initial GUI varies slightly depending on the image format used.

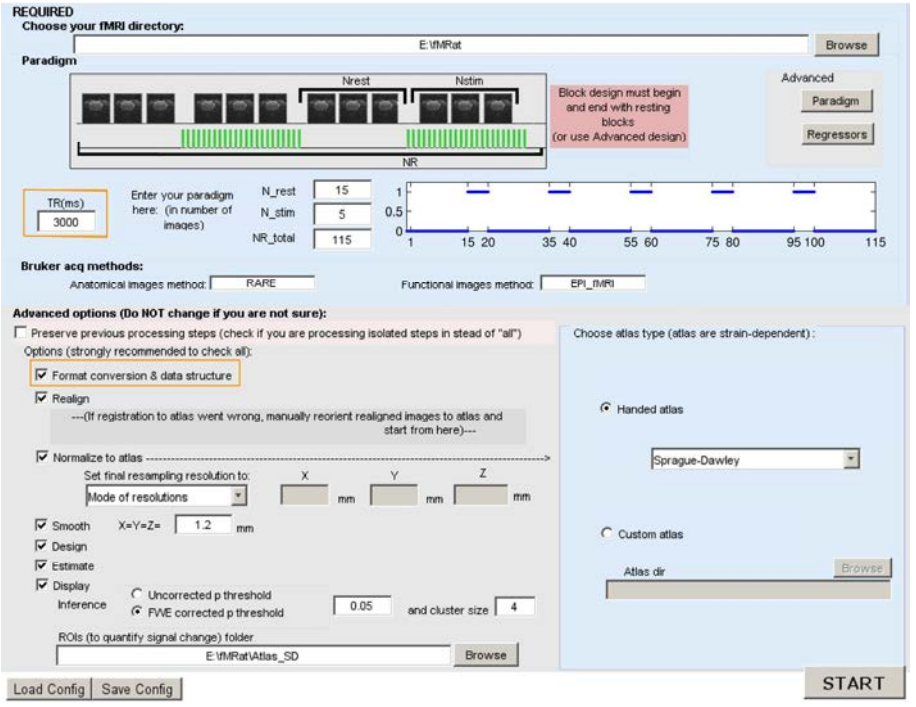

Figure 22. Main GUI (Bruker format). Required inputs in *blue panels*: directory, block design, TR, Bruker acquisition methods and strain or atlas directory. Optional arguments for advanced users are shown in *grey panels,* and specific features for Nifti (TR is required) or Bruker format (the first format conversion step) are highlighted in orange.

For Nifti images, the user is prompted for the acquisition repetition time (TR) and an extra Nifti selector, which serves to define the correspondence between functional and structural images, whereas for the Bruker format, all the information required to build the data structure (geometrical parameters, data type, and acquisition sequence) is read from the acquisition parameter Bruker files (acqp, method, and reco files).

Advanced users can also choose specific steps in the pipeline and adjust additional parameters such as the application of a user-defined atlas for normalization, the degree

of smoothing, the statistical correction applied (familywise error, FWE, or uncorrected p value) and the cluster size.

Required basic information and advanced parameters are displayed in separate panels. Advanced parameters include non-blocked paradigms, extra regressors, format conversion, realignment, atlas normalization, final resolution after normalization, smoothing, matrix design, estimation, statistical p-threshold, cluster size, and ROIs folder. These input data can be saved and reloaded as templates from the GUI. Once the "Start" button is pressed, the tool no longer prompts the user. Any possible processing errors are recorded into a text log file.

Default automatic processing pipeline: preprocessing steps

First, user input arguments are parsed and checked, an error log file is opened, and adequate SPM default parameters for rat studies are loaded. If the user is working with the Bruker format, a preprocessing step recursively detects all subjects and studies under the directory selected, as well as the structural and functional images within each study and the Bruker scout (Tripilot) images, if present. Based on this information, each functional image is associated with the latest structural image acquired within the study, thus overcoming the problem of having different sample positions within the same study. The complete data structure is saved into a tracking mat file that is used in further steps. The outcome of this step is to convert the functional 4D raw data into 1-volume-per-file images in Nifti format.

The Nifti images conforming a series are then rigidly realigned to their mean image [218] and normalized [219] to an anatomical atlas in order to achieve spatial concordance for subsequent group analyses. If desired, normalization can also be manually initialized to ensure convergence of the optimization algorithm, as is commonly required in human fMRI analysis. This normalization to the atlas is achieved via intermediate affine registration to the anatomical image [220]. The user can either select one of the 2 atlases (for Sprague-Dawley and Wistar strains) provided

with the tool or apply a user-provided atlas [221, 222]. At this step of atlas normalization, the tool also enables the user to specify a custom final pixel size for the warped functional images.

Both registration steps (functional-structural intrasubject rigid registration and structural-atlas normalization) were implemented using the spm_coreg m and spm_affreg.m SPM functions, which perform 2-level multiresolution rigid transformations by maximizing the normalized mutual information and a subsequent least squares affine registration respectively. As mentioned above, the structural images are also registered to the atlas, thus providing a fused display after the analysis.

Once all the functional and anatomical images are in the geometrical space of the atlas, the user can apply an optional Gaussian smoothing kernel with a user-specified FWHM (full width at half maximum).

Default automatic processing pipeline: GLM estimation and results

After the preprocessing steps, the tool builds a GLM design matrix, where rows correspond to different volume acquisitions (temporal axis) and columns to possible regressors. The first column corresponds to the convolution of the applied stimuli with a squared finite impulse response, the next 6 regressors represent the translation and rotation parameters obtained from the spatial realignment, and the last regressor is the mean voxel value at each time point. This automatic default design matrix corresponds to the typical block paradigms most frequently used in rodent fMRI. We included the realignment parameters in the design in order to allow for the correction of residual movement artifacts in the final statistical map [223]. In the “Advanced” panel, the advanced user may select more flexible paradigms as well as additional regressors to be used as covariates.

Statistical assessment was based on a restricted maximum likelihood algorithm [23]. The complete fMRI model includes a high-pass temporal filter, which suppresses

baseline drifts caused by the scanner and other low-frequency biological signals, and an autoregressive estimation of temporal correlations in the fMRI series.

Once the linear model has been estimated, the software applies 2 contrasts to detect areas where signal intensity is higher/lower in stimulation blocks than in rest blocks ("positive"/"negative" contrast respectively). After optional correction for multiple comparisons (FWE), the software applies extent and amplitude thresholding and provides a fused display that overlays the final t- and Z- statistical maps onto their corresponding normalized structural image. Positive and negative contrasts are represented with different color scales.

Maximum, mean and standard deviation of the percentage of signal change are also calculated, averaged, and written to text files for the whole masked brain and for any optional mask-delimited ROIs defined by the user.

Assessment

The tool and the default processing parameters were assessed with 460 rat time series. We tested 5 smoothing kernel sizes, the inclusion of the realignment parameters in the design matrix, and 3 different hemodynamic models.

The assessment was performed using images from 32 different rats (25 Sprague-Dawley and 7 Wistar [weight 300 g to 400 g]). The functional images were acquired with a 7T Bruker Biospec 70/20 scanner following the protocol described in [14]: axial orientation, TE/TR = 30 / 3000 ms; FOV 1.92 x 1.92 x 1 cm; matrix of 64 x 64 x 5 voxels. Hindlimbs and forelimbs were stimulated alternatively with sensorial electrical stimuli (1 mA, 0.3 ms duration) through a synchronized stimuli generator (a customized STG 4002, Multi Channel Systems GmbH, Reutlingen, Germany). Each time series consisted of 115 SE-EPI volumes acquired using a block design paradigm. Resting blocks comprised 15 images (45 s), whereas stimulation blocks comprised 5 images (15 s). The first and last blocks corresponded to resting periods in such a way that there were 6 resting blocks and 5 stimulation blocks per series.

We included in the package sample anatomical atlases for 2 rat strains (Wistar and Sprague-Dawley). These were built by means of rigid registration of the RARE T2-weighted axial anatomical images acquired during the fMRI sessions: 7 subjects for the Wistar atlas and 16 for the Sprague-Dawley atlas (256 x 256 x 15 voxels [0.075 mm x 0.075 mm x 1 mm resolution]). Images were reoriented, re-sliced in order to improve the axial resolution, averaged, and smoothed with FWHM=0.3 mm in the axial direction. For the quantitative analysis of our experiments, we segmented the following ROIs on the atlas: S1FL (primary somatosensorial cortex forelimb region left), S1FR (primary somatosensorial cortex forelimb region right), S1HL (primary somatosensorial cortex hindlimb region left), S1HR (primary somatosensorial cortex hindlimb region right), and the whole brain. Users may define any ROIs, as long as they are stored in Nifti format.

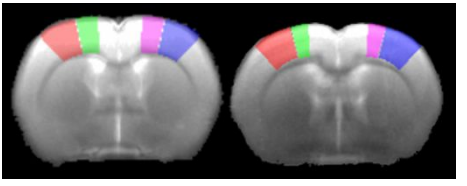

Figure 23. Axial slices of the atlas created and provided for each strain of rat (*left* = Sprague-Dawley, *right* = Wistar). The overlaid ROIs correspond to S1FL (*red*), S1FR (*purple*), S1HL (*green*), and S1HR (*pink*).

In order to select an optimum degree of smoothing to be used as a default setting, we tested 5 different 3D isotropic smoothing kernels, with FWHM ranging from 1 (no smoothing) to 5 times the voxel size. The optimum value provided as a default setting was chosen by visual inspection and by comparison of the maximum t-values obtained (see Results section).

Regarding the design matrix, we tested 2 issues: 1) whether the inclusion of the realignment parameters as regressors of no interest improves data fitting [224] (groups WITH and WITHOUT); and 2) which specific hemodynamic response function

provides better results with rats. The use of a generic boxcar-shaped hemodynamic response (BOXCAR) was compared to the "canonical function" proposed by Friston (FRISTON HRF) for humans and to a gamma function adapted for rat hemodynamics (RAT HRF) using the parameters reported by Martin et al. [46] for oxyhemoglobin in anesthetized rat cortex (mean=4.28 s, width=4.12 s). In both cases (realignment parameters and hemodynamic response), we assessed the goodness-of-fit of the linear model by comparing the median of variance images, assuming that a lower variance implies a better fit. Significance was assessed using the Wilcoxon signed rank test (realignment) and Friedman test (hemodynamic response).

6.3 RESULTS

Figure 21 and Figure 22 show an outline of the program flow and a snapshot of the main GUI. Figure 23 illustrates the 2 atlases built for Wistar and Sprague-Dawley rat strains, with segmented ROI masks overlaid.

Smoothing

In our experiments, the maximum t value was obtained with the 1.2-mm FWHM filter, which corresponds to four times the voxel size (Figure 24). This is in accordance with the postulate in [33], which states that the smoothing kernel should match the activation areas expected in size. In fact, this is the filter that best enhances signal-to-noise ratio (SNR) according to the "matched filter" principle in detection theory. In our study, 1.2 mm is approximately the activation extension expected, according to the Paxinos atlas [183]. Visual inspection of the activation maps shows accurate S1 cortex localization (Figure 25).

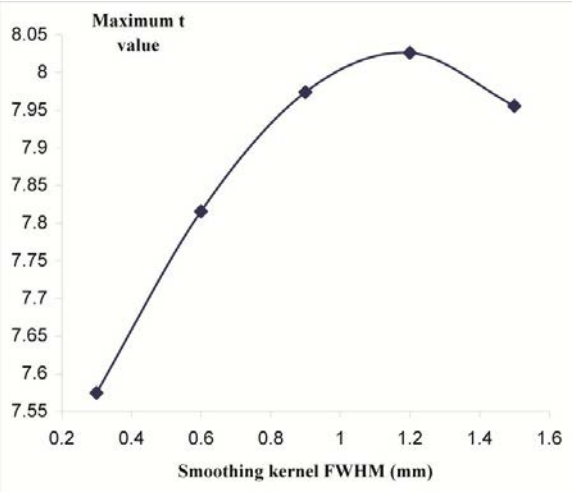

Figure 24. Effect of smoothing kernel size on the final maximum t value in the activation map (whole brain maximum).

Design matrix

Median residual variance of the linear model was higher for the analyses which did not include the realignment parameters as regressors. A Wilcoxon signed-rank test yielded significant between-group differences ($p < 1e{-}3$, between the WITH and WITHOUT realignment parameters analyses).

As for hemodynamic functions, we did not find significant differences between the gamma models (FRISTON HRF–RAT HRF), although the boxcar approach ($p < 1e{-}3$) led to significantly lower residual variance. Post hoc analysis yielded $p = 0.21$ for FRISTON HRF–RAT HRF, $p < 1e{-}3$ for BOXCAR–RAT HRF, and $p = 1e{-}3$ for BOXCAR–FRISTON HRF, thus confirming that the difference was due to the boxcar group, which led to lower variance values.

Tool output

The tool output consists of two mosaics per acquisition, two text files per study summarizing the ROI values of all the acquisitions within the study and all the intermediate images as generated by SPM. The two mosaics show the activation maps of positive (hot red scale) and negative (cool blue scale) contrasts, overlaid on the background anatomical image. One shows the t value map, and the other the Z score map (t value and Z value mosaics are similar but with a different normalization of the activation), both of which are overlaid onto the same background structural image. For each subject, the tool generates two text files (for the positive and negative contrasts, respectively) reporting the number of activated voxels and the percentage of signal change in the ROIs (mean, standard deviation, maximum and localization of the maximum). These ROIs include the whole image (with background), the masked brain and any user-defined ROIs analyzed.

All intermediate images (as generated by SPM) are also stored in a new folder named "Processed" inside each acquisition folder. The "Processed" folder enables the user to check the result of individual steps in the pipeline.

Figure 25 shows an example of the Z map image mosaic, as printed by the tool, and an example of a text file containing the input default parameters and the percentage of signal change measured at the different ROIs.

Quantitative assessment

We carried out a quantitative assessment comparing the percentage of signal change between our tool and the values reported by Marsbar [216] on the four regions mentioned in the previous section: S1FL, S1FR, S1HL and S1HR for n = 8 different acquisitions—with different BOLD contrasts.

Average differences (in absolute value) and correlation between measurements from both tools were computed. The mean percentage difference between both tools was 0.07 %, and the correlation coefficient was 0.95.

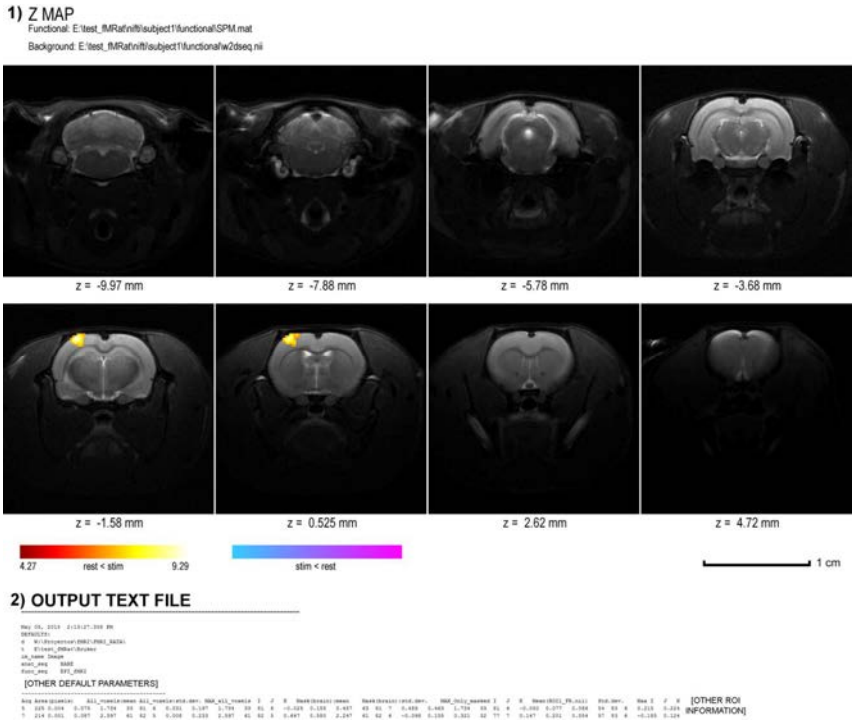

Figure 25. 1) Example of output image mosaics (in this case, the Z score map overlaid onto the warped structural image). 2) Example of the output text files printed: date and hour when the analysis was finished, default parameters –input of the analysis–, and ROI values in tabbed columns –output–.

6.4 DISCUSSION

We present an automatic tool developed for the analysis of rodent fMRI series. It comprises a user-friendly interface that enables statistical parametrical maps to be obtained in a fully automated way and provides the additional flexibility required by advanced users who wish to execute only specific steps of the processing pipeline. For example, the smoothing could be sometimes excessive when activated regions are

small, as suggested by Worsley et al. [33]. Such an approach enables to skip some computationally expensive steps, which may be particularly valuable in an experimental fMRI acquisition context, where an immediate analysis may provide important feedback about the animal physiology for tuning the next fMRI series before the acquisition process is complete.

We also investigated the optimum pipeline for rat studies, concluding that the inclusion of realignment parameters in the design matrix yielded less residual variance once the model was adjusted and, therefore, led to a more accurate fitting. The side effect is that it might decrease sensitivity in those cases where the movement is highly correlated with the stimuli of interest; consequently, care should be taken depending on the particular fMRI experiment [224]. Regarding hemodynamic response functions, our results suggest that for small animals such as rats, which have fast vascular dynamics [225], the simpler approach using a short boxcar response led to a better fit of the model than more complex approaches, at least at the relatively low temporal resolutions of our scans (acquisition time per volume = 3 s). We did not test other types of hemodynamic response functions, such as Fourier series [137] or derivative models, which would give good results for higher temporal resolutions.

Our study is subject to some limitations. Firstly, the tool may not be completely automatic if the user wishes to normalize to an external atlas, because manual initialization is sometimes required to ensure convergence of normalization. This problem occurs similarly in human studies. Secondly, the tool has only been tested with typical rat studies, and additional testing with mice or using different geometries or parameters is warranted.

Our tool offers the advantage of a thorough analysis in an automated pipeline. Simpler software packages, such as Bruker proprietary software or Stimulate (University of Minnesota), also provide a straightforward online analysis, but they lack relevant features such as series realignment, adjustment to a GLM model, or multiple comparison correction. Our tool automates all these steps, including ROI quantification in a single pipeline.

6.5 CONCLUSIONS

To conclude, we present a new tool for the online analysis of rat brain fMRI series. The tool provides a user-friendly interface for both standard and expert users, which enables an immediate and complete analysis to be obtained, even during the acquisition and with the functionality of four different tools in one. The tool is programmed in a modular fashion, thus enabling the advanced user to perform partial analyses in order to test specific hypotheses. Furthermore, it enables intensive offline analysis, including automatic multi-subject detection for Bruker format datasets.

The automation achieved reduces user interaction, thus preventing possible mistakes derived from manual operation of previous and more complicated analysis approaches. Besides, the GUI, the multi-subject automatic detection and the adaptation to preclinical studies could make fMRat a very valuable tool for preclinical research in fMRI.

The tool fMRat, its code and some sample images are publicly available to encourage a wider use from the scientific community and can be downloaded from:

https://github.com/HGGM-LIM/fmrat

7 CONCLUSIONS

The main objective of this thesis was to investigate new techniques for rodent fMRI that could improve the experimental practice and the quality of results at three different stages: the experimental setup, the data acquisition and the image processing.

Therefore, for the three stages mentioned, the main contributions of this thesis have been 1) the optimization of an anesthetic protocol with sevoflurane for rat fMRI, 2) the exploration of three different compressed sensing algorithms to speed up acquisition by exploiting the temporal redundancy in fMRI and 3) the proposal of a new automatic analysis tool for rodent fMRI.

The first contribution dealt with animal preparation and the problem of using anesthetics. fMRI statistical maps are very sensitive to head movement, and awake studies in rodents convey more difficulties than advantages, thus the use of an anesthetic is compulsory. On the other hand, anesthetics may suppress the neuronal activity in certain brain areas and some of them are toxic in the long term. Subcutaneous medetomidine constant infusion of 0.15 mg/kg/h had been adopted as a non-toxic sedative protocol appropriate for longitudinal studies. However, inhaled anesthetics are also non-toxic and preferred in the preclinical daily practice because of their faster induction and recovery. Specifically, sevoflurane is of great interest due to its use in the pediatric context, and there were no previous reports of its use in preclinical fMRI studies before this thesis. This first contribution addressed the definition of an optimal setup for rat fMRI studies under sevoflurane regarding the sevoflurane dose and the stimulation scheme for achieving the maximum BOLD signal possible. Results were compared with the previously established medetomidine protocol. Our results show that fMRI under sevoflurane is feasible in rats and produces a BOLD contrast as high as the one obtained under medetomidine protocol but the animal preparation takes longer and may discourage its use.

The second contribution deals with data acquisition and reconstruction. Long experiments may compromise the assumption of a stable physiological condition of the subject during data acquisition, which is critical for most experimental fMRI paradigms. In addition, due to the weak intensity of the BOLD signal, any fMRI task experiment requires many repetitions for the posterior statistical analysis. This frequently leads to fMRI runs of several minutes with total experimental time of hours. Although the interest of reducing acquisition time is obvious, conventional accelerated acquisition schemes are prone to produce aliasing artifacts. Compressed sensing has demonstrated to overcome these limitations in other imaging fields, but there are only a few works of its application to fMRI. Furthermore, it has been proved that each particular application may benefit from a specific optimization to better exploit its information redundancy. In this work we addressed the exploitation of the temporal redundancy of rat fMRI data and applied (for the first time in fMRI) three different state-of-the-art algorithms which had had yielded promising results in other applications such as CT (PICCS algorithm), cardiac MRI (TTV algorithm) or resting state human fMRI (k-t FASTER).

The third contribution of this thesis addresses the image postprocessing. A typical fMRI analysis involves many pre-processing and processing steps in order to ensure a robust statistical inference, what results in a wide variety of parameter combinations that the user must select. The existing processing tools were originally designed for humans and, though they can be adapted for rodents, typically require significant user interaction and computing skills. We developed a new tool, specifically optimized for rodent fMRI, which provides a fully automated multisubject analysis with a user friendly interface . The tool makes use of core SPM package functions and reports the statistical maps, displayed in a mosaic fashion, and the percentage signal change of any user provided ROI. Besides, it also includes advanced features that enable a more flexible analysis for expert users, such as advanced paradigm designs, additional regressors or the execution of individual processing steps. It was programmed as a plugin for the SPM software package and its code was made publicly available from Github website.

The specific conclusions reached during the progress of this thesis are:

1. It is feasible to perform BOLD experiments in rats under sevoflurane anesthesia. The electrical stimulation frequency at which BOLD contrast is in general more robust is 9Hz for sevoflurane anesthesia. The average dose at which BOLD contrast arises is 1.8% of sevoflurane, but the emergence of BOLD contrast is delayed about 100 minutes from the start of the anesthetic maintenance, which considerably increases the total fMRI experiment duration.

2. The percentage signal change measured in the primary sensorial cortex corresponding to the forelimbs is higher for the medetomidine anesthetic protocol than for the sevoflurane protocol, but the differences are not statistically significant.

3. The compressed sensing framework allowed the reconstruction of retrospectively undersampled rat fMRI datasets and provided significant statistical maps. The PICCS algorithm performed similarly to k-t FASTER in a high SNR scenario, but much better in a low SNR scenario, where k-t FASTER failed to provide significant maps. Spatiotemporal total variation also provided consistent statistical maps but with less sensitivity/specificity on the BOLD contrast detection than the other two algorithms.

4. Our results suggest that acceleration factors up to x8 are feasible with the PICCS algorithm.

5. A new tool, fMRat has been developed for a fully automated multisubject analysis of rodent fMRI. fMRat performs a thorough analysis including all the preprocessing steps and the GLM corrections typically performed with human tools such as SPM package. Its code and some sample images are publicly available to encourage a wider use from the scientific community.

6. fMRat has been validated with datasets from 32 different rats of both Wistar and Sprague-Dawley strains. For a subset of eight datasets, fMRat percentage

signal changes and those obtained with Marsbar (a ROI quantification SPM plugin) had a correlation coefficient of 0.95.

8 FUTURE LINES

Based on the contributions of this thesis, research can still be carried out to further improve the three stages that comprise a rodent fMRI experiment, as described below:

- To explore the possible causes of the delay in the BOLD emergence under sevoflurane anesthesia, for instance by simultaneously examining the vascular reactivity during the fMRI experiment acquisition.
- To compare the signal obtained under sevoflurane and isoflurane sedation, in order to elucidate possible differences in the underlying neuro-vascular coupling mechanisms for the two halogenated ethers.
- To implement the compressed sensing acquisition in order to check the maximum acceleration actually achievable for rodent fMRI.
- To study the feasibility of pseudo-randomly undersampling the EPI sequence and the modifications required in the conventional EPI corrections applied to the k-spaces.
- To implement and test a new algorithm that exploited the sparsity in other domains, such as the spatial domain of the statistical maps. This would mean iteratively evaluating the statistical final map inside the reconstruction algorithm and therefore would require an exploration of the processing steps that should be included inside the reconstruction algorithm.
- To extend the testing of fMRat tool to mice and pathological subjects. Further testing should be performed in order to ensure the robustness of the tool but unfortunately we had no datasets available other than healthy Wistar and Sprague-Dawley rats. We hope that the public availability of the tool will help to test it with a greater variety of subjects.

- To extend fMRat in order to automatically perform second level (group) analysis. .

9 PUBLICATIONS

9.1 DIRECTLY RELATED TO THIS THESIS

Articles

Chavarrias, C., Abascal, J.F., Montesinos, P. and Desco, M.,"Exploitation of temporal redundancy in compressed sensing reconstruction of fMRI studies with a prior-based algorithm (PICCS)". Med Phys, 42(7): p. 3814 (2015).

Chavarrías, C., García-Vázquez, V., Alemán-Gómez, Y., Montesinos, P., Pascau, J. and Desco, M.,"fMRat: an extension of SPM for a fully automatic analysis of rodent brain functional magnetic resonance series". Medical & Biological Engineering & Computing: p. 1-10 (2015).

Conferences

Chavarrias C., García-Vázquez V, Soto-Montenegro ML, Desco M. Rat fMRI study under sevoflurane anaesthesia. European Molecular Meeting EMIM 2014 (04/06/2014- 06/06/2014, Antwerp, Belgium). Poster #139.

Chavarrías, C., Abascal, J.F.P.J. , Montesinos, P., Desco, M. How Does Compressed Sensing Affect Activation Maps in Rat fMRI?. XIII Mediterranean Conference on Medical and Biological Engineering and Computing 2013 (MEDICON 2013, 25/09/2013- 28/09/2013, Sevilla, Spain). Published in IFMBE Proceedings Vol 41 p 202-205.

9.2 OTHER PUBLICATIONS

Articles

Chavarrías, C., Vaquero, J.J., Sisniega, A., Rodríguez-Ruano, A., Soto-Montenegro, M.L., García-Barreno, P. and Desco, M.,"Extraction of the respiratory signal from small-animal CT projections for a retrospective gating method". *Phys Med Biol*, **53**(17): p. 4683-4695 (2008).

Conferences

Chavarrías, C., Vaquero, J.J., Sisniega, A., Rodríguez, A., Soto-Montenegro, M.L., Desco, M. Reduction of respiratory blurring in small-animal CT scans based on a fast retrospective gating method. 22nd International Congress and Exhibition on Computer Assisted Radiology and Surgery (CARS 2008, 25/06/2008- 28/06/2008 Barcelona, Spain). Published in: Int J CARS Vol.3 Suppl.1 S13-S14

Chavarrías, C., Vaquero, J.J., Sisniega, A., Rodríguez, A., Soto-Montenegro, M.L., Desco, M. Validation of a Retrospective Respiratory Gating Method for Small-Animal CT Scanners. 2008 IEEE Nuclear Science Symposium and Medical Imaging Conference (IEEE NSS/MIC, 19/10/2008-25/10/2008, Dresde, Germany). Published in 2008 IEEE Nuclear Science Symposium Conference Record p 4303-4305.

Benito, M., Fernández, S., **Chavarrías, C.**, Montesinos, P., Vaquero, J.J., Desco, M. Fat Composition Assessment by 1H and 13C Spectroscopy in Mice. ISMRM 17th Scientific Meeting & Exhibition (ISMRM 2009, 18/04/2009- 24/04/2009, Honolulu, Hawai). Published in Proc Intl Soc Mag Reson Med Vol.17 p 4345.

Chavarrías, C., Benito, M., Montesinos, P., García-Vázquez, V., Taylor, J., Goiriena, E., Desco, M. Adquisición de imágenes de resonancia magnética funcional

(fMRI) en cerebro de rata. XXVII Congreso Anual de la Sociedad Española de Ingeniería Biomédica (CASEIB 2009, 18/11/2009- 20/11/2009, Cádiz, Spain). Published in Actas del XXVII Congreso Anual de la Sociedad Española de Ingeniería Biomédica (CASEIB) p 117-120 (Universidad de Cádiz).

Benito, M., Rodríguez-Ruano, A., **Chavarrías, C**., Montesinos, P., Desco, M. Vessel contrast in Susceptibility Weigthed Imaging (SWI) under inhalated anesthesia with different oxygen pressure. The ISMRM-ESMRMB Joint Annual Meeting (ISMRM 2010, 01/05/2010- 07/05/2010, Stockholm, Sweden). Published in Proc Intl Soc Mag Reson Med Vol.18 p 4451.

Carcavilla, A., Reig, S., Santomé, L., Guillén-Navarro, E., Lapunzina, P., López-Siguero, J.P., Sánchez del Pozo, J., Alonso, M., García-Sagredo, J.M., Pérez-Aytés, A., Pinto, I., **Chavarrías, C.**, Aragonés, A., Desco, M., Ezquieta, B. Morphometric analysis of facial photographs as a diagnostic tool in Noonan syndrome. 49th Annual Meeting of the European Society for Paediatric Endocrinology (ESPE 2010, 22/09/2010- 25/09/2010, Prague, Czech Republic). Published in Horm Res Paediatr 2010 74 Supl.3 p 106.

Montesinos, P., Benito, M., **Chavarrías, C**., Vaquero, J.J., Desco, M. MP2RAGE: una secuencia ponderada en T1 puro insensible a densidad protónica, contraste T2* e inhomogeneidades de campo. XXVIII Congreso Anual de la Sociedad Española de Ingeniería Biomédica (CASEIB 2010, 24/11/2010- 26/11/2010, Madrid, Spain). Published in Libro de actas del XXVIII Congreso Anual de la Sociedad Española de Ingeniería Biomédica (CASEIB) p 211.

López-Miranda, V., Cussó, L., González, C., Soto-Montenegro, M.L., Herradón, E., Vera, G., Cabezos, P.A., Benito, M., **Chavarrías, C**., Desco, M., Abalo, R., Martín, M.I. Cardiac disturbances in zucker diabetic fatty rats: effect of a chronic resveratrol treatment. 4th International Congress on Prediabetes and the Metabolic Syndrome (06/04/2011- 09/04/2011, Madrid, Spain). Published in Journal of Diabetes 3(S1) p 212.

Montesinos, P., Pérez-Juste Abascal, J.F., Chamorro, J., **Chavarrías, C**., Benito, M., Vaquero, J.J., Desco, M. High-Resolution Dynamic Cardiac MRI on Small Animals Using Reconstruction Based on Split Bregman Methodology. IEEE Nuclear Science Symposium and Medical Imaging Conference (2011 NSS-MIC, 23/10/2011- 29/10/2011, Valencia, Spain). Published in Abstract Book of the IEEE Nuclear Science Symposium and Medical Imaging Conference p 349.

Abascal, J.F., Sisniega, A., **Chavarrías, C.**, Vaquero, J.J., Desco, M., Abella, M. Investigation of Different Compressed Sensing Approaches for Respiratory Gating in Small Animal CT. IEEE Nuclear Science Symposium and Medical Imaging Conference (IEEE 2012, 27/10/2012- 03/11/2012, Anaheim, California, USA). Published in 2012 IEEE Nuclear Science Symposium and Medical Imaging Conference Record (NSS/MIC) p 3344-3346.

Sisniega, A., **Chavarrías, C**., Ezquieta, B., Carcavilla, A., Ramos, F.J., Desco, M. Clasificación de niños con síndromes de Noonan y Cornelia de Lange mediante análisis morfométrico facial 2D: un estudio preliminar. XXX Congreso Anual de la Sociedad Española de Ingeniería Biomédica (CASEIB 2012, 19/11/2012- 21/11/2012, San Sebastián, Spain). Published in Libro de Actas XXX CASEIB 2012

García-Vázquez, V., Cussó, L., Chamorro-Servent, J., Mirones, I., García-Castro, J., López-Sánchez, L., Peña-Zalbidea, S., Montesinos, P., **Chavarrías, C**., Pascau, J., Desco, M. Registration of Small-Animal SPECT/MRI Studies for Tracking Human Mesenchymal Stem Cells. XIII Mediterranean Conference on Medical and Biological Engineering and Computing 2013 (MEDICON 2013, 25/09/2013- 28/09/2013, Sevilla, Spain). Published in IFMBE Proceedings Vol 41 p 399-402.

Montesinos, P., Abascal, J.F.P.J., **Chavarrías, C**., Vaquero, J.J., Desco, M. Compressed Sensing for Cardiac MRI Cine Sequences: A Real Implementation on a Small-Animal Scanner. XIII Mediterranean Conference

on Medical and Biological Engineering and Computing 2013 (MEDICON 2013, 25/09/2013- 28/09/2013, Sevilla, Spain). Published in IFMBE Proceedings Vol 41 p 214-217.

10 REFERENCES

[1] *Logothetis, N.K.,"The underpinnings of the BOLD functional magnetic resonance imaging signal". J. Neurosci.,* ***23****(10): p. 3963-71 (2003).*

[2] *Logothetis, N.K.,"What we can do and what we cannot do with fMRI". Nature,* ***453****(7197): p. 869-878 (2008).*

[3] *Martin, C.,"Contributions and complexities from the use of in vivo animal models to improve understanding of human neuroimaging signals". Front. Neurosci.,* ***8****: p. 211 (2014).*

[4] *Smucny, J., Wylie, K.P. and Tregellas, J.R.,"Functional magnetic resonance imaging of intrinsic brain networks for translational drug discovery". Trends Pharmacol. Sci.,* ***35****(8): p. 397-403 (2014).*

[5] *Wise, R.G. and Tracey, I.,"The role of fMRI in drug discovery". J. Magn. Reson. Imaging,* ***23****(6): p. 862-876 (2006).*

[6] *Zhao, F., Welsh, D., Williams, M., Coimbra, A., Urban, M.O., Hargreaves, R., Evelhoch, J. and Williams, D.S.,"fMRI of pain processing in the brain: a within-animal comparative study of BOLD vs. CBV and noxious electrical vs. noxious mechanical stimulation in rat". NeuroImage,* ***59****(2): p. 1168-79 (2012).*

[7] *Silverman, J. and Muir, W.W.,"A review of laboratory animal anesthesia with chloral hydrate and chloralose". Lab Anim Sci,* ***43****(3): p. 210-216 (1993).*

[8] *Ueki, M., Mies, G. and Hossmann, K.A.,"Effect of alpha-chloralose, halothane, pentobarbital and nitrous oxide anesthesia on metabolic coupling in somatosensory cortex of rat". Acta Anaesthesiol Scand,* ***36****(4): p. 318-22 (1992).*

[9] *Gaertner, D.J., Hallman, T.M., Hankenson, F.C. and Batchelder, M.A., Chapter 10 - Anesthesia and Analgesia for Laboratory Rodents, in Anesthesia and Analgesia in Laboratory Animals (Second Edition), R.E. Fish, et al., Editors. 2008, Academic Press: San Diego. p. 239-297.*

[10] *Masamoto, K., Kim, T., Fukuda, M., Wang, P. and Kim, S.G.,"Relationship between neural, vascular, and BOLD signals in isoflurane-anesthetized rat somatosensory cortex". Cereb. Cortex,* ***17****(4): p. 942-50 (2007).*

[11] *Pawela, C.P., Biswal, B.B., Hudetz, A.G., Schulte, M.L., Li, R., Jones, S.R., Cho, Y.R., Matloub, H.S. and Hyde, J.S.,"A protocol for use of medetomidine anesthesia in rats for extended studies using task-induced BOLD contrast and*

resting-state functional connectivity". NeuroImage, ***46****(4): p. 1137-1147 (2009).*

[12] *Sanganahalli, B.G., Herman, P., Blumenfeld, H. and Hyder, F. "Comparision of α-chloralose and domitor anesthesia for fMRI and electrophysiology studies" in Proc. Intl. Soc. Magn. Reson. Med. (2009), p. 3723.*

[13] *Sommers, M.G., van Egmond, J., Booij, L.H. and Heerschap, A.,"Isoflurane anesthesia is a valuable alternative for alpha-chloralose anesthesia in the forepaw stimulation model in rats". NMR Biomed.,* ***22****(4): p. 414-8 (2009).*

[14] *Weber, R., Ramos-Cabrer, P., Wiedermann, D., van Camp, N. and Hoehn, M.,"A fully noninvasive and robust experimental protocol for longitudinal fMRI studies in the rat". Neuroimage,* ***29****(4): p. 1303-10 (2006).*

[15] *Patel, S.S. and Goa, K.L.,"Sevoflurane. A review of its pharmacodynamic and pharmacokinetic properties and its clinical use in general anaesthesia". Drugs,* ***51****(4): p. 658-700 (1996).*

[16] *Griswold, M.A., Jakob, P.M., Heidemann, R.M., Nittka, M., Jellus, V., Wang, J., Kiefer, B. and Haase, A.,"Generalized autocalibrating partially parallel acquisitions (GRAPPA)". Magn. Reson. Med.,* ***47****(6): p. 1202-10 (2002).*

[17] *Pruessmann, K.P., Weiger, M., Scheidegger, M.B. and Boesiger, P.,"SENSE: sensitivity encoding for fast MRI". Magn. Reson. Med.,* ***42****(5): p. 952-62 (1999).*

[18] *Feinberg, D.A., Reese, T.G. and Wedeen, V.J.,"Simultaneous echo refocusing in EPI". Magn. Reson. Med.,* ***48****(1): p. 1-5 (2002).*

[19] *Moeller, S., Yacoub, E., Olman, C.A., Auerbach, E., Strupp, J., Harel, N. and Uğurbil, K.,"Multiband multislice GE-EPI at 7 tesla, with 16-fold acceleration using partial parallel imaging with application to high spatial and temporal whole-brain fMRI". Magn. Reson. Med.,* ***63****(5): p. 1144-1153 (2010).*

[20] *Lee, G.R., Griswold, M.A. and Tkach, J.A.,"Rapid 3D radial multi-echo functional magnetic resonance imaging". NeuroImage,* ***52****(4): p. 1428-1443 (2010).*

[21] *Poser, B.A., Koopmans, P.J., Witzel, T., Wald, L.L. and Barth, M.,"Three dimensional echo-planar imaging at 7 Tesla". NeuroImage,* ***51****(1): p. 261-266 (2010).*

[22] *Posse, S., Ackley, E., Mutihac, R., Rick, J., Shane, M., Murray-Krezan, C., Zaitsev, M. and Speck, O.,"Enhancement of temporal resolution and BOLD sensitivity in real-time fMRI using multi-slab echo-volumar imaging". NeuroImage,* ***61****(1): p. 115-130 (2012).*

[23] *Candes, E.J., Romberg, J. and Tao, T.,"Robust uncertainty principles: Exact signal reconstruction from highly incomplete frequency information". IEEE Trans. Inf. Theory,* ***52****(2): p. 489-509 (2006).*

[24] *Donoho, D.L.,"Compressed sensing". IEEE Trans. Inf. Theory,* ***52****(4): p. 1289-1306 (2006).*

[25] *Lustig, M., Donoho, D. and Pauly, J.M.,"Sparse MRI: The application of compressed sensing for rapid MR imaging". Magn. Reson. Med.,* ***58****(6): p. 1182-1195 (2007).*

[26] *Lustig, M., Santos, J.M., Donoho, D. and Pauly, J.M. "k-t SPARSE : High frame rate dynamic MRI exploiting spatio-temporal sparsity" in Proc. Intl. Soc. Magn. Reson. Med. (2006), p. 2420.*

[27] *Jung, H., Sung, K., Nayak, K.S., Kim, E.Y. and Ye, J.C.,"k-t FOCUSS: A general compressed sensing framework for high resolution dynamic MRI". Magn. Reson. Med.,* ***61****(1): p. 103-116 (2009).*

[28] *Nguyen, H. and Glover, G. "A Generalized Series Approach to Sparsely-Sampled fMRI" in Proc. Intl. Soc. Magn. Reson. Med. (2013), p. 2676.*

[29] *Chiew, M., Smith, S.M., Koopmans, P.J., Graedel, N.N., Blumensath, T. and Miller, K.L. "k-t FASTER: Acceleration of functional MRI data acquisition using low rank constraints" in Magn. Reson. Med. Vol. early view August 2014. (2014, early view August).*

[30] *Fischl, B.,"FreeSurfer". NeuroImage,* ***62****(2): p. 774-781 (2012).*

[31] *Friston, K., Ashburner, J., Kiebel, S., Nichols, T. and Penny, W., (2007).Statistical Parametric Mapping: The Analysis of Functional Brain Images edited by K. Friston, et al. (Academic Press, Elsevier).*

[32] *Friston, K.J., Holmes, A.P., Poline, J.B., Grasby, P.J., Williams, S.C.R., Frackowiak, R.S.J. and Turner, R.,"Analysis of fMRI Time-Series Revisited". NeuroImage,* ***2****(1): p. 45-53 (1995).*

[33] *Worsley, K.J. and Friston, K.J.,"Analysis of fMRI Time-Series Revisited—Again". NeuroImage,* ***2****(3): p. 173-181 (1995).*

[34] *Cox, R.W.,"AFNI: Software for Analysis and Visualization of Functional Magnetic Resonance Neuroimages". Computers and Biomedical Research,* ***29****(3): p. 162-173 (1996).*

[35] *Beckmann, C.F., Jenkinson, M., Woolrich, M.W., Behrens, T.E.J., Flitney, D.E., Devlin, J.T. and Smith, S.M.,"Applying FSL to the FIAC data: Model-based and model-free analysis of voice and sentence repetition priming". Hum. Brain Mapp.,* ***27****(5): p. 380-391 (2006).*

[36] *Ogawa, S., Lee, T.M., Kay, A.R. and Tank, D.W.,"Brain magnetic resonance imaging with contrast dependent on blood oxygenation". Proc. Natl. Acad. Sci. U. S. A.,* ***87****: p. 9868-9872 (1990b).*

[37] *Ogawa, S., Lee, T.M., Nayak, A.S. and Glynn, P.,"Oxygenation-sensitive contrast in magnetic resonance image of rodent brain at high magnetic fields". Magn. Reson. Med.,* ***14****: p. 68-78 (1990a).*

[38] *Pauling, L. and Coryell, C.D.,"The Magnetic Properties and Structure of Hemoglobin, Oxyhemoglobin and Carbonmonoxyhemoglobin". Proc. Natl. Acad. Sci. U. S. A.,* ***22****(4): p. 210-6 (1936).*

[39] *Hyder, F., Behar, K., Martin, M. and Shulman, R. "Activation of the somatosensory motor cortex in anesthetized rats during forepaw stimulation localized by magnetic resonance imaging" in Proc. Intl. Soc. Magn. Reson. Med. Vol. S3. (1993), p. 1379.*

[40] *Uğurbil, K.,"Two decades of functional imaging with magnetic resonance: from nuclear spins to cortical columns". Cognitive Critique,* ***4****: p. 121 (2011).*

[41] *Di Salle, F., Formisano, E., Linden, D.E., Goebel, R., Bonavita, S., Pepino, A., Smaltino, F. and Tedeschi, G.,"Exploring brain function with magnetic resonance imaging". Eur. J. Radiol,* ***30****(2): p. 84-94 (1999).*

[42] *Hu, X. and Yacoub, E.,"The story of the initial dip in fMRI". NeuroImage,* ***62****(2): p. 1103-8 (2012).*

[43] *Buxton, R.B., Wong, E.C. and Frank, L.R.,"Dynamics of blood flow and oxygenation changes during brain activation: the balloon model". Magn. Reson. Med.,* ***39****(6): p. 855-64 (1998).*

[44] *Davis, T.L., Kwong, K.K., Weisskoff, R.M. and Rosen, B.R.,"Calibrated functional MRI: mapping the dynamics of oxidative metabolism". Proc. Natl. Acad. Sci. U. S. A.,* ***95****(4): p. 1834-9 (1998).*

[45] *Hyder, F.,"Neuroimaging with calibrated FMRI". Stroke,* ***35****(11 Suppl 1): p. 2635-41 (2004).*

[46] *Martin, C., Martindale, J., Berwick, J. and Mayhew, J.,"Investigating neural–hemodynamic coupling and the hemodynamic response function in the awake rat". NeuroImage,* ***32****(1): p. 33-48 (2006).*

[47] *Iadecola, C. and Nedergaard, M.,"Glial regulation of the cerebral microvasculature". Nat. Neurosci.,* ***10****(11): p. 1369-1376 (2007).*

[48] *Logothetis, N.K.,"The ins and outs of fMRI signals". Nat. Neurosci.,* ***10****(10): p. 1230-1232 (2007).*

[49] *Colonnese, M.T., Phillips, M.A., Constantine-Paton, M., Kaila, K. and Jasanoff, A.,"Development of hemodynamic responses and functional connectivity in rat somatosensory cortex". Nat. Neurosci.,* ***11****(1): p. 72-79 (2008).*

[50] *Hyder, F. and Rothman, D.L.,"Quantitative fMRI and oxidative neuroenergetics". NeuroImage,* ***62****(2): p. 985-94 (2012).*

[51] *Liao, L.-D., Lin, C.-T., Shih, Y.-Y.I., Lai, H.-Y., Zhao, W.-T., Duong, T.Q., Chang, J.-Y., Chen, Y.-Y. and Li, M.-L.,"Investigation of the cerebral hemodynamic response function in single blood vessels by functional photoacoustic microscopy". J. Biomed. Opt., **17**(6): p. 061210 (2012).*

[52] *Urban, A., Mace, E., Brunner, C., Heidmann, M., Rossier, J. and Montaldo, G.,"Chronic assessment of cerebral hemodynamics during rat forepaw electrical stimulation using functional ultrasound imaging". NeuroImage, **101**(0): p. 138-149 (2014).*

[53] *Kainerstorfer, J.M., Sassaroli, A., Tgavalekos, K.T. and Fantini, S.,"Cerebral autoregulation in the microvasculature measured with near-infrared spectroscopy". J. Cereb. Blood Flow Metab., **35**(6): p. 959-66 (2015).*

[54] *Budohoski, K.P., Czosnyka, M., Kirkpatrick, P.J., Smielewski, P., Steiner, L.A. and Pickard, J.D.,"Clinical relevance of cerebral autoregulation following subarachnoid haemorrhage". Nat Rev Neurol, **9**(3): p. 152-163 (2013).*

[55] *Lassen, N.A.,"Cerebral Blood Flow and Oxygen Consumption in Man". Physiol. Rev., **39**(2): p. 183-238 (1959).*

[56] *Brew, N., Walker, D. and Wong, F.Y.,"Cerebral vascular regulation and brain injury in preterm infants". Am. J. Physiol.-Regul. Integr. Comp. Physiol., **306**(11): p. R773-86 (2014).*

[57] *Hamner, J.W. and Tan, C.O.,"Relative Contributions of Sympathetic, Cholinergic, and Myogenic Mechanisms to Cerebral Autoregulation". Stroke, **45**(6): p. 1771-1777 (2014).*

[58] *Attwell, D., Buchan, A.M., Charpak, S., Lauritzen, M., Macvicar, B.A. and Newman, E.A.,"Glial and neuronal control of brain blood flow". Nature, **468**(7321): p. 232-43 (2010).*

[59] *Sofroniew, M. and Vinters, H.,"Astrocytes: biology and pathology". Acta Neuropathol., **119**(1): p. 7-35 (2010).*

[60] *Meng, L. and Gelb, A.W.,"Regulation of cerebral autoregulation by carbon dioxide". Anesthesiology, **122**(1): p. 196-205 (2015).*

[61] *Caffrey, M.K. and Febo, M.,"Cocaine-associated odor cue re-exposure increases blood oxygenation level dependent signal in memory and reward regions of the maternal rat brain". Drug Alcohol Depend., **134**: p. 167-177 (2014).*

[62] *Longden, T.A., Dabertrand, F., Hill-Eubanks, D.C., Hammack, S.E. and Nelson, M.T.,"Stress-induced glucocorticoid signaling remodels neurovascular coupling through impairment of cerebrovascular inwardly rectifying K+ channel function". Proc. Natl. Acad. Sci. U. S. A., **111**(20): p. 7462-7 (2014).*

[63] *Tuor, U.I., McKenzie, E. and Tomanek, B.,"Functional magnetic resonance imaging of tonic pain and vasopressor effects in rats". Magn. Reson. Imaging, **20**(10): p. 707-12 (2002).*

[64] *Devor, A., Dunn, A.K., Andermann, M.L., Ulbert, I., Boas, D.A. and Dale, A.M.,"Coupling of total hemoglobin concentration, oxygenation, and neural activity in rat somatosensory cortex". Neuron,* ***39****(2): p. 353-9 (2003).*

[65] *Sirotin, Y.B. and Das, A.,"Anticipatory haemodynamic signals in sensory cortex not predicted by local neuronal activity". Nature,* ***457****(7228): p. 475-9 (2009).*

[66] *Smith, A.J., Blumenfeld, H., Behar, K.L., Rothman, D.L., Shulman, R.G. and Hyder, F.,"Cerebral energetics and spiking frequency: the neurophysiological basis of fMRI". Proc Natl Acad Sci U S A,* ***99****(16): p. 10765-70 (2002).*

[67] *Zhao, F., Wang, P., Hendrich, K., Ugurbil, K. and Kim, S.G.,"Cortical layer-dependent BOLD and CBV responses measured by spin-echo and gradient-echo fMRI: insights into hemodynamic regulation". NeuroImage,* ***30****(4): p. 1149-60 (2006).*

[68] *Yu, X., Glen, D., Wang, S., Dodd, S., Hirano, Y., Saad, Z., Reynolds, R., Silva, A.C. and Koretsky, A.P.,"Direct imaging of macrovascular and microvascular contributions to BOLD fMRI in layers IV-V of the rat whisker-barrel cortex". NeuroImage,* ***59****(2): p. 1451-60 (2012).*

[69] *Bosshard, S.C., Baltes, C., Wyss, M.T., Mueggler, T., Weber, B. and Rudin, M.,"Assessment of brain responses to innocuous and noxious electrical forepaw stimulation in mice using BOLD fMRI". Pain,* ***151****(3): p. 655-63 (2010).*

[70] *Chang, C. and Shyu, B.C.,"A fMRI study of brain activations during non-noxious and noxious electrical stimulation of the sciatic nerve of rats". Brain Res,* ***897****(1-2): p. 71-81 (2001).*

[71] *Governo, M.R.J., Morris, P.G., Prior, M.J., Marsden, C.A. and Chapman, V.,"Capsaicin-evoked brain activation and central sensitization in anaesthetised rats: a functional magnetic resonance imaging study". Pain,* ***126****(1-3): p. 35-45 (2006).*

[72] *Governo, R.J., Morris, P.G., Marsden, C.A. and Chapman, V.,"Gabapentin evoked changes in functional activity in nociceptive regions in the brain of the anaesthetized rat: an fMRI study". Br J Pharmacol,* ***153****(7): p. 1558-67 (2008).*

[73] *Governo, R.J., Prior, M.J., Morris, P.G., Marsden, C.A. and Chapman, V.,"Validation of an automated punctate mechanical stimuli delivery system designed for fMRI studies in rodents". J Neurosci Methods,* ***163****(1): p. 31-7 (2007).*

[74] *Lowe, A.S., Beech, J.S. and Williams, S.C.,"Small animal, whole brain fMRI: innocuous and nociceptive forepaw stimulation". NeuroImage,* ***35****(2): p. 719-28 (2007).*

[75] *Malisza, K.L. and Docherty, J.C.,"Capsaicin as a source for painful stimulation in functional MRI". J Magn Reson Imaging,* ***14****(4): p. 341-7 (2001).*

[76] *Malisza, K.L., Gregorash, L., Turner, A., Foniok, T., Stroman, P.W., Allman, A.A., Summers, R. and Wright, A.,"Functional MRI involving painful stimulation of the ankle and the effect of physiotherapy joint mobilization". Magn Reson Imaging,* ***21****(5): p. 489-96 (2003).*

[77] *Tuor, U.I., Malisza, K., Foniok, T., Papadimitropoulos, R., Jarmasz, M., Somorjai, R. and Kozlowski, P.,"Functional magnetic resonance imaging in rats subjected to intense electrical and noxious chemical stimulation of the forepaw". Pain,* ***87****(3): p. 315-24 (2000).*

[78] *Hess, A., Sergejeva, M., Budinsky, L., Zeilhofer, H.U. and Brune, K.,"Imaging of hyperalgesia in rats by functional MRI". Eur J Pain,* ***11****(1): p. 109-19 (2007).*

[79] *Matthews, P.M., Pharmacological Applications of fMRI, in fMRI Techniques and Protocols, M. Filippi, Editor. 2009. p. 751-767.*

[80] *Grohn, O.H. and Kauppinen, R.A.,"Assessment of brain tissue viability in acute ischemic stroke by BOLD MRI". NMR Biomed,* ***14****(7-8): p. 432-40 (2001).*

[81] *Kim, Y.R., Huang, I.J., Lee, S.R., Tejima, E., Mandeville, J.B., van Meer, M.P., Dai, G., Choi, Y.W., Dijkhuizen, R.M., Lo, E.H. and Rosen, B.R.,"Measurements of BOLD/CBV ratio show altered fMRI hemodynamics during stroke recovery in rats". J Cereb Blood Flow Metab,* ***25****(7): p. 820-9 (2005).*

[82] *Shen, Q., Ren, H., Cheng, H., Fisher, M. and Duong, T.Q.,"Functional, perfusion and diffusion MRI of acute focal ischemic brain injury". J Cereb Blood Flow Metab,* ***25****(10): p. 1265-79 (2005).*

[83] *Dijkhuizen, R.M., Ren, J., Mandeville, J.B., Wu, O., Ozdag, F.M., Moskowitz, M.A., Rosen, B.R. and Finklestein, S.P.,"Functional magnetic resonance imaging of reorganization in rat brain after stroke". Proc Natl Acad Sci U S A,* ***98****(22): p. 12766-71 (2001).*

[84] *Goloshevsky, A.G., Wu, C.W., Dodd, S.J. and Koretsky, A.P.,"Mapping cortical representations of the rodent forepaw and hindpaw with BOLD fMRI reveals two spatial boundaries". NeuroImage,* ***57****(2): p. 526-38 (2011).*

[85] *Pawela, C.P., Biswal, B.B., Hudetz, A.G., Li, R., Jones, S.R., Cho, Y.R., Matloub, H.S. and Hyde, J.S.,"Interhemispheric neuroplasticity following limb deafferentation detected by resting-state functional connectivity magnetic resonance imaging (fcMRI) and functional magnetic resonance imaging (fMRI)". NeuroImage,* ***49****(3): p. 2467-78 (2010).*

[86] *Endo, T., Spenger, C., Hao, J., Tominaga, T., Wiesenfeld-Hallin, Z., Olson, L. and Xu, X.J.,"Functional MRI of the brain detects neuropathic pain in experimental spinal cord injury". Pain,* ***138****(2): p. 292-300 (2008).*

[87] *Endo, T., Spenger, C., Tominaga, T., Brene, S. and Olson, L.,"Cortical sensory map rearrangement after spinal cord injury: fMRI responses linked to Nogo signalling". Brain,* ***130****(Pt 11): p. 2951-61 (2007).*

[88] *Ghosh, A., Sydekum, E., Haiss, F., Peduzzi, S., Zorner, B., Schneider, R., Baltes, C., Rudin, M., Weber, B. and Schwab, M.E.,"Functional and anatomical reorganization of the sensory-motor cortex after incomplete spinal cord injury in adult rats". J Neurosci,* ***29****(39): p. 12210-9 (2009).*

[89] *Benson, R.R., FitzGerald, D.B., LeSueur, L.L., Kennedy, D.N., Kwong, K.K., Buchbinder, B.R., Davis, T.L., Weisskoff, R.M., Talavage, T.M., Logan, W.J., Cosgrove, G.R., Belliveau, J.W. and Rosen, B.R.,"Language dominance determined by whole brain functional MRI in patients with brain lesions". Neurology,* ***52****(4): p. 798-809 (1999).*

[90] *Gotman, J.,"Epileptic networks studied with EEG-fMRI". Epilepsia,* ***49 Suppl 3****: p. 42-51 (2008).*

[91] *Hertz-Pannier, L., Chiron, C., Jambaque, I., Renaux-Kieffer, V., Van de Moortele, P.F., Delalande, O., Fohlen, M., Brunelle, F. and Le Bihan, D.,"Late plasticity for language in a child's non-dominant hemisphere: a pre- and post-surgery fMRI study". Brain,* ***125****(Pt 2): p. 361-72 (2002).*

[92] *Lehericy, S., Cohen, L., Bazin, B., Samson, S., Giacomini, E., Rougetet, R., Hertz-Pannier, L., Le Bihan, D., Marsault, C. and Baulac, M.,"Functional MR evaluation of temporal and frontal language dominance compared with the Wada test". Neurology,* ***54****(8): p. 1625-33 (2000).*

[93] *Mueller, W.M., Yetkin, F.Z., Hammeke, T.A., Morris, G.L., 3rd, Swanson, S.J., Reichert, K., Cox, R. and Haughton, V.M.,"Functional magnetic resonance imaging mapping of the motor cortex in patients with cerebral tumors". Neurosurgery,* ***39****(3): p. 515-20; discussion 520-1 (1996).*

[94] *Tieleman, A., Deblaere, K., Van Roost, D., Van Damme, O. and Achten, E.,"Preoperative fMRI in tumour surgery". Eur Radiol,* ***19****(10): p. 2523-34 (2009).*

[95] *Dobkin, B.H., Firestine, A., West, M., Saremi, K. and Woods, R.,"Ankle dorsiflexion as an fMRI paradigm to assay motor control for walking during rehabilitation". NeuroImage,* ***23****(1): p. 370-81 (2004).*

[96] *Barcia, J.A., Sanz, A., Balugo, P., Alonso-Lera, P., Brin, J.R., Yus, M., Gonzalez-Hidalgo, M., Acedo, V.M. and Oliviero, A.,"High-frequency cortical subdural stimulation enhanced plasticity in surgery of a tumor in Broca's area". Neuroreport,* ***23****(5): p. 304-9 (2012).*

[97] *Blatow, M., Delmaire, C., Duffau, H., Eyssen, M., Goebel, R., Juengling, F.D., Kassubek, J., Kovacs, S., Krakow, K., Lehéricy, S., Lengler, U., Naidich, T.P., Peeters, R., Sage, C., Stippich, C., Sunaert, S., Thomas, B., Tronnier, V., Moortele, P.-F.V.d. and Yousry, T.A., (2007).Clinical Functional MRI.*

Presurgical Functional Neuroimaging edited by M. Stippich C. (Springer Berlin Heidelberg).

[98] *Hyder, F., Behar, K.L., Martin, M.A., Blamire, A.M. and Shulman, R.G.,"Dynamic magnetic resonance imaging of the rat brain during forepaw stimulation". J Cereb Blood Flow Metab,* ***14****(4): p. 649-55 (1994).*

[99] *Gyngell, M.L., Bock, C., Schmitz, B., Hoehn-Berlage, M. and Hossmann, K.A.,"Variation of functional MRI signal in response to frequency of somatosensory stimulation in alpha-chloralose anesthetized rats". Magn Reson Med,* ***36****(1): p. 13-5 (1996).*

[100] *Keilholz, S.D., Silva, A.C., Raman, M., Merkle, H. and Koretsky, A.P.,"Functional MRI of the rodent somatosensory pathway using multislice echo planar imaging". Magn Reson Med,* ***52****(1): p. 89-99 (2004).*

[101] *Austin, V.C., Blamire, A.M., Allers, K.A., Sharp, T., Styles, P., Matthews, P.M. and Sibson, N.R.,"Confounding effects of anesthesia on functional activation in rodent brain: a study of halothane and alpha-chloralose anesthesia". Neuroimage,* ***24****(1): p. 92-100 (2005).*

[102] *Kida, I. and Yamamoto, T.,"Stimulus frequency dependence of blood oxygenation level-dependent functional magnetic resonance imaging signals in the somatosensory cortex of rats". Neurosci Res,* ***62****(1): p. 25-31 (2008).*

[103] *Lawrence, J., Stroman, P.W. and Malisza, K.L.,"Functional MRI of the cervical spinal cord during noxious and innocuous thermal stimulation in the alpha-chloralose- and halothane-anesthetized rat". Magn. Reson. Imaging,* ***26****(1): p. 1-10 (2008).*

[104] *de Celis Alonso, B., Makarova, T. and Hess, A.,"On the use of alpha-chloralose for repeated BOLD fMRI measurements in rats". J Neurosci Methods,* ***195****(2): p. 236-40 (2011).*

[105] *Zong, X., Lee, J., John Poplawsky, A., Kim, S.-G. and Ye, J.C.,"Compressed sensing fMRI using gradient-recalled echo and EPI sequences". NeuroImage,* ***92****(0): p. 312-321 (2014).*

[106] *Van Camp, N., Verhoye, M., De Zeeuw, C.I. and Van der Linden, A.,"Light stimulus frequency dependence of activity in the rat visual system as studied with high-resolution BOLD fMRI". J Neurophysiol,* ***95****(5): p. 3164-70 (2006).*

[107] *Pawela, C.P., Hudetz, A.G., Ward, B.D., Schulte, M.L., Li, R., Kao, D.S., Mauck, M.C., Cho, Y.R., Neitz, J. and Hyde, J.S.,"Modeling of region-specific fMRI BOLD neurovascular response functions in rat brain reveals residual differences that correlate with the differences in regional evoked potentials". NeuroImage,* ***41****(2): p. 525-34 (2008).*

[108] *Bonvento, G., Charbonne, R., Correze, J.L., Borredon, J., Seylaz, J. and Lacombe, P.,"Is alpha-chloralose plus halothane induction a suitable anesthetic*

regimen for cerebrovascular research?". Brain Res., ***665****(2): p. 213-21 (1994).*

[109] *Sicard, K., Shen, Q., Brevard, M.E., Sullivan, R., Ferris, C.F., King, J.A. and Duong, T.Q.,"Regional cerebral blood flow and BOLD responses in conscious and anesthetized rats under basal and hypercapnic conditions: implications for functional MRI studies". J. Cereb. Blood Flow Metab.,* ***23****(4): p. 472-81 (2003).*

[110] *Stefanovic, B., Warnking, J.M., Rylander, K.M. and Pike, G.B.,"The effect of global cerebral vasodilation on focal activation hemodynamics". NeuroImage,* ***30****(3): p. 726-34 (2006).*

[111] *Kolbitsch, C., Lorenz, I.H., Hormann, C., Kremser, C., Schocke, M., Felber, S., Moser, P.L., Hinteregger, M., Pfeiffer, K.P. and Benzer, A.,"Sevoflurane and nitrous oxide increase regional cerebral blood flow (rCBF) and regional cerebral blood volume (rCBV) in a drug-specific manner in human volunteers". Magn. Reson. Imaging,* ***19****(10): p. 1253-60 (2001).*

[112] *Alkire, M.T., Hudetz, A.G. and Tononi, G.,"Consciousness and anesthesia". Science,* ***322****(5903): p. 876-80 (2008).*

[113] *Sommers, M.G., van Egmond, J., Booij, L.H. and Heerschap, A.,"Isoflurane anesthesia is a valuable alternative for alpha-chloralose anesthesia in the forepaw stimulation model in rats". NMR Biomed,* ***22****(4): p. 414-8 (2009).*

[114] *Goense, J.B. and Logothetis, N.K.,"Neurophysiology of the BOLD fMRI signal in awake monkeys". Curr. Biol.,* ***18****(9): p. 631-40 (2008).*

[115] *Peeters, R.R., Tindemans, I., De Schutter, E. and Van der Linden, A.,"Comparing BOLD fMRI signal changes in the awake and anesthetized rat during electrical forepaw stimulation". Magn. Reson. Imaging,* ***19****(6): p. 821-6 (2001).*

[116] *Erdos, B., Lacza, Z., Toth, I.E., Szelke, E., Mersich, T., Komjati, K., Palkovits, M. and Sandor, P.,"Mechanisms of pain-induced local cerebral blood flow changes in the rat sensory cortex and thalamus". Brain Res.,* ***960****(1-2): p. 219-27 (2003).*

[117] *Deshpande, G., Kerssens, C., Sebel, P.S. and Hu, X.,"Altered local coherence in the default mode network due to sevoflurane anesthesia". Brain Res.,* ***1318****: p. 110-21 (2010).*

[118] *Goa, K.L., Noble, S. and Spencer, C.M.,"Sevoflurane in paediatric anaesthesia: a review". Paediatr Drugs,* ***1****(2): p. 127-53 (1999).*

[119] *Lerman, J., Sikich, N., Kleinman, S. and Yentis, S.,"The pharmacology of sevoflurane in infants and children". Anesthesiology,* ***80****(4): p. 814-24 (1994).*

[120] *Peltier, S.J., Kerssens, C., Hamann, S.B., Sebel, P.S., Byas-Smith, M. and Hu, X.,"Functional connectivity changes with concentration of sevoflurane anesthesia". Neuroreport,* ***16****(3): p. 285-8 (2005).*

[121] *Qiu, M., Ramani, R., Swetye, M. and Constable, R.T.,"Spatial nonuniformity of the resting CBF and BOLD responses to sevoflurane: in vivo study of normal human subjects with magnetic resonance imaging". Hum Brain Mapp,* ***29****(12): p. 1390-9 (2008).*

[122] *Silva, A.C. and Koretsky, A.P.,"Laminar specificity of functional MRI onset times during somatosensory stimulation in rat". Proc Natl Acad Sci U S A,* ***99****(23): p. 15182-7 (2002).*

[123] *Schridde, U., Khubchandani, M., Motelow, J.E., Sanganahalli, B.G., Hyder, F. and Blumenfeld, H.,"Negative BOLD with large increases in neuronal activity". Cereb Cortex,* ***18****(8): p. 1814-27 (2008).*

[124] *Van Camp, N., D'Hooge, R., Verhoye, M., Peeters, R.R., De Deyn, P.P. and Van der Linden, A.,"Simultaneous electroencephalographic recording and functional magnetic resonance imaging during pentylenetetrazol-induced seizures in rat". NeuroImage,* ***19****(3): p. 627-36 (2003).*

[125] *Pro-Sistiaga, P., Lamberton, F., Boraud, T., Saulnier, R., Young, A.R., Bioulac, B., Gross, C. and Mazoyer, B.,"High resolution 3T fMRI in anesthetized monkeys". J Neurosci Methods,* ***205****(1): p. 86-95 (2012).*

[126] *Paul, M., Fokt, R.M., Kindler, C.H., Dipp, N.C. and Yost, C.S.,"Characterization of the interactions between volatile anesthetics and neuromuscular blockers at the muscle nicotinic acetylcholine receptor". Anesth Analg,* ***95****(2): p. 362-7, table of contents (2002).*

[127] *Borsook, D. and Becerra, L.,"CNS Animal fMRI imaging in Pain and Analgesia". Neuroscience and biobehavioral reviews,* ***35****(5): p. 1125-1143 (2011).*

[128] *Chin, C.L., Tovcimak, A.E., Hradil, V.P., Seifert, T.R., Hollingsworth, P.R., Chandran, P., Zhu, C.Z., Gauvin, D., Pai, M., Wetter, J., Hsieh, G.C., Honore, P., Frost, J.M., Dart, M.J., Meyer, M.D., Yao, B.B., Cox, B.F. and Fox, G.B.,"Differential effects of cannabinoid receptor agonists on regional brain activity using pharmacological MRI". Br J Pharmacol,* ***153****(2): p. 367-79 (2008).*

[129] *Martin, C., Jones, M., Martindale, J. and Mayhew, J.,"Haemodynamic and neural responses to hypercapnia in the awake rat". Eur J Neurosci,* ***24****(9): p. 2601-10 (2006).*

[130] *Friston, K.J., Fletcher, P., Josephs, O., Holmes, A., Rugg, M.D. and Turner, R.,"Event-related fMRI: characterizing differential responses". Neuroimage, 7(1): p. 30-40 (1998).*

[131] *Hoge, R.D., Atkinson, J., Gill, B., Crelier, G.R., Marrett, S. and Pike, G.B.,"Investigation of BOLD signal dependence on cerebral blood flow and oxygen consumption: the deoxyhemoglobin dilution model". Magn Reson Med,* ***42****(5): p. 849-63 (1999).*

[132] *Hare, H.V., Blockley, N.P., Gardener, A.G., Clare, S. and Bulte, D.P.,"Investigating the field-dependence of the Davis model: Calibrated fMRI at 1.5, 3 and 7T". NeuroImage,* ***112****: p. 189-96 (2015).*

[133] *Kim, S.G. and Ogawa, S.,"Biophysical and physiological origins of blood oxygenation level-dependent fMRI signals". J Cereb Blood Flow Metab,* ***32****(7): p. 1188-206 (2012).*

[134] *Hyder, F., Kida, I., Behar, K.L., Kennan, R.P., Maciejewski, P.K. and Rothman, D.L.,"Quantitative functional imaging of the brain: towards mapping neuronal activity by BOLD fMRI". NMR Biomed,* ***14****(7-8): p. 413-31 (2001).*

[135] *Kida, I., Kennan, R.P., Rothman, D.L., Behar, K.L. and Hyder, F.,"High-resolution CMR(O2) mapping in rat cortex: a multiparametric approach to calibration of BOLD image contrast at 7 Tesla". J Cereb Blood Flow Metab,* ***20****(5): p. 847-60 (2000).*

[136] *Hoge, R.D.,"Calibrated FMRI". NeuroImage,* ***62****(2): p. 930-7 (2012).*

[137] *Friston, K.J., Ashburner, J., Kiebel, S., Nichols, T. and Penny, W., (2007).Statistical Parametric Mapping: The Analysis of Functional Brain Images edited by K. Friston, et al. (Academic Press, Elsevier).*

[138] *Cox, R.W., Ashburner, J., Breman, H., Fissell, K., Haselgrove, C., Holmes, C.J., Lancaster, J.L., Rex, D.E., Smith, S.M., Woodward, J.B. and Strother, S.C., A (Sort of) New Image Data Format Standard: NIfTI-1, in Hum Brain Mapp 25 2004.*

[139] *Friston, K.J., Josephs, O., Zarahn, E., Holmes, A.P., Rouquette, S. and Poline, J.,"To smooth or not to smooth? Bias and efficiency in fMRI time-series analysis". NeuroImage,* ***12****(2): p. 196-208 (2000).*

[140] *Worsley, K.J.,"Spatial smoothing of autocorrelations to control the degrees of freedom in fMRI analysis". NeuroImage,* ***26****(2): p. 635-41 (2005).*

[141] *Jochimsen, T.H., Norris, D.G., Mildner, T. and Moller, H.E.,"Quantifying the intra- and extravascular contributions to spin-echo fMRI at 3 T". Magn Reson Med,* ***52****(4): p. 724-32 (2004).*

[142] *Uludag, K., Muller-Bierl, B. and Ugurbil, K.,"An integrative model for neuronal activity-induced signal changes for gradient and spin echo functional imaging". NeuroImage,* ***48****(1): p. 150-65 (2009).*

[143] *Mansfield, P.,"Multi-planar image formation using NMR spin echoes". Journal of Physics C: Solid State Physics,* ***10****(3): p. L55 (1977).*

[144] *Hyder, F., Rothman, D.L. and Blamire, A.M.,"Image reconstruction of sequentially sampled echo-planar data". Magn Reson Imaging,* ***13****(1): p. 97-103 (1995).*

[145] *Lee, G.R., Griswold, M.A. and Tkach, J.A.,"Rapid 3D radial multi-echo functional magnetic resonance imaging". NeuroImage,* ***52****(4): p. 1428-43 (2010).*

[146] *Lee, J.H., Pauly, J.M. and Nishimura, D.G. "Partial k-space reconstruction for radial k-space trajectories in magnetic resonance imaging". Patent no. US7277597 B2. 2 Oct 2007.*

[147] *Lindquist, M.A., Zhang, C.-H., Glover, G. and Shepp, L.,"Rapid three-dimensional functional magnetic resonance imaging of the initial negative BOLD response". J. Magn. Reson.,* ***191****(1): p. 100-111 (2008).*

[148] *Menon, R.G., Walsh, E.G., Twieg, D.B., Cantrell, C.G., Vakil, P., Jonathan, S.V., Batjer, H.H. and Carroll, T.J.,"Snapshot MR technique to measure OEF using rapid frequency mapping". J Cereb Blood Flow Metab,* ***34****(7): p. 1111-6 (2014).*

[149] *Pipe, J.G.,"Motion correction with PROPELLER MRI: application to head motion and free-breathing cardiac imaging". Magn Reson Med,* ***42****(5): p. 963-9 (1999).*

[150] *Shu, Y. and Bernstein, M.A. "Accelerated shells trajectory MRI acquisition". Patent no. US8214013 B2. 3 Jul 2012.*

[151] *Hu, Y. and Glover, G.H.,"Three-dimensional spiral technique for high-resolution functional MRI". Magn. Reson. Med.,* ***58****(5): p. 947-951 (2007).*

[152] *Swisher, J.D., Sexton, J.A., Gatenby, J.C., Gore, J.C. and Tong, F.,"Multishot versus single-shot pulse sequences in very high field fMRI: a comparison using retinotopic mapping". PLoS ONE,* ***7****(4): p. e34626 (2012).*

[153] *Hu, Y. and Glover, G.H.,"Partial-k-space acquisition method for improved SNR efficiency and temporal resolution in 3D fMRI". Magn Reson Med,* ***55****(5): p. 1106-13 (2006).*

[154] *Posse, S., Ackley, E., Mutihac, R., Rick, J., Shane, M., Murray-Krezan, C., Zaitsev, M. and Speck, O.,"Enhancement of temporal resolution and BOLD sensitivity in real-time fMRI using multi-slab echo-volumar imaging". NeuroImage,* ***61****(1): p. 115-30 (2012).*

[155] *Poser, B.A. and Norris, D.G.,"Investigating the benefits of multi-echo EPI for fMRI at 7 T". NeuroImage,* ***45****(4): p. 1162-72 (2009).*

[156] *Tsao, J., Boesiger, P. and Pruessmann, K.P.,"k-t BLAST and k-t SENSE: dynamic MRI with high frame rate exploiting spatiotemporal correlations". Magn Reson Med,* ***50****(5): p. 1031-42 (2003).*

[157] *Utting, J.F., Kozerke, S., Schnitker, R. and Niendorf, T.,"Comparison of k-t SENSE/k-t BLAST with conventional SENSE applied to BOLD fMRI". J Magn Reson Imaging,* ***32****(1): p. 235-41 (2010).*

[158] *Feinberg, D.A., Moeller, S., Smith, S.M., Auerbach, E., Ramanna, S., Gunther, M., Glasser, M.F., Miller, K.L., Ugurbil, K. and Yacoub, E.,"Multiplexed echo planar imaging for sub-second whole brain FMRI and fast diffusion imaging". PLoS ONE,* ***5****(12): p. e15710 (2010).*

[159] *Candès, E.J., Romberg, J.K. and Tao, T.,"Stable signal recovery from incomplete and inaccurate measurements". Communications on Pure and Applied Mathematics,* ***59****(8): p. 1207-1223 (2006).*

[160] *Abascal, J.F.P.J., Montesinos, P., Marinetto, E., Pascau, J., Vaquero, J.J. and Desco, M. "A Prior-Based Image Variation (PRIVA) Approach Applied to Motion-Based Compressed Sensing Cardiac Cine MRI" in XIII Mediterranean Conference on Medical and Biological Engineering and Computing 2013, IFMBE Proceedings, Seville, Spain. Vol. 41. (Springer International Publishing, 2013), p. 233-236.*

[161] *Montesinos, P., Abascal, J.F.P.J., Cussó, L., Vaquero, J.J. and Desco, M.,"Application of the compressed sensing technique to self-gated cardiac cine sequences in small animals". Magn. Reson. Med.,* ***72****(2): p. 369-380 (2014).*

[162] *Jung, H., Ye, J.C. and Kim, E.Y.,"Improved k-t BLAST and k-t SENSE using FOCUSS". Phys Med Biol,* ***52****(11): p. 3201-26 (2007).*

[163] *Avdal, J., Kristoffersen, A., Håberg, A. and Goa, P.E.,"Functional MRI employing Compressed Sensing and separation of signal and noise in k-space". Proc. Intl. Soc. Mag. Reson. Med. 20: p. 2269 (2012).*

[164] *Holland, D., Liu, C., Bowen, C.V., Sederman, A., Gladden, L. and Beyea, S.D.,"Highly Sparse Spiral fMRI Reconstructed with Compressed Sensing: Trajectory Optimization for BOLD Contrast". Proc. Intl. Soc. Mag. Reson. Med. 19, (2011).*

[165] *Holland, D.J., Liu, C., Song, X., Mazerolle, E.L., Stevens, M.T., Sederman, A.J., Gladden, L.F., D'Arcy, R.C.N., Bowen, C.V. and Beyea, S.D.,"Compressed sensing reconstruction improves sensitivity of variable density spiral fMRI". Magn. Reson. Med.,* ***70****(6): p. 1634-1643 (2013).*

[166] *Nguyen, H. and Glover, G. "Field-corrected imaging for sparsely-sampled fMRI by exploiting low-rank spatiotemporal structure" in Proc. Intl. Soc. Magn. Reson. Med. (2014), p. 0327.*

[167] *Jenkinson, M., Beckmann, C.F., Behrens, T.E., Woolrich, M.W. and Smith, S.M.,"Fsl". NeuroImage,* ***62****(2): p. 782-90 (2012).*

[168] *Sawiak, S.J., Wood, N.I., Williams, G.B., Morton, A.J. and Carpenter, T.A. "SPMMouse: A new toolbox for SPM in the animal brain" in Proc. Intl. Soc. Magn. Reson. Med. (2009), p. 1086.*

[169] *Bruker Biospin Paravision 5.0 Users Manual edited (Bruker AXS GmbH, Germany).*

[170] *Strupp, J.P.,"Stimulate: A GUI based fMRI analysis software package". NeuroImage, **3**(3, Supplement): p. S607 (1996).*

[171] *Zhao, F., Zhao, T., Zhou, L., Wu, Q. and Hu, X.,"BOLD study of stimulation-induced neural activity and resting-state connectivity in medetomidine-sedated rat". NeuroImage, **39**(1): p. 248-260 (2008).*

[172] *Franceschini, M.A., Radhakrishnan, H., Thakur, K., Wu, W., Ruvinskaya, S., Carp, S. and Boas, D.A.,"The effect of different anesthetics on neurovascular coupling". NeuroImage, **51**(4): p. 1367-77 (2010).*

[173] *Lindauer, U., Villringer, A. and Dirnagl, U.,"Characterization of CBF response to somatosensory stimulation: model and influence of anesthetics". Am J Physiol, **264**(4 Pt 2): p. H1223-8 (1993).*

[174] *Fish, R.E., Chapter 1 - Pharmacology of Injectable Anesthetics, in Anesthesia and Analgesia in Laboratory Animals, D.F. Kohn, et al., Editors. 1997, Academic Press: San Diego. p. 1-28.*

[175] *Ueki, M., Mies, G. and Hossmann, K.A.,"Effect of alpha-chloralose, halothane, pentobarbital and nitrous oxide anesthesia on metabolic coupling in somatosensory cortex of rat". Acta Anaesthesiol. Scand., **36**(4): p. 318-22 (1992).*

[176] *Camp, N.V., Verhoye, M. and der Linden, A.V.,"Stimulation of the rat somatosensory cortex at different frequencies and pulse widths". NMR Biomed., **19**(1): p. 10-17 (2006).*

[177] *Gyngell, M.L., Bock, C., Schmitz, B., Hoehn-Berlage, M. and Hossmann, K.A.,"Variation of functional MRI signal in response to frequency of somatosensory stimulation in alpha-chloralose anesthetized rats". Magn. Reson. Med., **36**(1): p. 13-5 (1996).*

[178] *Sommers, M.G., Pikkemaat, J.A., Booij, L.H.D.J. and Heerschap, A. "Improved anesthesia protocols for fMRI studies in rats: the use of medetomidine for stable, reversible sedation" in Proc. Intl. Soc. Mag. Reson. Med. . (2002), p. 38.*

[179] *Weber, R., Ramos-Cabrer, P., Wiedermann, D., Hoehn, M. "A robust non-invasive protocol for longitudinal fMRI studies in the rat" in Proc. Intl. Soc. Magn. Reson. Med. (2005), p. 310.*

[180] *Brunson, D.B., Chapter 2 - Pharmacology of Inhalation Anesthetics, in Anesthesia and Analgesia in Laboratory Animals, D.F. Kohn, et al., Editors. 1997, Academic Press: San Diego. p. 1-28.*

[181] *Campagna, J.A., Miller, K.W. and Forman, S.A.,"Mechanisms of Actions of Inhaled Anesthetics". New England Journal of Medicine,* ***348****(21): p. 2110-2124 (2003).*

[182] *Liu, Z.M., Schmidt, K.F., Sicard, K.M. and Duong, T.Q.,"Imaging oxygen consumption in forepaw somatosensory stimulation in rats under isoflurane anesthesia". Magn Reson Med,* ***52****(2): p. 277-85 (2004).*

[183] *Paxinos, G., Watson, C.R. and Emson, P.C.,"AChE-stained horizontal sections of the rat brain in stereotaxic coordinates". J. Neurosci. Methods,* ***3****(2): p. 129-49 (1980).*

[184] *Hyder, F., Behar, K.L., Martin, M.A., Blamire, A.M. and Shulman, R.G.,"Dynamic Magnetic Resonance Imaging of the Rat Brain During Forepaw Stimulation". J. Cereb. Blood Flow Metab.,* ***14****(4): p. 649-655 (1994).*

[185] *Poplawsky, A.J. and Kim, S.-G.,"Layer-dependent BOLD and CBV-weighted fMRI responses in the rat olfactory bulb". NeuroImage,* ***91****(0): p. 237-251 (2014).*

[186] *Madore, B., Glover, G.H. and Pelc, N.J.,"Unaliasing by fourier-encoding the overlaps using the temporal dimension (UNFOLD), applied to cardiac imaging and fMRI". Magn. Reson. Med.,* ***42****(5): p. 813-28 (1999).*

[187] *Wang, Y.L., Yang, J.F., Yin, W.T. and Zhang, Y.,"A New Alternating Minimization Algorithm for Total Variation Image Reconstruction". SIAM J. Imaging Sci.,* ***1****(3): p. 248-272 (2008).*

[188] *Yang, J., Zhang, Y. and Yin, W.,"A Fast Alternating Direction Method for TVL1-L2 Signal Reconstruction From Partial Fourier Data". IEEE J. Sel. Top. Signal Process.,* ***4****(2): p. 288-297 (2010).*

[189] *Ajraoui, S., Parra-Robles, J. and Wild, J.M.,"Incorporation of prior knowledge in compressed sensing for faster acquisition of hyperpolarized gas images". Magn. Reson. Med.,* ***69****(2): p. 360-369 (2013).*

[190] *Chavarrias, C., Abascal, J.F.P.J., Montesinos, P. and Desco, M. "How does compressed sensing affect activation maps in rat fMRI" in XIII Mediterranean Conference on Medical and Biological Engineering and Computing 2013, IFMBE Proceedings, Seville, Spain. Vol. 41. (Springer International Publishing, 2014), p. 202-205.*

[191] *Lingala, S.G., Hu, Y., DiBella, E. and Jacob, M.,"Accelerated dynamic MRI exploiting sparsity and low-rank structure: k-t SLR". IEEE Trans. Med. Imaging,* ***30****(5): p. 1042-54 (2011).*

[192] *Abascal, J.F., Abella, M., Sisniega, A., Vaquero, J.J. and Desco, M.,"Investigation of Different Sparsity Transforms for the PICCS Algorithm in Small-Animal Respiratory Gated CT". PLoS ONE,* ***10****(3): p. e0120140 (2015).*

[193] *Chen, G.H., Tang, J. and Leng, S.,"Prior image constrained compressed sensing (PICCS): a method to accurately reconstruct dynamic CT images from highly undersampled projection data sets". Med. Phys.,* ***35****(2): p. 660-3 (2008).*

[194] *Leng, S., Tang, J., Zambelli, J., Nett, B., Tolakanahalli, R. and Chen, G.H.,"High temporal resolution and streak-free four-dimensional cone-beam computed tomography". Phys. Med. Biol.,* ***53****(20): p. 5653-73 (2008).*

[195] *Nett, B.E., Brauweiler, R., Kalender, W., Rowley, H. and Chen, G.H.,"Perfusion measurements by micro-CT using prior image constrained compressed sensing (PICCS): initial phantom results". Phys. Med. Biol.,* ***55****(8): p. 2333-2350 (2010).*

[196] *Qi, Z. and Chen, G.H.,"Extraction of tumor motion trajectories using PICCS-4DCBCT: a validation study". Med. Phys.,* ***38****(10): p. 5530-8 (2011).*

[197] *Tang, J., Hsieh, J. and Chen, G.H.,"Temporal resolution improvement in cardiac CT using PICCS (TRI-PICCS): performance studies". Med. Phys.,* ***37****(8): p. 4377-88 (2010).*

[198] *Mistretta, C.A., Wieben, O., Velikina, J., Block, W., Perry, J., Wu, Y. and Johnson, K.,"Highly constrained backprojection for time-resolved MRI". Magn. Reson. Med.,* ***55****(1): p. 30-40 (2006).*

[199] *Johnson, K.M., Velikina, J., Wu, Y., Kecskemeti, S., Wieben, O. and Mistretta, C.A.,"Improved waveform fidelity using local HYPR reconstruction (HYPR LR)". Magn. Reson. Med.,* ***59****(3): p. 456-62 (2008).*

[200] *O'Halloran, R.L., Wen, Z., Holmes, J.H. and Fain, S.B.,"Iterative projection reconstruction of time-resolved images using highly-constrained back-projection (HYPR)". Magn. Reson. Med.,* ***59****(1): p. 132-9 (2008).*

[201] *Samsonov, A., Wieben, O. and Block, W. "HYPR-Constrained Compressed Sensing Reconstruction for Accelerated Time Resolved Imaging" in Proc. Intl. Soc. Magn. Reson. Med. (2008), p. 339.*

[202] *Lam, F., Zhao, B., Liu, Y., Liang, Z.-P., Weiner, M. and Schuff, N. "Accelerated fMRI using Low-Rank Model and Sparsity Constraints" in Proc. Intl. Soc. Magn. Reson. Med. (2013), p. 2620.*

[203] *Goldstein, T. and Osher, S.,"The Split Bregman Method for L1-Regularized Problems". SIAM J. Imaging Sci.,* ***2****(2): p. 323-343 (2009).*

[204] *Osher, S., Burger, M., Goldfarb, D., Xu, J.J. and Yin, W.T.,"An iterative regularization method for total variation-based image restoration". Multiscale Mod. Simul.,* ***4****(2): p. 460-489 (2005).*

[205] *Abascal, J., Chamorro-Servent, J., Aguirre, J., Arridge, S., Correia, T., Ripoll, J., Vaquero, J.J. and Desco, M.,"Fluorescence diffuse optical tomography using the split Bregman method". Med. Phys.,* ***38****(11): p. 6275-6284 (2011).*

[206] *Abascal, J.F., Montesinos, P., Marinetto, E., Pascau, J. and Desco, M.,"Comparison of total variation with a motion estimation based compressed sensing approach for self-gated cardiac cine MRI in small animal studies". PLoS ONE,* ***9****(10): p. e110594 (2014).*

[207] *Candes, E.J. and Plan, Y.,"Matrix Completion With Noise". Proc. IEEE,* ***98****(6): p. 925-936 (2010).*

[208] *Chavarrias, C., García-Vázquez, V., Soto-Montenegro, M. and Desco, M. "fMRI in rats under sevoflurane anesthesia" in European Molecular Imaging Meeting 2014. (ESMI, 2014). #139*

[209] *Keilholz, S.D., Silva, A.C., Raman, M., Merkle, H. and Koretsky, A.P.,"Functional MRI of the rodent somatosensory pathway using multislice echo planar imaging". Magn. Reson. Med.,* ***52****(1): p. 89-99 (2004).*

[210] *Sawiak, S.J., Wood, N.I., Williams, G.B., Morton, A.J. and Carpenter, T.A.,"Voxel-based morphometry in the R6/2 transgenic mouse reveals differences between genotypes not seen with manual 2D morphometry". Neurobiol. Dis.,* ***33****(1): p. 20-27 (2009).*

[211] *Lu, J., Dai, G., Egi, Y., Huang, S., Kwon, S.J., Lo, E.H. and Kim, Y.R.,"Characterization of cerebrovascular responses to hyperoxia and hypercapnia using MRI in rat". Neuroimage,* ***45****(4): p. 1126-1134 (2009).*

[212] *Tang, J., Nett, B.E. and Chen, G.H.,"Performance comparison between total variation (TV)-based compressed sensing and statistical iterative reconstruction algorithms". Phys. Med. Biol.,* ***54****(19): p. 5781-5804 (2009).*

[213] *Hugger, T., Zahneisen, B., LeVan, P., Lee, K.J., Lee, H.-L., Zaitsev, M. and Hennig, J.,"Fast Undersampled Functional Magnetic Resonance Imaging Using Nonlinear Regularized Parallel Image Reconstruction". PLoS ONE,* ***6****(12): p. e28822 (2011).*

[214] *Nguyen, H.M. and Glover, G.H.,"A modified generalized series approach: application to sparsely sampled FMRI". IEEE Trans. Biomed. Eng.,* ***60****(10): p. 2867-77 (2013).*

[215] *Logothetis, N.K. and Pfeuffer, J.,"On the nature of the BOLD fMRI contrast mechanism". Magn. Reson. Imaging,* ***22****(10): p. 1517-1531 (2004).*

[216] *Brett, M., Anton, J., Valabregue, R. and Poline, J.,"Region of interest analysis using an SPM toolbox. ". Neuroimage,* ***16****(2, Supp.1): p. 769–1198 (2002).*

[217] *Draganski, B., Gaser, C., Kempermann, G., Kuhn, H.G., Winkler, J., Buchel, C. and May, A.,"Temporal and spatial dynamics of brain structure changes during extensive learning". J Neurosci,* ***26****(23): p. 6314-7 (2006).*

[218] *Friston, K., Ashburner, J., Frith, C., Poline, J., Heather, J. and Frackowiak, R.,"Spatial Registration and Normalization of Images". Hum Brain Mapp,* ***2****: p. 165-189 (1995).*

[219] *Hill, D., Studholme, C. and Hawkes, D. "Voxel Similarity Measures for Automated Image Registration" in Proc. SPIE. Vol. 2359. (1994), p. 205-216.*

[220] *Carp, J.,"The secret lives of experiments: methods reporting in the fMRI literature". Neuroimage,* ***63****(1): p. 289-300 (2012).*

[221] *Johnson, G.A., Calabrese, E., Badea, A., Paxinos, G. and Watson, C.,"A multidimensional magnetic resonance histology atlas of the Wistar rat brain". NeuroImage,* ***62****(3): p. 1848-1856 (2012).*

[222] *Schwarz, A., Danckaert, A., Reese, T., Gozzi, A., Paxinos, G., Watson, C., Merlo-Pich, E. and Bifone, A.,"A stereotaxic MRI template set for the rat brain with tissue class distribution maps and co-registered anatomical atlas: application to pharmacological MRI". NeuroImage,* ***32****(2): p. 538-550 (2006).*

[223] *Friston, K.J., Penny, W., Phillips, C., Kiebel, S., Hinton, G. and Ashburner, J.,"Classical and Bayesian Inference in Neuroimaging: Theory". NeuroImage,* ***16****(2): p. 465-483 (2002).*

[224] *Friston, K.J., Williams, S., Howard, R., Frackowiak, R.S.J. and Turner, R.,"Movement-Related effects in fMRI time-series". Magn. Reson. Med.,* ***35****(3): p. 346-355 (1996).*

[225] *Chen, B.R., Bouchard, M.B., McCaslin, A.F.H., Burgess, S.A. and Hillman, E.M.C.,"High-speed vascular dynamics of the hemodynamic response". NeuroImage,* ***54****(2): p. 1021-1030 (2011)*